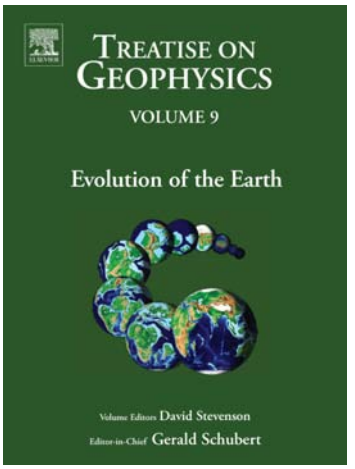

9.10 History of Earth Rotation

W. R. Peltier, University of Toronto, Toronto, ON, Canada

9.10.1 Polar Motion and Length-of-Day Variations through (Geological) Time

Observations of the evolving state of planetary rotation reveal the occurrence of variability on timescales ranging from daily to annual, to interannual, decadal, and millennial, and extending even to the timescale of hundreds of millions of years on which the process of mantle convection governs planetary evolution and to the 4.56 billion year age of the planet itself. These variations in the state of rotation are most usefully discussed in terms of changes in the rate of planetary rotation about the instantaneous spin axis and thus variations in the length of the day, on the one hand, or in terms of the wobble of the spin axis as observed in a body-fixed frame of reference on the other. On relatively short subannual to annual timescales, variations in the length of day (l.o.d.) have been clearly shown to arise primarily as a consequence of the exchange of angular momentum between the solid Earth and its overlying atmosphere (e.g., Hide *et al.*, 1980) and oceans. On the interannual timescale, an important recent discovery concerning

l.o.d. variability has been the documentation of a significant excitation associated with El Niño–Southern Oscillation (ENSO) events (Cox and Chao, 2002; Dickey *et al.*, 2002). Concerning the sources of wobble excitation, it is clear that on the timescale of the seasonal cycle of climate change, the excitation of the annual component of wobble variability is due to the interhemispheric exchange of atmospheric mass. The Chandler wobble, however, a free oscillation of Earth's spin axis in a body-fixed frame of reference with a period close to 14 months, is apparently significantly forced by the dynamical state of the oceans (e.g., Gross, 2000) as well as by the atmosphere. These most recent analyses of the problem of Chandler wobble excitation, to be reviewed in what follows, appear to have finally resolved what had remained an unresolved problem for decades.

On the longer timescale of millennia, both of these 'anomalies' in Earth rotation exhibit apparent secular variations that are caused primarily by the Late Pleistocene cycle of glaciation and deglaciation (Peltier, 1982) that has been an enduring feature of climate system variability for the past 900 000 years of Earth history (e.g., Deblonde and Peltier, 1991). A primary focus of the discussion to follow in this chapter will be upon the manner in which, through the process of glacial isostatic adjustment (GIA), these ice-age-engendered variations in Earth rotation feed back upon postglacial relative sea-level (RSL) history, thus enabling detailed tests to be performed on the quality of the theory that has been developed to compute the rotational response to the GIA process (Peltier, 2005). The importance of an accurate attribution of the source of excitation of the observed secular changes in the l.o.d. and polar motion to the GIA process concerns the important role that these observations may be invoked to play in the inference of the viscosity of the deep Earth, a parameter that is required in the construction of models of the mantle convection and continental drift processes. An interesting additional aspect of the history of Earth's rotation on the timescale of the Late Pleistocene ice-age cycle concerns the way in which temporal variations in the precession and obliquity components of the evolving geometry of Earth's orbit around the Sun, forced by gravitational n-body effects in the solar system, have been employed to refine the timing of the ice-age cycle itself (Shackleton *et al.*, 1990).

On the very longest timescales on which the thermal evolution of the planet is governed by the mantle convection process, there also exists the distinct possibility that relatively rapid and large amplitude changes in the rotational state could have occurred in association with an 'avalanche effect' during which the style of the mantle convective circulation switches from one characterized by significant radial layering of the thermally forced flow, to one of 'whole mantle' form (e.g., Peltier and Solheim, 1994a, 1994b). This process could conceivably act so as to induce the inertial interchange true polar wander (IITPW) instability that was suggested initially by Gold (1955) and which has recently been invoked by Kirschvink *et al.* (1997) as plausibly having occurred in the Early Cambrian period of Earth history.

Figure 1 provides a schematic depiction of the extremely broad range of processes that contribute to the excitation of variations in Earth rotation on all timescales. The centipedes in the sketch, following the colorful analogy by Gold (1955), are intended to represent, by their ability to move over the surface and thereby slowly (?) modify the moment of inertia tensor of the planet, the excitation of a rotational response due to the action of the internal mantle

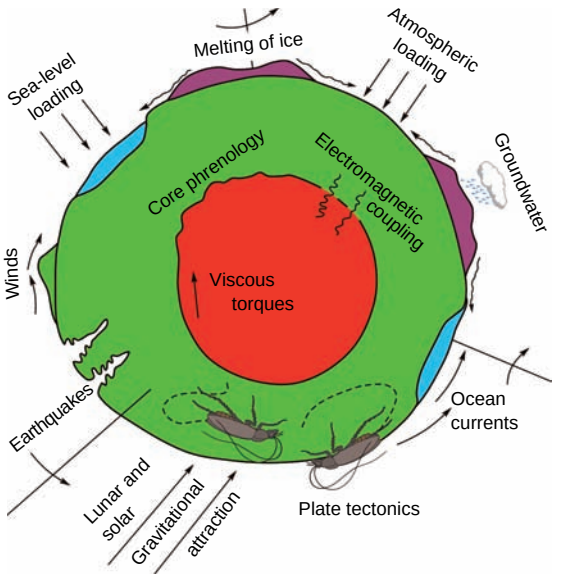

Figure 1 Schematic diagram illustrating the range of processes that contribute to the excitation of variations in the rotational state of the planet. The centipedes in the figure, which are a modification of the beetles employed by Gold (1955) for the same illustrative purpose, are intended to represent the contribution to rotational excitation due to the mantle convection process. This schematic is a modification of that in Lambeck's (1980a) paper commenting upon the important paper of Hide *et al.* (1980).

convective mixing process. How important this component of the rotational excitation could be is still a matter of considerable debate, as is discussed in the final section of this chapter.

9.10.2 Theoretical and Observational Background I: Angular Momentum Conservation on Subannual to Interannual Timescales

9.10.2.1 Theoretical Preliminaries

An instantaneous state of Earth rotation is described entirely by the three Cartesian components of the planet's evolving angular velocity vector with components $\omega_i(t)$. The evolution of the angular velocity vector is itself determined by a solution of the classical Euler equation describing the conservation of angular momentum of a system subjected to external torques τ_j, as:

$$\frac{\mathrm{d}}{\mathrm{d}t}\left(\mathcal{J}_{ij}\omega_i\right) + \in_{ijk}\omega_j\mathcal{J}_{kl}\omega_l = \tau_j \qquad [1]$$

Here, the $\mathcal{J}_{ij}$ are the elements of the moment of inertia tensor and $\in_{ijk}$ is the Levi–Civita (alternating) tensor. Restricting attention to small departures from a modern state of steady rotation with angular velocity Ω_o, we may construct a solution to [1], accurate to first order in perturbation theory, by expanding:

$$\omega_i = \Omega_o(\delta_{i3} + m_i),\ m_i = \omega_i/\Omega_o \qquad [2a]$$

$$\mathcal{J}_{11} = A + I_{11} \qquad [2b]$$

$$\mathcal{J}_{22} = B + I_{22} \qquad [2c]$$

$$\mathcal{J}_{33} = C + I_{33} \qquad [2d]$$

$$\mathcal{J}_{ij} = I_{ij},\ i \neq j \qquad [2e]$$

Substitution of these expansions into eqn [1], keeping only terms of first order, leads to the standard set of governing equations for polar wander and the length of day, respectively (see, for example, Munk and McDonald (1960)), as:

$$\left.\begin{aligned}\frac{\mathrm{d}m_1}{\mathrm{d}t} + \frac{(C-B)}{A}\Omega_o m_2 &= \Psi_1\\ \frac{\mathrm{d}m_2}{\mathrm{d}t} + \frac{(C-A)}{B}\Omega_o m_1 &= \Psi_2\end{aligned}\right\}\ \text{polar wander} \qquad [3a, b]$$

$$\left.\frac{\mathrm{d}m_3}{\mathrm{d}t} = \Psi_3\right\}\ \text{length of day} \qquad [3c]$$

in which the 'excitation functions' are defined as

$$\Psi_1 = \left(\frac{\Omega_o}{A}\right)I_{23} - \frac{(\mathrm{d}I_{13}/\mathrm{d}t)}{A} + \tau_1 \qquad [4a]$$

$$\Psi_2 = -\left(\frac{\Omega_o}{B}\right)I_{13} - \frac{(\mathrm{d}I_{23}/\mathrm{d}t)}{B} + \tau_2 \qquad [4b]$$

$$\Psi_3 = -\left(\frac{I_{33}}{C}\right) + \tau_3 \qquad [4c]$$

Now, it is important to recognize that we are here distinguishing between two different ways of describing the rotational excitation, due respectively to externally applied torques τ_i and to 'internally' originating perturbations I_{ij} to the moment of inertia tensor. In this section, a brief review will be provided of our current understanding of the nature and origins of the variations in Earth rotation that occur on subannual to interannual timescales. These variations are most simply understood by considering the rotational response of an 'almost-rigid' solid Earth to externally applied torques derivative of the action upon it of the atmosphere and oceans as well as to the redistributions of mass that occur both subseasonally and interannually within these components of the Earth system. As we will see in Section 9.10.4, it will be more natural to describe the process involved in the excitation of millennial timescale variations of Earth rotation by invoking 'internally' generated changes in the moment of inertia tensor.

9.10.2.2 Variations in the l.o.d

Focusing first upon changes in the l.o.d. on relatively short timescales, the connection of variations on these timescales to the exchange of angular momentum between the solid Earth and overlying atmosphere was first established most clearly in the important paper by Hide *et al.* (1980). It will be useful to revisit their initial order of magnitude arguments here in order to fix ideas. If one denotes the total axial angular momentum of the Earth system by the sum $M + M_a$, as in Hide *et al.*, which has the approximate value $5.85 \times 10^{33}\,\mathrm{kg\,m^2\,s^{-1}}$, and divides this by the axial moment of inertia that the atmosphere plus solid Earth system would have if the whole system were in a state of rigid body rotation, namely $I + I_a \approx 8.04 \times 10^{37}\,\mathrm{kg\,m^2}$, then one would obtain for the angular velocity of the Earth system $\Omega_R \approx 0.726 \times 10^{-4}\,\mathrm{rad\,s^{-1}}$. A consequence of the fact that the atmosphere of the Earth is differentially heated by the Sun is that the complex general circulation of its atmosphere is characterized by a marked differential rotation between it and the solid Earth.

This leads to a net increase in the angular momentum of the atmosphere by the (approximate) amount $\delta M_a \approx 1.5 \times 10^{26}\,\mathrm{kg\,m^2\,s^{-1}}$ as determined on the basis of direct atmospheric observations. Given the approximate value of the moment of inertia of the atmosphere, $I_a \approx 1.42 \times 10^{32}\,\mathrm{kg\,m^2}$, this leads to an approximate value for the change in angular velocity of magnitude $\delta M_a / I_a \approx 10^{-6}\,\mathrm{rad\,s^{-1}} \approx 3 \times 10^{-8}\,\Omega_R$ or, given that the l.o.d. is just $2\pi/\Omega_R$, one obtains an approximate magnitude for the change in the l.o.d. due to the solar differential heating forced general circulation of the atmosphere of 3×10^{-3} s. Detailed astronomical measurements by the Bureau Internationale de l'Heure (BIH) directly demonstrate that on the annual and interannual timescales this is in fact the order of magnitude of the variations in the l.o.d. observed.

Figure 2 reproduces a figure from the original paper of Hide *et al.* in which a detailed analysis of the angular momentum budget of the atmosphere was performed by evaluating the axial component of the relative angular momentum m_a as

$$m_a = \frac{a^2}{g} \int_{-\pi/2}^{+\pi/2} \int_0^{2\pi} \int_0^{p_g} u(p,\, \theta,\, \lambda,\, t) \cos^2\theta \, \mathrm{d}p \, \mathrm{d}\lambda \, \mathrm{d}\theta \quad [5]$$

in which a is the radius of the Earth, g is the surface gravitational acceleration, u is the zonal component of the velocity of atmospheric air in a frame of reference rotating with the solid Earth, p is atmospheric pressure, p_g is the pressure at the surface of the Earth, θ is latitude, λ is longitude, and t is time. The radial part of the required volume integral has been converted to an integral over pressure by employing the hydrostatic approximation. Based upon the use of independent sets of reanalysis data from the UK Meteorological Office (MO) and from the US National Meteorological Center (NMC), the authors inferred the changes in the l.o.d. that should have occurred if the atmosphere was simply exchanging its axial angular momentum with that of the solid Earth. These estimates of temporal changes in the l.o.d. were compared directly to the astronomically derived measurements provided by the BIH over a 9 month period extending from the winter of 1978 to the summer of 1979. These results, which have since only been reconfirmed by later and more detailed analysis, clearly establish that on these short timescales, changes in the l.o.d. are primarily associated with the exchange of angular momentum between the solid Earth and its overlying atmosphere.

Considered over a period of many years, rather than decades, one begins to see additional structure in the variability in the l.o.d. that includes the measurable influence of an effect due to the changing axial component of the moment of inertia of the solid Earth, an influence that is generally measured in

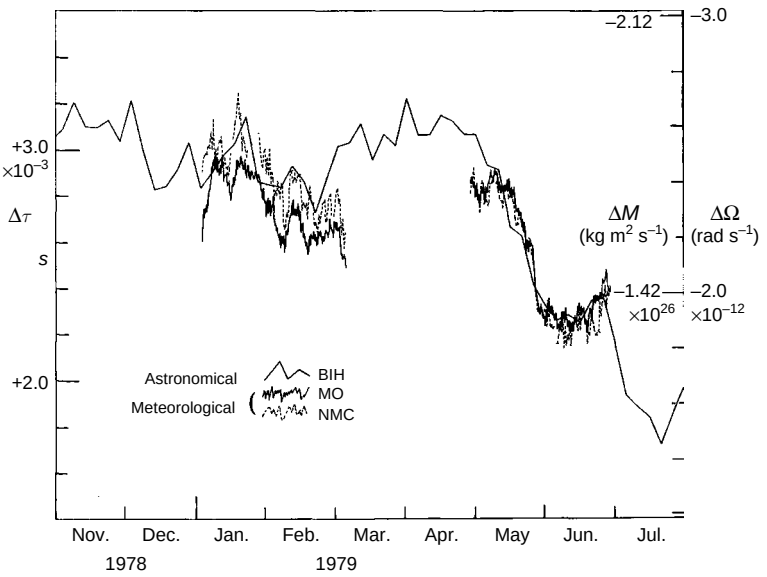

Figure 2 Comparison of the expected changes in the l.o.d., represented by the parameter $\Delta\tau$ measured in milliseconds and derived from the meteorological results (either MO or NMC), with the observed changes based upon the astronomical measurements of the BIH. Reproduced from Hide R, Birch NT, Morrison LV, Shea DJ, and White AA (1980) Atmospheric angular momentum fluctuations an changes in the length of the day. *Nature* 286: 114–117.

terms of a parameter $\dot{\mathcal{J}}_2$ which will be discussed at length in subsequent sections of this chapter. The parameter $\mathcal{J}_2$ is the nondimensional degree 2 and order zero coefficient in the spherical harmonic expansion of the gravitational field of the planet. The connection between this parameter and the angular velocity of the planet and thus the l.o.d. is given by the following simple expression:

$$\dot{\mathcal{J}}_2 = \frac{3}{2}\frac{C}{a^2 m_e}\dot{m}_3 \qquad [6]$$

in which a and m_e are the Earth's radius and mass, respectively, and $m_3 = \omega_3/\Omega_0$.

Superimposed upon the secular trend in $\mathcal{J}_2$, an effect we will show to be unambiguously connected to the GIA process, analyses by Cox and Chao (2002) were the first in which an interannual timescale variation of this quantity was detected that was apparently associated with the ENSO phenomenon. This internal oscillatory ENSO mode of climate system variability is supported by coupling between the atmosphere and the oceans across the equatorial Pacific region and recurs on a timescale that varies from 3 to 7 years. Further analysis of this interannual variability of $\mathcal{J}_2$, which at the time of writing is still not entirely understood, was presented by Dickey *et al.* (2002), in which an attempt was made to ascribe the El Niño influence to a particular related process having to do with "a recent surge in subpolar glacial melting and by mass shifts in the Southern, Pacific and Indian Oceans." **Figure 3** displays a sequence of time series of the parameter $\mathcal{J}_2$, that marked **A** being the time series of the raw data from the BIH. Although prior to late 1996 the time series reveals a consistent secular decrease in the value of this parameter, such that a least-squares best fit of a straight line to the data delivers a best estimate of $\dot{\mathcal{J}}_2$ of approximately -2.9×10^{-11} yr^{-1}, beginning in late 1996 the onset of a significant deviation developed from this secular trend. The timing of this excursion in the time series was coincident with the onset of the intense El Niño event that occurred in 1998. The remaining time series shown on **Figure 3** display the alterations to it that obtain upon successive removal of the influence of the forcing associated with four plausible influences, respectively in (**B**) integrated ocean effects as determined using a data-constrained ocean model, (**C**) subpolar glacier wasting effects, (**D**) integrated atmospheric effects derived on the basis of National Centers for Environmental Prediction (NCEP) reanalysis data, and (**E**) integrated groundwater effects based upon NCEP reanalysis data.

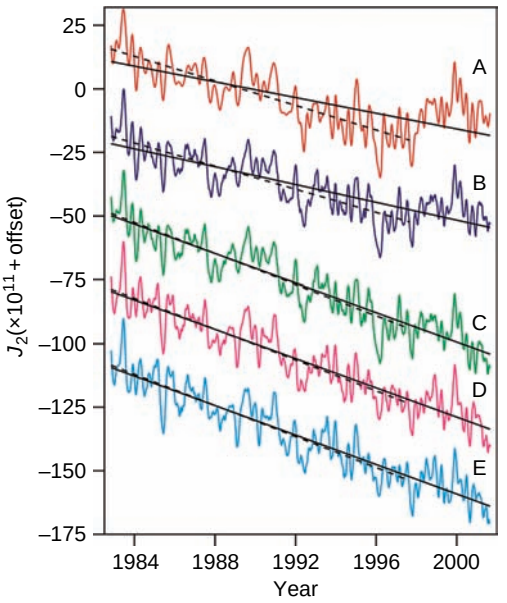

Figure 3 Illustrates as (**A**) the geodetically observed time series of the parameter J_2 over the time period 1983–2002, and residuals (**B**)–(**E**) obtained by successive removal of modeled source terms related respectively to the processes of (**B**) integrated ocean effects, (**C**) subpolar glacial effects, (**D**) integrated atmospheric effects, and (**E**) integrated groundwater effects. Reproduced from Dickey JO, Marcus SL, de Viron O, and Fukumori I (2002) Recent Earth oblateness variations: Unravelling climate and postglacial rebound effects. *Science* 298: 1975–1977.

Although it remains an issue as to whether the attribution of the influence of ENSO upon the $\mathcal{J}_2$ excursion as due to an enhanced wasting of subpolar glaciers is correct, there can be no doubt that the warming associated with the strong 1998 ENSO event induced a substantial variation in the l.o.d. Although the BIH data prior to 1984 were not of sufficient accuracy to generate a longer time series of the variability in this parameter that is equally useful as that shown on **Figure 3**, it is nevertheless extremely important that the dominant secular variation in the time series is essentially the same as that previously inferred on the basis of the analysis of ancient eclipse observations as we will discuss in the following sections of this chapter.

9.10.2.3 Polar Motion: The Annual and Chandler Wobbles

The Chandler wobble or free Eulerian nutation of the spin axis of the Earth in a body-fixed frame of reference was first discovered by S. C. Chandler

(1891). A detailed theory of the Chandler wobble from a 'normal-mode' perspective was first presented by Dahlen and Smith (1974) and has been more fully developed since by Wahr (1982, 1983), whose investigation focused upon the important influence of the atmosphere and oceans upon the phenomenon. Although manipulation of eqns [3a,b] predicts the existence of a simple harmonic 'free oscillation' solution of frequency $\sigma_R = \Omega_0(C-A/A)$, which is referred to from here on as the Chandler wobble frequency of the rigid Earth, this expression substantially errs in its prediction of the period of the actual Chandler wobble because of the importance of these components of the Earth system as well as the existence of the fluid core upon wobble dynamics. Furthermore, this system of equations would predict a Chandler wobble that would have infinite Q in the sense that, once excited, it would never decay in amplitude.

Aside from the Chandler wobble, which has a variable amplitude that ranges between *c.* 100 and 200 milliarcseconds (mas) in the angular displacement of the pole, several additional physical processes contribute to the complete range of polar motion that is observed using the space geodetic techniques of very long baseline interferometry, satellite and Lunar Laser Ranging, and Global Positioning System interferometry. These include: (1) a forced annual wobble with an amplitude of approximately 100 mas which occurs in response to the seasonal variability of the atmosphere and oceans, (2) a weaker but quasi-periodic variation on decadal timescales with an amplitude of approximately 30 mas that is often referred to as the Markowitz wobble, and, most important from the perspective of this chapter, (3) a linear trend corresponding to a secular drift in the position of the pole that is presently occurring at a rate of approximately 3.5 mas yr^{-1}. The latter ultra-low-frequency feature, which will be a primary focus in the main body of this chapter to follow, is the polar motion counterpart to the secular variation in the l.o.d. represented in terms of $\dot{J}_2$ and discussed in the last subsection. The rate of 3.5 mas yr^{-1} corresponds to a rate of drift of the pole across the surface of approximately 0.95° per million years.

Although each of the highest frequency contributions to the motion of the pole has been studied in depth, it has been the development of a detailed understanding of the Chandler wobble that has attracted the greatest interest, as the explanation of its excitation mechanism has proven to be extremely elusive. Attempts were made to ascribe its excitation to the atmosphere (Wilson and Haubrich, 1976; Wahr, 1983), to core–mantle interactions (Rochester and Smylie, 1965; Jault and Le Muel, 1993), to the occurrence of earthquakes (Sauriau and Cazanave, 1985; Gross, 1986), and even to continental water storage (Chao *et al.*, 1987; Kuehne and Wilson, 1991). More recent research has however suggested that the primary excitation may in fact be oceanographic (Gross, 2000), although aided to significant degree by the atmosphere.

In attempting to attribute the excitation of the Chandler wobble to any particular forcing function, it is also important to recognize that this important mode of rotational free oscillation also has a finite Q, so that if all sources of excitation were to vanish, the amplitude of the polar motion would decay to zero. For this reason, a simple heuristic model, derivable from the linearized Liouville equations [3a, b] above, given the extremely small amplitude of the observed motion, is just (e.g., Lambeck, 1980):

$$\Gamma + \frac{\mathrm{i}}{\sigma_{CW}}\frac{\mathrm{d}\Gamma}{\mathrm{d}t} = \chi(t) \qquad [7]$$

in which $\Gamma = x_p - \mathrm{i}y_p$ where x_p and y_p are respectively the displacements of the pole from the Conventional International Origin along the Greenwich and 90° west meridians, σ_{CW} is the complex Chandler wobble frequency of the real anelastic Earth for which the Q of the Chandler wobble has been estimated by Wilson and Vincente (1990) to be 179 with 1σ bounds of 74 and 789. Equation [7] describes simple harmonic motion in the complex plane subject to the forcing represented by the function $\chi(t)$, an excitation function that Wahr (1982) has shown may be written as

$$\chi(t) = \frac{1.61}{\Omega_0(C-A)}\left[h(t) + \frac{\Omega_0 I(t)}{1.44}\right] \qquad [8]$$

in which the complex-valued function $I(t) = I_{13}(t) + \mathrm{i}I_{23}(t)$ where I_{13} and I_{23} are the perturbations of the inertia tensor associated with the variations in the mass distributions in the atmosphere and the oceans that may be responsible for wobble excitation. The function $h(t) = h_1(t) + \mathrm{i}h_2(t)$ represents changes of relative angular momentum associated, for example, with atmospheric winds and ocean currents. The numerical factors 1.61 and 1.44 respectively account for the influences of core decoupling and the yielding of the solid Earth under the weight of the changing surface mass load.

In the paper by Gross (2000), detailed analyses of Chandler wobble excitation were presented that

were based upon the assumption of the validity of the estimates of the Chandler period and Q by Wilson and Vincente (1990), an analysis in which the estimates were based upon the longest time series of polar motion data available at that time (86 years), the only study in which the duration of the data set analyzed was longer than the e-folding time for the decay of the Chandler amplitude. Since the polar motion is resonant at the Chandler period, most analyses of the excitation mechanism have been conducted in the frequency domain by direct comparison of the spectrum of the rotational response to the spectrum of the excitation as computed on the basis of assumed *a priori* knowledge of a range of plausible excitation mechanisms. **Figure 4**(**a**) presents such an intercomparison, one that focused upon assessing the effectiveness of both atmospheric and oceanographic processes.

Inspection of this figure demonstrates, as shown earlier by Wilson and Haubrich (1976) and Wahr (1983), that the net effect of the sum of atmospheric wind and pressure fluctuations (determined on the basis of NCEP/NCAR reanalysis data) is insufficient to explain the Chandler excitation in terms of available as compared to required power (whereas this excitation is entirely adequate insofar as the annual

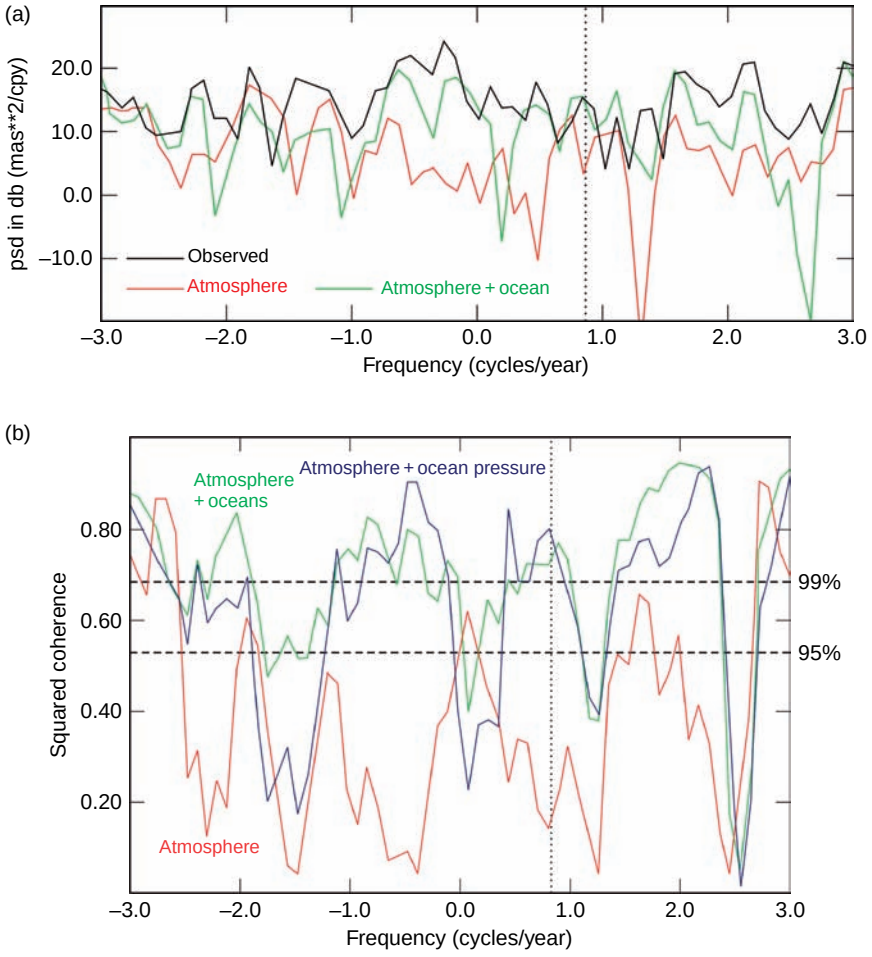

Figure 4 (a) The power spectral density (PSD) estimates in decibels (db) computed from time series of polar motion excitation functions ($\chi(t)$) for the period 1985.0–1996.0 for the observed polar motion excitation function derived from space-geodetic Earth rotation measurements (black curve), for the sum of the excitation functions due to atmospheric wind and pressure changes (red curve) (where the atmospheric pressure term is computed by assuming the validity of the inverted barometer approximation), and for the sum of all atmospheric and oceanic excitation processes (green curve). (b) Squared coherence between the observed polar motion excitation functions in the period 1985.0–1996.0 and the excitation functions due to the sum of atmospheric wind and (inverted barometer) pressure changes (red curve), due to the sum of atmospheric pressure and ocean bottom pressure fluctuations (blue curve), and due to the sum of all atmospheric and oceanic excitation processes. From Gross RS (2000) The excitation of the Chandler wobble. *Geophysical Research Letters* 27: 2329–2342.

wobble is concerned as previously remarked) (NCAR = National Center for Atmospheric Research). On the other hand, when the oceanographic excitation is added to the forcing at the Chandler period, with this determined on the basis of output of the MIT ocean general circulation model (Ponte *et al.*, 1998) driven by 12 h wind stress and 24 h surface heat and freshwater fluxes from NCEP, the total power in the forcing at the Chandler period was found to fit the requirements of the observations extremely well.

In the Gross (2000) paper, this analysis in terms of the available power in the total forcing by the atmosphere and ocean was complemented by an analysis of the coherence between the observed and modeled excitation, the results from which are reproduced here in **Figure 4**(**b**). Inspection of the results of this analysis demonstrates that the atmospheric excitation alone is not coherent with the observed excitation, whereas the atmospheric plus oceanographic excitation is highly coherent with the observed excitation. Through detailed analysis, the author of this paper concludes "that the Chandler wobble is being excited by a combination of atmospheric and oceanic processes" and that "the single most important mechanism exciting the Chandler wobble has been ocean bottom pressure fluctuations which contribute about twice as much excitation power in the Chandler frequency band as do atmospheric pressure fluctuations." It would appear on the basis of these results that our understanding of the Chandler component of Earth's polar motion has become as well understood as are the similarly high-frequency variations in the l.o.d. discussed in the previous subsection.

In the following section of this chapter, the characteristic timescale of our interest in Earth rotation history is extended to include the last million years, a period during which the surface of the solid Earth has been continuously subjected to a quasi-cyclic glaciation–deglaciation cycle involving extremely large exchanges of mass between the oceans and the surface of the continents on which massive continental ice sheets formed. It should not be surprising, given the magnitude of this mass redistribution over the surface, that this 'ice-age cycle' has had and continues to have a profound impact upon the rotational state of the planet. What is often seen as very surprising, however, is the fidelity with which the Earth has conspired to remember the details of both the rotational excitation to which it was subjected and the response to it.

9.10.3 Theoretical Background II: The Viscoelastic Rotational Response to the Late Pleistocene Ice-Age Cycle

Given the extremely broad range of processes that contribute to the excitation of variations in Earth's rotational state (see **Figure 1**) it is always an issue as to the degree to which one is able to uniquely ascribe the observed variability in a particular range of timescales to any one particular process. On the characteristic timescale of millennia and tens to hundreds of millenniums, however, it is apparently the case that the excitation mechanism is so strongly dominated by the Late Pleistocene process of glaciation and deglaciation that such unambiguous attribution has come to be quite generally accepted. This is due to the advances that have been achieved over the past several decades in the development of a detailed viscoelastic theory of the GIA process.

9.10.3.1 Global Theory of the GIA Process

The modern theory of global glacial isostasy addresses the question of the changes in the Earth's shape and gravitational field caused by the variations in surface mass load that occur when water is irreversibly removed from the oceans and delivered to the high-latitude continents to form large accumulations of land ice. Since the amount of water removed from the ocean basins in a typical 100 ky cycle of glaciation and deglaciation has been such as to cause mean sea level to fall by approximately 120 m, it should not be surprising that this process has been accompanied by highly significant variations in Earth rotation, variations of sufficient amplitude as to leave indelible imprints in the geological record of RSL history. The dominant timescale of the Late Pleistocene ice-age cycle is most clearly appreciated on the basis of oxygen-isotopic measurements in deep-sea sedimentary cores. One example of such a record is shown in **Figure 5**. The oxygen-isotopic anomaly $\delta^{18}O$, as measured on the tests of foraminifera extracted as a function of depth from such cores, provides a high-quality proxy for the amount of ice that exists on the continents as a function of time in the past, determined by the depth in the core from which the individual samples are taken (Shackleton, 1967). This is a simple consequence of the fact that the process whereby water is irreversibly removed from the oceans to build the ice sheets is a process that fractionates mass. $H_2{}^{16}O$ is preferentially

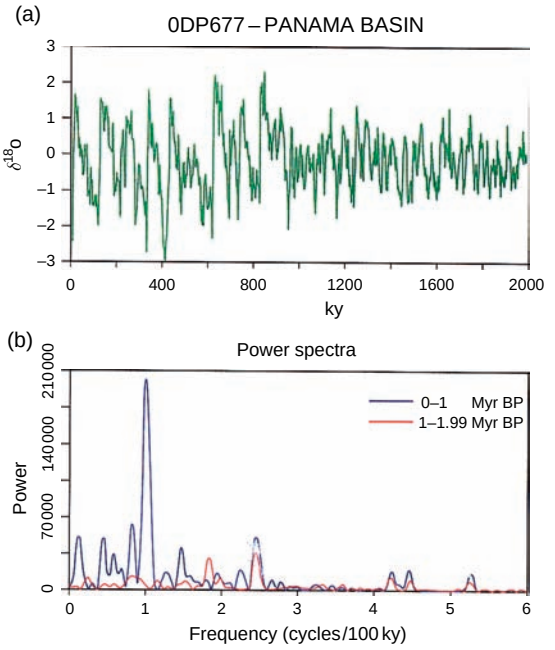

Figure 5 Oxygen-isotopic record from Ocean Drilling Programme Site 677 in the Panama Basin extending to 2 My BP. Also shown are the power spectra for the first and last million years of the record illustrating the onset of the 100 000 year cycle of glaciation and deglaciation in mid-Pleistocene time. Also evident in this continental ice-volume proxy record are the additional spectral lines associated with the variations of orbital obliquity and with the eccentricity modulation of the precessional effect (see Section 9.10.6 for further discussion). From Shackleton NJ, Berger A, and Peltier WR (1990) An alternative astronomical calibration of the lower Pleistocene timescale based upon ODP 677. *Transactions of the Royal Society of Edinburgh: Earth Sciences* 81: 251–261.

removed from the oceans through the evaporation and precipitation processes whereby water is delivered to the high-latitude continents, resulting in an ocean that is anomalously rich in $H_2{}^{18}O$ at a time in the past when large-scale continental ice sheets are in place, an anomaly that is recorded in the shells of foraminifera so long as these remain open systems. This isotopic anomaly is defined as

$$\delta^{18}\mathrm{O} = \left(\frac{[{}^{18}\mathrm{O}/{}^{16}\mathrm{O}]_{\mathrm{sample}}}{[{}^{18}\mathrm{O}/{}^{16}\mathrm{O}]_{\mathrm{standard}}} - 1 \right) \qquad [9]$$

The record shown in **Figure 5**, from Ocean Drilling Program Site 677 in the Panama Basin off the west coast of the South American continent, remains one of the highest-resolution records available and was employed in Shackleton *et al.* (1990) to refine the entire chronology of the Pleistocene epoch (see Section 9.10.6). Inspection of the power spectrum of this record, which is also shown in **Figure 5** for both the first and last million years of the Pleistocene epoch, will show that for the most recent 900 000 years (see Deblonde and Peltier (1991) for a statistical assessment of the sharpness of this 'mid-Pleistocene climate transition') the climate system has been dominated by a quasi-cyclic variation of ice cover with an average period of approximately 100 000 years. Also evident by inspection of the power spectrum of this record are the additional weaker spectral peaks, one at a period of approximately 41 000 years and a triplet of very weak spectral lines at periods of 19 000, 22 000, and 23 000 years. These additional spectral lines are associated with the component of ice-volume variability that is directly forced by the weak variations in solar radiation caused by the changing geometry of Earth's orbit around the Sun that are in turn due to gravitational n-body effects in the solar system. Because the Earth and Sun are not alone in the solar system, the planet's orbit around the Sun does not consist of a time-invariant Keplerian ellipse but rather one whose ellipticity varies slowly with time at a dominant period of 100 000 years. Furthermore, the spin axis of the Earth as it continuously executes its almost elliptical orbit, and which presently makes an angle of approximately 23.5° with the plane of the ecliptic, also varies with time with a dominant period of 41 000 years. As is discussed with more detail in Section 9.10.6, it is these sources of variability in Earth's rotational state that are responsible for the ice ages themselves.

Given the large variations in surface mass load that have accompanied the growth and decay of continental ice sheets over the past ~900 000 years of Earth history, during which a quasi-periodic ice-age cycle has persisted with a period of approximately 100 000 years, it should be clear that the key to understanding the excitation of Earth rotation that has accompanied the process must involve the ability to construct a detailed model of the variations in the moment of inertia tensor caused by the process. This requires the solution of what is here referred to as the sea-level equation (SLE), an equation that accurately describes the way in which water must be distributed over the ocean basins when ice sheets melt so as to ensure that the evolving surface of the ocean remains a surface of constant gravitational potential. An initial version of this equation was first solved in papers by Clark *et al.* (1978) and Peltier *et al.* (1978) based upon

the combination of results obtained in Peltier (1974, 1976) and Farrell and Clark (1976). Since this original work, the theory underlying the SLE has been significantly extended, however, and it is these extensions that have proven crucial to the accurate understanding of the important role that the Earth's rotational response to the GIA process plays in the theory.

The solution of the SLE delivers a prediction of the history of RSL change, $S(\theta, \lambda, t)$ say, that is caused by an assumed known history of the variations in continental ice mass, represented by a history of continental ice-sheet thickness variations $I(\theta, \lambda, t)$. In these expressions, θ is latitude, λ is longitude, and t is time. The form of the SLE that relates these quantities is as follows:

$$S(\theta, \lambda, t) = C(\theta, \lambda, t) \times \left[\int_{-\infty}^{t} \mathrm{d}t' \int \int_{\Omega} \mathrm{d}\Omega' \{ L(\theta', \lambda', t') G_{\phi}^{\mathrm{L}}(\phi, t-t') + \Psi^{\mathrm{R}}(\theta', \lambda', t') G_{\phi}^{\mathrm{T}}(\phi, t-t') \} + \frac{\Delta\Phi(t)}{g} \right] \quad [10]$$

In this equation, $C(\theta, \lambda, t)$ is the 'ocean function', which is, as defined by Munk and Macdonald (1960), unity over the oceans and zero over the continents. The function C is time dependent because the removal of water from, and its addition to, the ocean basins causes the coastline to migrate, an effect that may be accurately computed on a global basis using the methodology described in Peltier (1994). The space-time-dependent surface mass load per unit area L in the above equation has the composite form:

$$L(\theta, \lambda, t) = \rho_{\mathrm{I}} I(\theta, \lambda, t) + \rho_{\mathrm{W}} S(\theta, \lambda, t) \quad [11]$$

in which ρ_{I} and ρ_{W} are the densities of ice and water, respectively. The angle ϕ in the Green functions G_{ϕ}^{L} and G_{ϕ}^{T} is the angular separation between the source point (θ', λ') and the field point (θ, λ). The function $\Psi^{\mathrm{R}}(\theta, \lambda, t)$ is the variation of the centrifugal potential due to the changing rotational state of the Earth that is caused by the surface loading and unloading process associated with the ice-age cycle. Following Dahlen (1976), this may be expressed, to first order in perturbation theory, in terms of the following spherical harmonic expansion, as

$$\Psi^{\mathrm{R}}(\theta, \lambda, t) = \Psi_{00} Y_{00}(\theta, \lambda, t) + \sum_{m=-1}^{+1} \Psi_{2m} Y_{2m}(\theta, \lambda, t) \quad [12]$$

with

$$\Psi_{00} = \frac{2}{3} \omega_3(t) \Omega_0 a^2 \quad [13a]$$

$$\Psi_{20} = -\frac{1}{3} \omega_3(t) \Omega_0 a^2 \sqrt{4/5} \quad [13b]$$

$$\Psi_{2,-1} = (\omega_1 - \mathrm{i}\omega_2)(\Omega_0 a^2/2)\sqrt{2/15} \quad [13c]$$

$$\Psi_{2,+1} = -(\omega_1 + \mathrm{i}\omega_2)(\Omega_0 a^2/2)\sqrt{2/15} \quad [13d]$$

The ω_i in the above equations are to be obtained as solutions to the appropriate version of eqns [3] in Section 9.10.2, the form from which the externally applied torques τ_i have been removed as the rotational excitation in this case must by considered to be internally generated. The remaining terms in the SLE consist of the surface mass loading and tidal potential loading Green functions which have been shown in Peltier (1976) to have the mathematical representations:

$$G_{\phi}^{\mathrm{L}}(\phi, t) = \frac{a}{m_{\mathrm{e}}} \sum_{l=0}^{\infty} (1 + k_l^{\mathrm{L}}(t) - h_l^{\mathrm{L}}(t)) P_l(\cos\theta) \quad [14a]$$

$$G_{\phi}^{\mathrm{T}}(\phi, t) = \frac{a}{g} \sum_{l=0}^{\infty} (1 + k_l^{\mathrm{T}}(t) - h_l^{\mathrm{T}}(t)) P_l(\cos\theta) \quad [14b]$$

in which k_l^{T}, h_l^{T} are the viscoelastic tidal potential loading Love numbers and k_l^{L}, h_l^{L} are the corresponding surface mass loading Love numbers. Peltier (1976, 1985) has shown that these time domain viscoelastic Love numbers may be expressed, in the case of impulsive point mass or gravitational potential loading at the surface of the planet, in the form of the following normal-mode expansions:

$$k_l^{\mathrm{T}}(t) = k_l^{\mathrm{T,E}} \delta(t) + \sum_{j=1}^{M} q_j^l e^{-s_j^l t} \quad [15a]$$

$$h_l^{\mathrm{T}}(t) = h_l^{\mathrm{T,E}} \delta(t) + \sum_{j=1}^{M} r_j^l e^{-s_j^l t} \quad [15b]$$

$$k_l^{\mathrm{L}}(t) = k_l^{\mathrm{L,E}} \delta(t) + \sum_{j=1}^{M} q_j^l e^{-s_j t} \quad [15c]$$

$$h_l^{\mathrm{L}}(t) = h_l^{\mathrm{L,E}} \delta(t) + \sum_{j=1}^{M} r_j^l e^{-s_j^l t} \quad [15d]$$

In these normal-mode expansions, the $k_l^{\mathrm{T,E}}$, $h_l^{\mathrm{T,E}}$, $k_l^{\mathrm{L,E}}$, and $h_l^{\mathrm{L,E}}$ are the elastic surface mass load and tidal potential loading Love numbers of Farrell (1972), the s_j^l are the inverse relaxation times of a discrete set of normal modes of viscoelastic relaxation determined as the zeros of an appropriate secular function (Peltier,

1985) or by collocation (Peltier, 1974, 1976), and the amplitudes q'^{l}_{j}, r'^{l}_{j}, q^{l}_{j}, r^{l}_{j} are the residues at these poles. Insofar as understanding the polar wander component of the rotational response of the planet to the GIA process is concerned, the parameter k_2^{T} plays an especially crucial role as is made clear in what follows.

9.10.3.2 Computation of the Rotational Response to Earth–Ice–Ocean Interactions in the Ice Age

The important role of the Love number $k_2^{\mathrm{T}}(t)$ may be understood by returning to eqns [4] of Section 9.10.2 and focusing upon the polar wander component of the rotational response of the planet in circumstances in which it may be assumed that externally applied torques vanish ($\tau_i \equiv 0$), and noting that in this case we must distinguish two distinct but intimately related sources of excitation. The first of these derives from the perturbations of inertia caused by the direct affect of the isostatic adjustment process, an influence that may be represented in the form (e.g., Peltier, 1982):

$$I_{ij}^{\mathrm{GIA}} = (1 + k_2^{\mathrm{L}}(t)) * I_{ij}^{\mathrm{R}}(t) \qquad [16]$$

in which the $I_{ij}^{\mathrm{R}}(t)$ are the perturbations of inertia that would obtain due to the variations in surface mass load if the Earth were a rigid body rather than viscoelastic and the symbol $*$ represents the temporal convolution operation.

The second contribution to the perturbations of inertia is that due to the changing rotation itself, and this may be derived from an application of a linearized version of MacCullagh's formula (see, for example, Munk and MacDonald (1960)) as

$$I_{13}^{\mathrm{ROT}} = \left(\frac{k_2^{\mathrm{T}} * a^5 \omega_1 \omega_3}{3G}\right) = \left(\frac{k_2^{\mathrm{T}}}{k_{\mathrm{f}}}\right) * m_1 (C-A) \qquad [17a]$$

$$I_{23}^{\mathrm{ROT}} = \left(\frac{\mathrm{k}_2^{\mathrm{T}} * a^5 \omega_2 \omega_3}{3G}\right) = \left(\frac{\mathrm{k}_2^{\mathrm{T}}}{\mathrm{k}_{\mathrm{f}}}\right) * m_2 (C-A) \qquad [17b]$$

with

$$k_{\mathrm{f}} = \left(\frac{3G}{a^5 \Omega_o^2}\right)(C-A) \qquad [17c]$$

in which $A = B$ has been assumed in eqns [4] and $k_2^{\mathrm{T}}(t)$ is the tidal potential loading Love number of degree 2 defined above, the parameter that will be seen to play a crucial role in what follows. Equally critical for the arguments to be presented is the so-called 'fluid Love number' k_{f}, the value of which is determined entirely on the basis of the well-known equatorial flattening of the planet that is represented by the difference between the polar and equatorial moments of inertia $(C-A)$ in eqn [17c]. Substituting in [17c] for Newton's gravitational constant G, the Earth's radius a (for which we will take the equatorial value), the present-day rate of angular rotation Ω_{o} and the polar and equatorial moments of inertia C and A, respectively, taking all data from the tabulation of Yoder (1995), one obtains for the value of k_{f} that

$$k_{\mathrm{f}} \cong 0.9414 \qquad [18]$$

An important part of the discussion to follow will involve understanding of the connection between k_{f} and $\lim_{t\to\infty} k_2^{\mathrm{T}}(t)$, the infinite time asymptote of the viscoelastic tidal loading Love number of degree 2.

Since the solution of eqn [3c] for the change in the axial rate of rotation is uncomplicated, it will suffice to focus first in what follows on the solution of [3a] and [3b] for the polar wander component of the response to surface loading. Substitution of [17a] and [17b] into [3a,b], the Laplace-transformed forms of the equations that follow are simply

$$s m_1 + \sigma\left(1 - \frac{k_2^{\mathrm{T}}(s)}{k_{\mathrm{f}}}\right) m_2 = \Psi_1(s) \qquad [19a]$$

$$s m_2 + \sigma\left(1 - \frac{k_2^{\mathrm{T}}(s)}{k_{\mathrm{f}}}\right) m_1 = \Psi_2(s) \qquad [19b]$$

where

$$\sigma = \Omega_{\mathrm{o}} \frac{(C-A)}{A} \qquad [19c]$$

is the Chandler wobble frequency of the rigid Earth, s is the Laplace transform variable, and again $A = B$ has been assumed. The Laplace-transformed forms of the excitation functions in [19a] and [19b] are simply

$$\Psi_1(s) = \left(\frac{\Omega_{\mathrm{o}}}{A}\right) I_{23}(s) - \left(\frac{s}{A}\right) I_{13}(s) \qquad [20a]$$

$$\Psi_2(s) = \left(\frac{\Omega_{\mathrm{o}}}{A}\right) I_{13}(s) - \left(\frac{s}{A}\right) I_{23}(s) \qquad [20b]$$

with

$$I_{ij}(s) = \left(1 + k_2^{\mathrm{L}}(s)\right) I_{ij}^{\mathrm{Rigid}}(s) \qquad [20c]$$

Now eqns [19a] and [19b] are elementary algebraic equations for $m_1(s)$ and $m_2(s)$ and these may be solved, neglecting terms of order s^2/σ^2, as is appropriate for the analysis of a physical process evolving on a

timescale that is much longer than the period of the Chandler wobble, to obtain

$$m_1(s) = \left(\frac{\Omega_o}{A\sigma}\right)\left[\frac{1+k_2^L(s)}{1-\frac{k_2^T(s)}{k_f}}\right] I_{13}^{Rigid}(s) = H(s) I_{13}^{Rigid}(s) \quad [21a]$$

$$m_2(s) = H(s) I_{23}^{Rigid}(s) \quad [21b]$$

A convenient short-hand form for the solution vector $(m_1, m_2) = \mathbf{m}$ is to write

$$\mathbf{m}(s) = \frac{\mathbf{\Psi}^L(s)}{\left[1-\frac{k_2^T(s)}{k_f}\right]} = H(s)\left(I_{13}^{Rigid}(s),\, I_{23}^{Rigid}(s)\right) \quad [22a]$$

where

$$\mathbf{\Psi}^L(s) = \left[\left(\frac{\Omega_o}{A\sigma}\right)(1+k_2^L(s)\left(I_{13}^{Rigid}(s),\, I_{23}^{Rigid}(s)\right)\right] \quad [22b]$$

From eqns [22], it will be clear that the polar wander solution $\mathbf{m}(s)$ will depend critically upon the ratio $k_2^T(s) / k_f$. This fact was more fully exposed in the analysis of Peltier (1982) and Wu and Peltier (1984) who rewrote the Laplace transform domain forms of $k_2^T(s)$ and $k_2^L(s)$ as (e.g., see equation 61 of Wu and Peltier (1984)):

$$k_2^T(s) = k_2^T(s=0) - s\sum_{j=1}^{N}\frac{(q_j'/s_j)}{(s+s_j)} \quad [23a]$$

$$k_2^L(s) = (-1+l_s) - s\sum_{j=1}^{N}\frac{(q_j/s_j)}{(s+s_j)} \quad [23b]$$

in which the superscript $\ell = 2$ on q_j^2, r_j^2, s_j^2 has been suppressed for convenience. Substituting [23a] into [22], this may be rewritten as

$$\mathbf{m}(s) = \frac{\mathbf{\Psi}^L(s)}{\left[1-\frac{k_2^T(s=0)}{k_f}\right] + \frac{s}{k_f}\sum_{j=1}^{N}\frac{(q_j'/s_j)}{(s+s_j)}} \quad [24]$$

In discussing the formal inversion of [24] into the time domain, the focus for the purpose of this chapter is on the results that follow from application of an important modified form of this equation.

9.10.3.3 The 'Equivalent Earth Model' Approach of Munk and McDonald (1960)

Since the surface of the Earth is broken into a large number of individually rigid lithospheric 'plates' whose boundaries are in general weak, it should be the case that, at spherical harmonic degree 2, the effective $k_2^T(s=0)$ will be close to k_f since in this limit the absence of strength at plate boundaries will enable the planet as a whole to adjust to the tidal (rotational) forcing as if the planet had no surface lithosphere at all. This is highly plausible on physical grounds as $\lim_{s\to 0} s k_2^T(s)$, via the Tauberian theorems (eg., Widder, 1946), is identical to $\lim_{t\to\infty} k_2^T(t)$. That $k_2^T(s=0)$ does tend toward k_f as the thickness of the lithosphere tends to zero will be clear on the basis of **Figure 6** (see also table 5 in Wu and Peltier (1984) and Mitrovica *et al.* (2005)). Based upon **Figure 6**, it will be clear that the deviation of $k_2^T(s=0)$, in the limit of zero lithospheric thickness, from k_f is by less than 1% in the model of Earth's radial viscoelastic structure being employed for present purposes. This model has its radial variation of density and elastic Lamé parameters fixed to those of the preliminary reference earth model of Dziewonski and Anderson (1981) and its viscosity structure fixed to that of the VM2 model of Peltier (1996). In the hydrostatic equilibrium state that develops in the limit of long time under the action of the rotational forcing it is only the internal density field that matters as in this hydrostatic limit of no motion the viscosity structure becomes irrelevant. There is some subtlety here, however, as there is a small effect due to nonlinearity in the exact theoretical determination in the hydrostatic limit

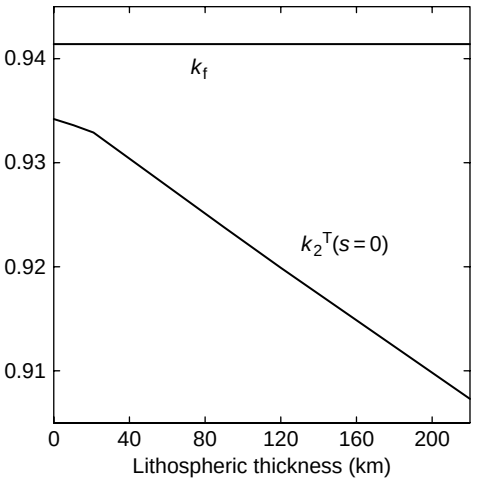

Figure 6 The infinite time asymptotic value of the tidal potential loading Love number of degree 2 is shown as a function of lithospheric thickness. This infinite time limit is identical to the limit in which the Laplace transform variable s equals zero. Also shown is the value of the fluid Love number k_f, which is a constant determined by the observed flattening of Earth's shape as measured by the difference between the polar and equatorial moments of inertia ($C-A$). Note that the difference between $k_2^T(s=0)$ and k_f in the limit of zero lithospheric thickness is <1%. See text for further discussion.

of the value of k_f (e.g., see Nakiboglu (1982)) and so it is not to be expected that a linear viscoelastic field theory for k_2^T will deliver an exact result for k_f in the limit $t \to \infty$. Since it is also the case that the observed flattening of the planet may be influenced to some (imperfectly known) degree by the nonhydrostatic dynamics of the mantle convection process, there is additional reason to expect that the prediction of linear viscoelastic field theory of the value of $k_2^T(s=0)$ could not be precisely equal to the observed k_f. However, since the dynamical contribution due to mantle convection will be invariant on the timescale of the GIA process, this will be of no consequence insofar as the results of the application of first-order perturbation theory are concerned.

Following the 'equivalent Earth model' approach of Munk and McDonald (1960, see p. 28), as in Peltier (1982) and Wu and Peltier (1984), we proceed in a first approximation by adjusting the asymptotic properties of the viscoelastic Earth model by assuming that the infinite time asymptote of the viscoelastic tidal Love number of degree 2 is identical to the fluid Love number based upon the observed flattening of the planet. Although this may somewhat underestimate the degree of stabilization provided by the Earth's actual rotational bulge, it is nevertheless a useful first approximation. In eqn [24], we then take:

$$1 - \frac{k_2^T(s=0)}{k_f} \equiv 0 \qquad [25]$$

Since the actual magnitude of the left-hand side of eqn (25) is extremely small, $k_2^T\ (s=0)$ differing from k_f by less than 1% in the limit of zero lithospheric thickness, the 'equivalent Earth model' approach would appear to be well justified in the context of an analysis based upon the application of first-order perturbation theory (as will be discussed further below). In this 'equivalent Earth model' limit, in which [25] is assumed, eqn [24] becomes

$$\begin{aligned}\mathbf{m}(s) &= \frac{\mathbf{\Psi}^L(s)}{\frac{s}{k_f}\sum_{j=1}^{N}\frac{(q_j/s_j)}{(s+s_j)}} \\ &= \left(\frac{\Omega_o}{A\sigma}\right)\frac{\left(1+k_2^L(s)\right)}{\frac{s}{k_f}\sum_{j=1}^{N}\frac{(q_j/s_j)}{(s+s_j)}}\left(I_{13}^{\text{Rigid}}(s),\ I_{23}^{\text{Rigid}}(s)\right) \\ &= H(s)\left(I_{13}^{\text{Rigid}}(s),\ I_{23}^{\text{Rigid}}(s)\right)\end{aligned} \qquad [26]$$

In order to accurately reconstruct the time domain solution, we need to rewrite the 'impulse response function' $H(s)$ in the above, following Peltier (1982), Wu and Peltier (1984), and Peltier and Jiang (1996), as

$$H(s) = \left(\frac{\Omega_o}{A\sigma_o}\right)\left[\frac{\lambda_s}{s} - \sum_{j=1}^{N}\frac{(q_j/s_j)}{(s+s_j)}\right]\frac{\prod_{j=1}^{N}(s+s_j)}{Q_{N-1}(s)} \qquad [27a]$$

where the degree $N-1$ polynomial Q_{N-1} with roots λ_i is such that

$$Q_{N-1} = \sum_{j=1}^{N} g_j\left[\prod_{i\neq j}(s+s_j)\right] = \prod_{i=1}^{N}(s+\lambda_i) \qquad [27b]$$

with

$$g_j = \frac{q_j'/s_j}{\sum_{j=1}^{N}(q_j'/s_j)} \qquad [27c]$$

is the relative strength of the jth mode of 'viscous gravitational relaxation', and the fully 'relaxed' Chandler wobble frequency of the viscoelastic Earth is defined to be

$$\sigma_o = \frac{\sigma}{k_f}\sum_{j=1}^{N}\frac{q_j'}{s_j} \qquad [28]$$

Using these definitions, the impulse response $H(s)$ may be further manipulated to write

$$\begin{aligned}H(s) =& \left(\frac{\Omega_o\lambda_s}{A\sigma_o}\right)\left[1-\frac{q(s)}{sQ_{N-1}(s)}\right] - \left(\frac{\Omega_o}{A\sigma_o}\right) \\ &\times \sum_{j=1}^{N}\frac{q_j}{s_j}\left[1-\frac{R_j(s)}{Q_{N-1}(s)}\right]\end{aligned} \qquad [29a]$$

where

$$q(s) = s\prod_{i=1}^{N-1}(s+\lambda_i) - \prod_{i=1}^{N}(s+s_i) \qquad [29b]$$

$$R_j(s) = \prod_{i=1}^{N-1}(s+\lambda_i) - \prod_{i\neq j}^{N-1}(s+s_i) \qquad [29c]$$

both of which are polynomials of degree $N-1$. With these factorizations, the Laplace transform of the impulse response, $H(s)$, may be directly inverted into the time domain. When this time domain impulse response is convolved with the time domain expression for the forcing ($I_{13}^{\text{Rigid}}(t)$ and $I_{23}^{\text{Rigid}}(t)$), we obtain the time domain solution of Peltier (1982) and Wu and Peltier (1984), namely:

$$\begin{aligned}m_j(t) =& \left(\frac{\Omega_o}{A\sigma_o}\right)\left\{\left[\lambda_s - \sum_{j=1}^{N}\frac{q_j}{s_j}\right]I_{j3}^{\text{Rigid}}(t)\right. \\ &+ \left(\frac{-\lambda_s q(o)}{\prod_{i=1}^{N-1}\lambda_i}\right)\int_o^t I_{j3}^{\text{Rigid}}(t')\mathrm{d}t' \\ &\left.+ \sum_{i=1}^{N-1}E_i e^{-\lambda_i t} * I_{j3}^{\text{Rigid}}(t)\right\}\end{aligned} \qquad [30a]$$

in which

$$E_i = \left[\frac{\lambda_s q(-\lambda_i)}{\lambda_i} + \sum_{j=1}^{N} \frac{q_j R_j(-\lambda_i)}{s_j}\right] \Big/ \prod_{k\neq i}^{N-1} (\lambda_k - \lambda_i) \quad [30b]$$

To obtain the components of the polar wander velocity vector required to compare with the observed polar wander velocity, we simply differentiate the $m_j(t)$, which are the direction cosines of the polar motion, with respect to time, to obtain

$$\dot{m}_j(t) = \left(\frac{\Omega_o}{A\sigma_o}\right)\left[\left(1 + k_2^{LE}\right) I_{j3} - \frac{\lambda_s q(o)}{\prod_{i=1}^{N-1} \lambda_i} I_{j3} + \sum_{i=1}^{N-1} E_i \frac{d}{dt}\left[e^{-\lambda_i t} * I_{j3}(t)\right]\right] \quad [31]$$

where the equality

$$1 - \sum_{j=1}^{N} (q_j/s_j) = 1 + k_2^{LE}$$

has been employed. To complete the solution for the polar wander component of the rotational response, we need to specify the time series $I_{13}^{Rigid}(t)$ and $I_{23}^{Rigid}(t)$. A specific model of these time-dependent perturbations of inertia will be described in the following subsection.

9.10.3.4 Models of the History of Variations in the Elements of Earth's Moment of Inertia Tensor on the Multimillenial Timescale of the Ice-Age Cycle

For the purpose of the results to be described in this chapter, the surface mass load forcing associated with the ice-age cycle of the Late Pleistocene will, for the most part, be taken to be that of the ICE-5G (VM2) model of Peltier (2004) although results will also be compared to those delivered by a version of the previous model ICE-4G (VM2) of Peltier (1994, 1996). **Figure 7** compares the contribution to the eustatic rise of sea level from LGM to the present for the ICE-5G model with that of a modified version of the precursor model ICE-4G. ICE-5G is characterized by a significant geographic redistribution of the surface mass load. The most important of these changes, which the interested reader will find discussed in detail in Peltier

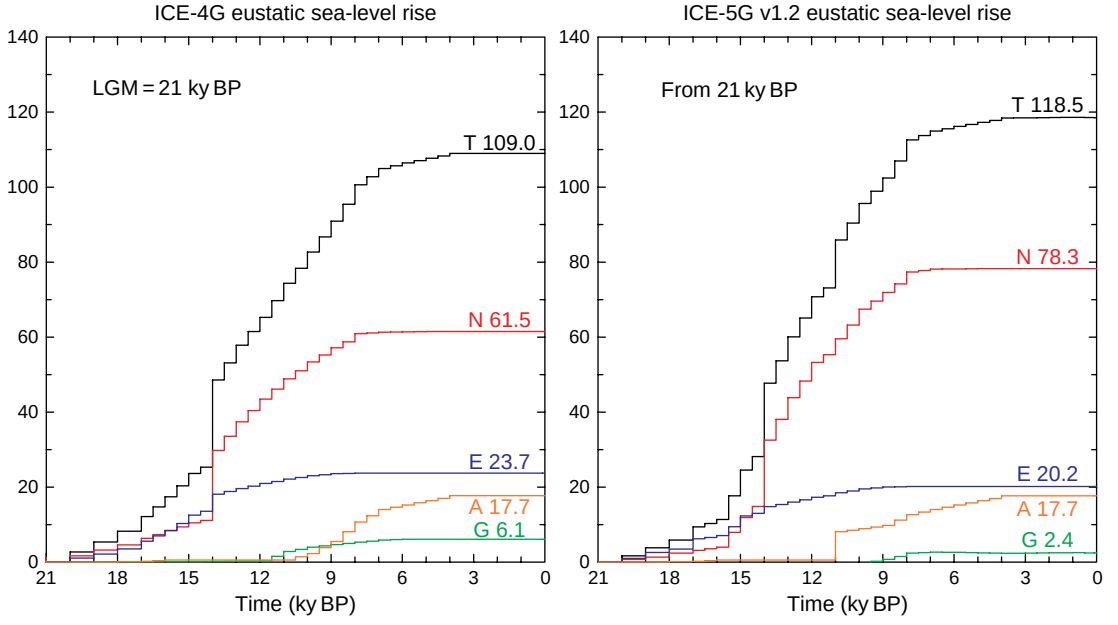

Figure 7 Eustatic sea level curves for the ICE-4G and ICE-5G V1.2 models of the last glacial–interglacial transition. Note that the most significant difference between these models concerns the net eustatic rise from LGM to present. For this version of the ICE-4G model, for which the reconstruction has been performed using the method described in Peltier (2005) in which the 'implicit ice' methodology is not employed, the net eustatic rise is 109.0 m. For the ICE-5G (N1.2) model, on the other hand, the net eustatic rise is 122.1 m. Also evident is the very significant increase in ice mass located over the North American continent (the component denoted 'N': E denotes Eurasia, A denotes Antarctica and South America, and G denotes Greenland). The increase in North American ice mass is partly accounted for by decreases in both Greenland and Eurasia. Also notable is the fact that in the ICE-5G V1.2 model the deglaciation of Antarctica is assumed to begin very abruptly at the time of occurrence of meltwater pulse 1b in the Barbados sea-level record. See the text for further discussion.

(2004), involves a significant shift in mass from Eurasia and Greenland toward the North American continent. It is expected that this will significantly impact both the direction and rate of TPW forced by the glaciation–deglaciation cycle. Also evident by inspection of **Figure 7** is the fact that the version of the ICE-4G model to be employed here has about 10% less LGM mass than the ICE-5G model, a consequence of the fact that it has been reconstructed using the methodology described in Peltier (2005) in which the previous 'implicit ice'-based formalism has been discarded in order that a meaningful full glacial cycle reconstruction could be employed in the present work.

Since the RSL data set from the island of Barbados has been employed to validate the total surface mass load, it will be useful to consider the extent to which the most recent of these models, the ICE-5G model of Peltier (2004), reconciles the observed sea level history at this site. **Figure 8**, which derives from the discussion of this issue in Peltier and Fairbanks (2006), compares the RSL history at this site with the prediction of the ICE-5G (VM2) model of the GIA process based upon eqn [10] and shown as the red curve. In the main portion of the figure, the actual Barbados data, which provide an excellent approximation to the eustatic (globally averaged) variation of sea level from LGM to the present (Peltier, 2002), are compared to both the ICE-5G prediction and the global ice equivalent eustatic sea-level curve proposed by Lambeck and Chappell (2001), which is represented by the color-coded crosses that the authors believed to be eustatic levels derived from the various locations listed in the figure Caption. It will be noted that the Lambeck and Chappell Barbados estimates, as well as those derived from J. Bonaparte Gulf (see Yokoyama *et al.*, 2000), are plotted approximately 20 m below the actual depth from which the samples from these sites were actually recovered. The LGM ice equivalent eustatic lowstand of the sea in the ICE-5G (VM2) model, assuming the modified LGM age of 26 ky proposed by Peltier and Fairbanks (2006) for the time of deepest glaciation, is approximately 122 m (see **Figure 8**, where the eustatic curve is shown as the step-discontinuous purple curve and the prediction of RSL history at this site is shown as the red curve), extremely close to the conventional oxygen-isotope-derived estimate of ~120 m (e.g., see Shackleton (2000)), which was based upon the assumption that the depth of the LGM lowstand was being accurately measured by the Barbados data. At the conventionally assumed LGM age of 21 ky, the eustatic depression of the sea is only 118.7 m in the ICE-5G model. It is a

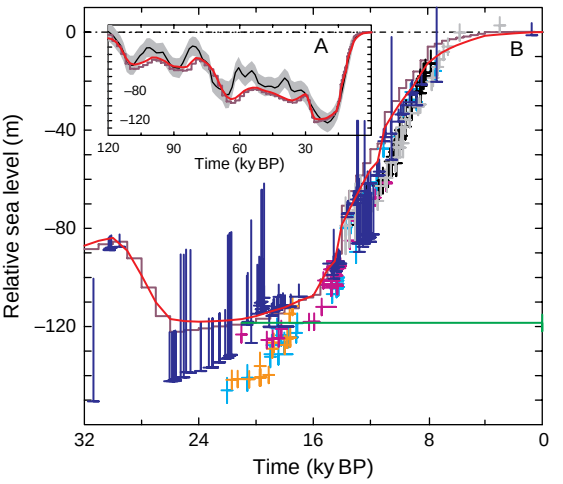

Figure 8 The fit of the predicted relative sea-level history at the island of Barbados to the extended coral-based data set from this location tabulated in Peltier and Fairbanks (2006). The blue symbols with error bars of various length represent these new Barbados data, the data represented by the shorter error bars of 5 m length derived from the *Acropora palmata* species of coral that provide the best constraints on sea level. The data represented by the error bars on intermediate 20 m length derive from the *Montastrea annularis* species of coral. The data represented by the longest error bars derive either from *Porites asteroides* species or the *Diploria* species. The green horizontal line denotes the 118.7 m depth level, which is the level corresponding to the samples of LGM if LGM is assumed to have occurred at the conventionally assumed age of 21 000 years (ago). In order to fit this observational datum, the eustatic depression of sea level at that age is almost precisely equal to the depth at which the sample of LGM age is found. This is a consequence of the fact that the Barbados record of relative sea-level is an excellent approximation to eustatic sea-level history itself. The color coding of the Lambeck and Chappell estimates, which are shown as the crosses, is as follows: cyan (Barbados), black (Huon Penninsula), gray (Tahiti), purple (Sunda Shelf). The inset to the figure shows the comparison between the eustatic history of the ICE-5G model and the complete 10^5 yr glacial cycle with that inferred by Waelbroecke *et al.* (2002) based upon benthic $\delta^{18}O$ records corrected for the influence of the change in abyssal ocean temperature.

further important property of the extended Barbados record of Peltier and Fairbanks that the data appear to strongly reject the hypothesis of Yokoyama *et al.* (2000) that a strong meltwater pulse occurred at 19 ka. In the ICE-5G reconstruction, such rapid melting events are taken to have occurred only at the times of meltwater pulses 1a and 1b originally identified by Fairbanks (1989).

Also evident by inspection of **Figure 7** is that the contribution to ice equivalent eustatic sea-level rise from the Antarctic continent in version 1.2 of the ICE-

5G (VM2) model is characterized by an abrupt onset at approximately 11 500 years BP. This late onset of Antarctic meltback has always been a characteristic of the ICE-NG sequence of models, it having been argued (e.g., see Peltier (2005)) that this region was the most likely source of the meltwater pulse 1b event that is now clearly evident in the extended Barbados sea level record discussed in Peltier and Fairbanks (2006). Very recently, this assumption in the ICE-5G and earlier reconstructions has been strikingly verified by accurately carbon-14 dating the age of the onset of shelf sedimentation from a large number of sites in coastal Antarctica that had been covered by grounded ice at LGM (e.g., see Domack *et al.* (2005)). These new observational results effectively rule out the claim in Clark *et al.* (2002) that the source of the earlier meltwater pulse 1a event was Antarctica. Peltier (2005) discussed additional evidence on the basis of which this suggestion must be considered implausible and Tarasov and Peltier (2005, 2006) have explicitly discussed the flaw in the Clark *et al.* (2002) suggestion. A sequence of predictions of RSL histories based upon the ICE-5G (VM2) model at a sequence of well-dated sites from Scotland derivative of isolation basin-based inferences of RSL (see Peltier *et al.* (2002) for a detailed discussion of these data) strongly reinforce the Antarctic origin of meltwater pulse 1b. As discussed in Peltier *et al.* (2002), the highly nonmonotonic nature of these RSL curves, which are so well fit by the theoretical predictions, is entirely a consequence of the assumed late glacial melting event emanating from Antarctica and its abrupt onset as is characteristic of the ICE-5G v1.2 reconstruction.

The primary model of the glaciation–deglaciation process that is to be employed here for the purpose of analyzing Earth's rotational response to the ice-age cycle is therefore ICE-5G (VM2), the extension of which in the interval between the Eemian interglacial and LGM is based upon the SPECMAP record of Imbrie *et al.* (1984). In the inset to **Figure 8**, the complete ICE-5G record of the most recent glaciation–deglaciation cycle is compared with the reconstruction of Waelbroeck *et al.* (2002), whose reconstruction was based upon deep-sea δ^{18}O records corrected for the influence of the temperature variability of the abyssal ocean. Comparison of this record with that for the ICE-5G (VM2) model demonstrates that the two approximations to the ice equivalent eustatic sea-level history over the most recent glaciation–deglaciation cycle are extremely similar. In order to construct a complete surface loading model for use in the computation of Earth rotation anomalies, however, a model that includes more than a single glacial cycle is required. Since approximately seven such cycles have occurred during the past 800 000 years of Earth history, for the purpose of the analyses to be discussed herein, it will be assumed that an approximately100 ky cycle of glaciation and deglaciation has continued to operate over this same period.

Construction of the polar wander and l.o.d. solutions requires the time series $I_{13}^{\mathrm{Rigid}}(t)$, $I_{23}^{\mathrm{Rigid}}(t)$, and $I_{33}^{\mathrm{Rigid}}(t)$, inputs to the calculation that may be computed from the definition of the I_{ij}^{Rigid}. This definition is

$$I_{ij}^{\mathrm{Rigid}}(t) = \int\int v(\theta,\,\phi,\,t)(a^2\delta_{ij} - x_i x_j)\;\mathrm{d}s \qquad [32]$$

where the integral is over the surface of the sphere and where $v(\theta,\,\phi,\,t)$ is the surface mass load per unit area. Since this may be expressed in the form of a spherical harmonic expansion as

$$v(\theta,\,\phi,\,t) = \sum_{\lambda=\mathrm{o}}^{\infty}\sum_{m=-\lambda}^{+\lambda} v_{\lambda m}(t)\,Y_{\lambda m}(\sigma,\,\phi) \qquad [33]$$

it follows that

$$I_{13}^{\mathrm{Rigid}}(t) + \mathrm{i}I_{23}^{\mathrm{Rigid}}(t) = -\left(\frac{32}{15}\right)^{1/2}\pi a^4 v_{21}(t) \qquad [34a]$$

$$I_{33}^{\mathrm{Rigid}}(t) = -\left(\frac{8}{3}\right)\pi a^4\left[\left(\frac{1}{5}\right)^{1/2} v_{20}(t) - 2v_{\mathrm{oo}}(t)\right] \qquad [34b]$$

An issue that immediately arises concerning the evaluation of these inputs to the theory concerns the way in which the component of the surface load is computed that is associated with the water that is extracted from or added to the oceans as the ice sheets grow and decay, respectively. Although the loading and unloading of the continents due to the growth and decay of the ice-sheets is an *a priori* specified input to the theory, the ocean loading component must be obtained self-consistently as a solution to the SLE [10]. However, this equation for the space-time history of the load on the ocean basins includes the influence of rotational feedback through the convolution of Ψ^{R} with G_{ϕ}^{T}. The problem of determining the rotational response to the ice-age cycle must therefore be determined iteratively. We first compute a solution for the ω_i by neglecting this feedback effect. We next add the feedback terms into eqn [10] and recompute the sea-level history and thus the modification to the ocean load needed to determine the inertia perturbations required for the computation of the $\omega_i(t)$, etc. The iteration sequence is found to converge rapidly. It is

also important to note that the ocean component of the surface load varies over a single glacial cycle in a way that depends somewhat upon the viscosity model of the Earth that is employed to represent the GIA process.

In order to complete the specification of the inputs for solution [26], we need to evaluate convolution integrals of the form

$$f(t) = e^{-\lambda_i t} * I^{\text{Rigid}}(t) = \int_{-\infty}^{t} I(t')e^{-\lambda_i(t-t')}dt' = e^{-\lambda_i t}\int_{-\infty}^{t} I(t')e^{\lambda_i t'}dt \quad [35]$$

These integrals may be computed to sufficient accuracy by assuming that the functions $I(t)$ consist of a series of periodic pulses, each of the form consistent with the ICE-5G (VM2) model of the most recent glacial cycle. Single-cycle integrals are computed numerically, and the impact of a large number of cycles is simply added with the appropriate phase delay (see Peltier (1982) and Wu and Peltier (1984) for an example in the special case that the pulse shape has a simple triangular form). In that case, the integrals may be evaluated analytically. In the general case treated here, they must be evaluated numerically. **Figure 9** compares time series for the ICE-5G (VM2) and ICE-4G (VM2) models for I_{13}^{Rigid}, I_{23}^{Rigid}, and I_{33}^{Rigid}. Given these models of the rotational forcing, we are in a position to compute the response in terms of both the l.o.d. and polar motion.

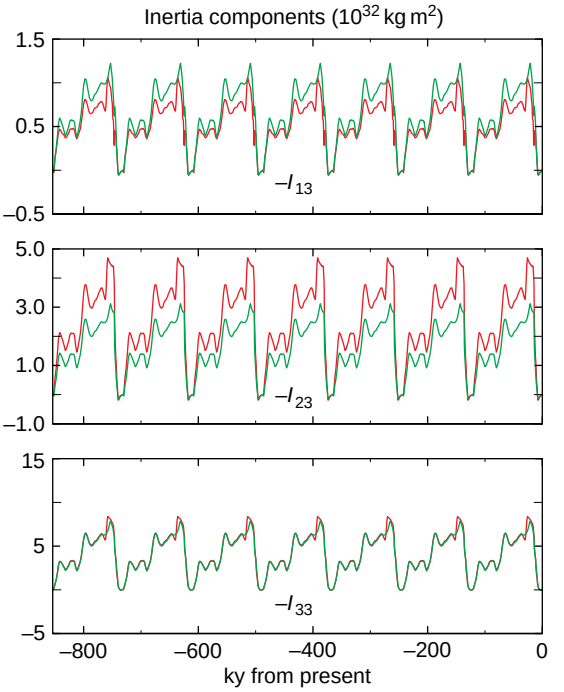

Figure 9 ICE-5G- (red) and ICE-4G- (green) based model histories for the variation of the I_{13}^R, I_{23}^R, and I_{33}^R components of the inertia tensor for a model history that assumes that seven cycles of glaciation and deglaciation have occurred with an approximate period of 100 ky. For the purpose of the calculations described in this chapter, Late Pleistocene glacial–interglacial cycle is assumed to have been precisely periodic. Since the system exhibits a fading memory of its past, this should not have a profound influence upon our conclusions.

9.10.4 Observations of Millenial-Scale Secular Variations in Earth Rotation Anomalies

Although the existence of a secular trend, persisting over thousands of years, in the nontidal variations of the l.o.d., has been known for at least the last quarter of the twentieth century, and an equivalently important secular drift in the position of the pole has also become evident in the same period, debate has continued as to the cause of these secular variations in the rotation anomalies. Only through the development of the theory described in the last subsection of this chapter has it proven possible to unambiguously attribute both signals to the GIA process. Prior to reviewing the analyses that have established this result, it will be useful to briefly review the observations themselves.

9.10.4.1 Ancient Eclipse Observations and the Nontidal Acceleration of Rotation

That an anomaly in Earth's rate of axial rotation did exist, beyond the relatively well-understood decrease due to the action of the tidal friction that arises because of the frictional dissipation of the tide raised in the Earth's oceans by (primarily) the gravitational attraction of the Moon, was first suggested (e.g., Newton, 1972; Morrison, 1973; Muller and Stephenson, 1975) on the basis of analyses of ancient eclipse data extending back more than 2500 years before present. For much of this interval of time, in both Babylon and China, naked eye astronomers kept careful records of the timing and place of occurrence of total eclipses of the Sun and Moon. On the basis of the assumption that tidal friction had remained constant over this interval, a highly reasonable assumption as sea level has not changed appreciably over this interval of the Late Holocene period, one may accurately predict when and where a total eclipse of the Sun or Moon should

have occurred. Analysis of such data, as described most recently in Stephenson and Morrison (1995) and Morrison and Stephenson (2001), clearly demonstrates that the further back in time for which an eclipse prediction is made, the larger is the error in timing, the sign of the error being such as to imply the action of a acceleration of rotation that is acting opposite to the effect of tidal friction. The compilation of data from the paper by Stephenson and Morrison (1995) is shown in **Figure 10**. Based upon the analysis of both lunar and solar eclipses that occurred between700 BC and AD 1600, these authors reported an increase in the length of the mean solar day (l.o.d) of (1.7 ± 0.5) ms per year, which implies a rate of decrease of the angular speed of rotation of $(-4.5 \pm 0.1) \times 10^{-22}\,\mathrm{rad\,s^{-2}}$ on average over the past 2.7 ky. After subtracting the contribution due to tidal friction, which is accurately known based upon observations of the rate of recession of the Moon using Lunar Laser Ranging, Stephenson and Morrison (1995) inferred an average rate of nontidal acceleration of $(1.6 \pm 0.4) \times 10^{-22}\,\mathrm{rad\,s^{-2}}$ over this period. This value for the nontidal acceleration of rotation corresponds to a value for $\dot{\mathcal{J}}_2$ of $(-3.5 \pm 0.8) \times 10^{-11}\,\mathrm{yr^{-1}}$. As discussed in Section 9.10.2, this parameter provides a direct measure of the oblateness of planetary shape such that the larger is $\mathcal{J}_2$ the larger the oblateness. The fact that the time derivative is negative therefore implies that the nontidal acceleration of rotation is derivative of a secular decrease in the oblateness of figure and therefore of a decrease in the value of the polar moment of inertia. That this is plausibly a consequence of the GIA process follows from the fact that at glacial maximum the oblateness would have been increased by the increased surface mass load at the poles. Once this load is eliminated during the deglaciation process, this ice-age contribution to enhanced oblateness would have begun to relax as the planet returned to the more spherical shape characteristic of an interglacial period. Since angular momentum is conserved in the absence of external torques, the rate of axial rotation would have continued to increase, thus leading to the observed nontidal acceleration of rotation.

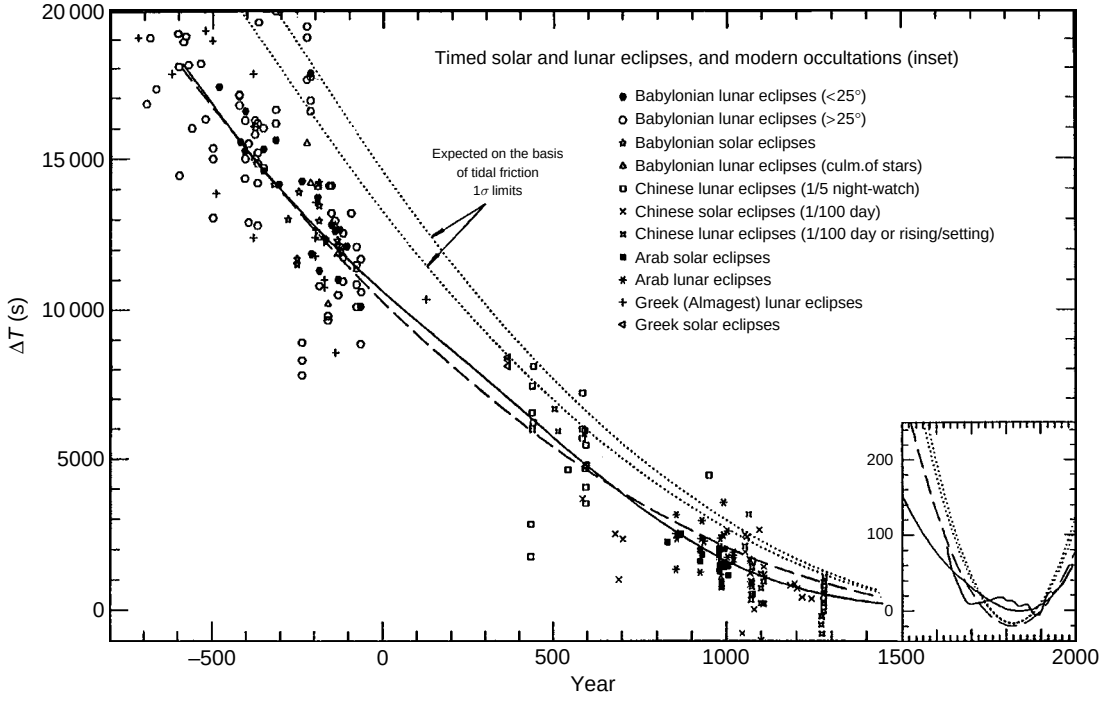

Figure 10 Results obtained for the time difference between the observed time of a total eclipse of the Sun or the Moon and the time at which the event was predicted to occur based upon the assumption of constant tidal torque. The inset (on a scale 25 times greater) includes the continuous curve derived frm the lunar occultations in the period AD 1620–1955.5, and the difference TAI-UT1 + 32.1845 from 1955.5 to 1990. The dashed curve is the best-fitting parabola 31 t^2 s. The solid curve is fitted using cubic splines. This curve, the best fitting parabola, and the parabola expected on the basis of tidal friction, are continued on the inset. From Stephenson ER and Morrison LV (1995) Long term fluctuations in the earth's rotation: 700 BC to AD 1990. *Philosophical Transactions of the Royal Society (London) Series A* 351: 165–202.

Beginning with the first publication and interpretation of data from the Laser Geodynamics Satellite (LAGEOS) by Yoder *et al.* (1983), which appeared simultaneously with the interpretation of the nontidal acceleration as a consequence of the GIA effect (Peltier 1982, 1983), the validity of the ancient eclipse-based inference of the nontidal acceleration was clearly established. Many estimates of the nontidal acceleration based upon the analysis of satellite laser ranging (SLR) data have now appeared (the effect observed is an acceleration in the rate of precession of the node of the orbit). The complete set of published estimates is shown in **Figure 11**, where the estimates of various authors are provided in terms of $\dot{J}_2$.

As a final comment upon the most recent research that has been conducted on l.o.d changes on millennial timescale, it is worth noting the work of Dunberry and Bloxham (2006) on the possibility of the existence of an oscillation in the l.o.d. that may be evident in the historical eclipse data set, an oscillation that the authors suggest may have a period of 1500 yr. A similar timescale is suggested to be evident from archeomagnetic artifacts, lake sediments, and lava flows (Daly and LeGoff, 1996; Hongre *et al.*, 1998; Korte and Constable, 2003). They interpret this as plausibly arising as a consequence of coupling between the outer core and the mantle across the core–mantle interface. It should be noted, however, that the existence of any such 1500 yr oscillatory component in the l.o.d. variations has been questioned by Dalmau (1997).

Although space limitations mitigate against providing a detailed review of an important very long timescale mechanism through which highly significant changes in the l.o.d. occur, namely through the action of tidal friction alone, it will be important to at least record the fact that such changes are large and that there exist extremely useful observations that can be brought to bear upon the problem. Because of the dominant control that the semi-diurnal M2 tide in the oceans exerts upon coastal marine sedimentological processes, it has been possible on the basis of the study of 'tidal rhythmites' to infer what the l.o.d has been at certain epochs in the distant past. For example, in Williams (2000), analyses are described of South Australian sequences for the Late Neoproterozoic (~620 My BP) that indicate a rotational state characterized by 13.1 ± 0.1 synodic (lunar) months/yr, 400 ± 7 solar days/yr, and an l.o.d of 21.9 ± 0.4 h. He also infers on the basis of these data a mean rate of lunar recession since that time of 2.17 ± 0.31 cm/yr, slightly more than half the present-day rate of lunar recession of 3.82 ± 0.07 cm/yr obtained on the basis of Lunar Laser Ranging. Similar data from earlier epochs are also discussed in Williams review paper, which suggest that a close approach of the Moon to the Earth did not occur during the Proterozoic (2450–620 Ma). These results are clearly important for our understanding of the origin of the Moon and of the processes that control tidal friction. The current configuration of the ocean basins is such that tidal friction is considerably larger than it has been over much of the geological past as a consequence of the fact that the ocean basins are currently of a spatial scale such that a near-resonant condition exists between the normal modes of the ocean basins and the tidal forcing. The interested reader will find a highly informative discussion of the tides as free oscillations of the ocean basins in Platzman (1971). This is a fascinating subject about which there is yet a great deal to be learned.

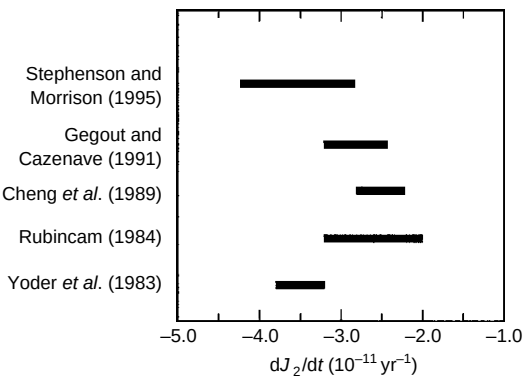

Figure 11 Published estimates of the parameter $\dot{J}_2$.

9.10.4.2 Millenial Timescale Polar Wander and the Glaciation–Deglaciation Cycle

Insofar as the second of the secular anomalies in Earth rotation is concerned, namely the true wander of the North Pole of rotation relative to the surface geography, the data originally obtained by the International Latitude Service that have been employed to constrain it are shown on **Figure 12**. The data initially tabulated by Vincente and Yumi (1969, 1970) were derived on the basis of observations of star transits using a Northern Hemisphere array of photo-zenith tubes. The data consist of time series of the x and y coordinates of the position of the North Pole of rotation relative to a reference frame fixed to the Earth's crust with origin at the Conventional International Origin (CIO). This reference frame is shown on the inset polar projection in **Figure 12** and has its x-axis aligned with the Greenwich meridian. Inspection of the x and y time series demonstrates

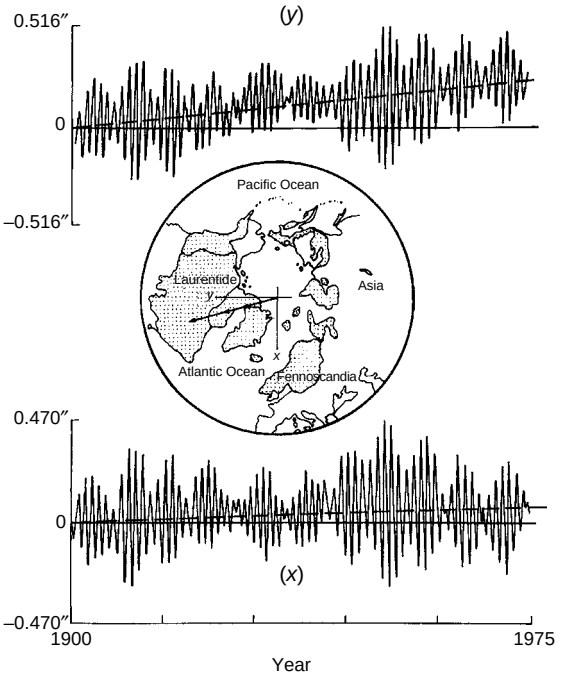

Figure 12 Time series of the location of the North Pole of rotation of the planet, as *x* and *y* coordinates relative to the coordinate system shown on the inset polar projection with origin at the Conventional International Origin (CIO). These data are those of the International Latitude Service (Vincente and Yumi, 1969, 1970) and they reveal a secular drift of the pole at arate near 0.95° per million years approximately along the 75.5° west meridian of longitude.

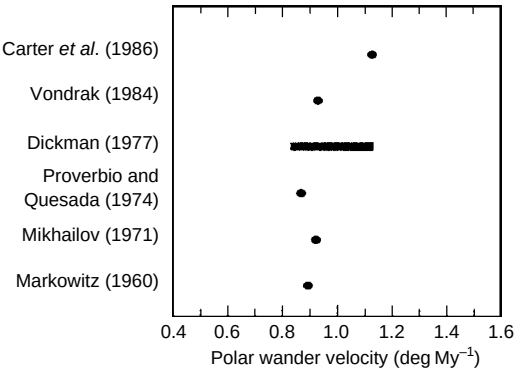

Figure 13 Published estimates of the speed of polar motion based primarily upon the ILS data.

them to be dominated by an oscillatory pattern of beats with a period of approximately 7 years. This pattern is well understood to arise as a consequence of the interference between the 12 month periodic annual wobble and the 14 month periodic Chandler wobble that were discussed in Section 9.10.2. Based upon the review of our understanding of these features of Earth rotation history discussed therein, it would appear that previous controversies concerning their excitation have now been satisfactorily resolved. According to Dickman (1977), the TPW, evident as the secular drift of the position of the pole upon which the oscillatory signal is superimposed, is occurring at a rate of $(0.95 \pm 0.15)^\circ$ per million years along the 75.5° west meridian as shown on the inset polar projection in **Figure 12**. An unambiguous connection of this Earth rotation anomaly to the GIA process was first suggested in Peltier (1982) and Wu and Peltier (1984), whose detailed theoretical analysis, since further generalized in Peltier and Jiang (1996), showed that the initial analysis by Munk and MacDonald (1960) of the excitation of polar wander by surface loading of a viscoelastic model of the Earth did not in fact rule out an explanation in terms of the GIA process even though the surface mass load during the Late Holocene interglacial period has been very nearly time invariant. The analysis of the data by Dickman (1977) was preceded by several earlier analyses and has been followed by others. Most of these results are shown on **Figure 13**, where they are accompanied by an early result derived on the basis of the analysis of VLBI observations by Carter *et al.* (1986).

The most recent analysis of the International Latitude Service (ILS) data is that of Argus and Gross (2004), who have investigated the possibility that all of these interpretations may be contaminated by the failure to account for the influence of surface plate-tectonic motions. Their analysis of the raw data delivered a best estimate of the speed of polar wander of 1.06° per million years. Depending upon how this estimate was corrected for the influence of plate tectonics, however, considerably different results could be obtained, as listed in **Table 1** of that paper. Whereas the ILS inference uncorrected for plate motion was that the ongoing polar wander was along the 75.5° west meridian, if the same data set is corrected by making the inference in the frame of reference in which the lithosphere exhibits no net rotation, then the corresponding speed and direction change slightly to 0.98° My^{-1} southward along the 79.9° west meridian. However, if the correction to these data is based upon the 'hot-spot frame', then one obtains, from the ILS data, according to Argus and Gross (2004), the values 1.12° My^{-1} for the speed and southward along the 69° west meridian for the direction, a significant difference. The fact that all of these inferences of polar wander direction

Table 1 Predictions of the polar wander speed and direction for the ICE-4G and ICE-5G models of the Late Pleistocene glaciation cycle, both including and excluding the influence of rotational feedback

	Observation	ICE-4G (N)	ICE-4G (R)	ICE-5G (N)	ICE-5G (R)
Polar wander speed (deg My^{-1})	0.8–1.1	0.81	0.57	1.06	0.72
Polar wander direction (degrees west longitude)	75.5	69.9	73.4	83.1	88.8

suggest it to be moving 'toward' what was the centroid of the ancient Laurentide ice sheet is nevertheless highly significant insofar as the explanation in terms of glacial isostasy is concerned. Since the constraint of angular momentum conservation requires that the pole must drift so as to align itself along the axis relative to which the moment of inertia is largest, it is clear why, as a consequence of the GIA effect, the pole should now be moving toward what was the centroid of the greatest concentration of land ice. Following deglaciation, there exists a residual depression of the land that is yet to be eliminated by the slow viscous process of GIA. This region therefore constitutes a localized deficit of mass relative to the state of gravitational equilibrium that will eventually be reached once the GIA-related relaxation of shape has been completed. It is toward this regional mass deficit that the pole must move in order to come into alignment with the axis of greatest inertia. That it need never reach and in general will not reach this region is simply a consequence of the fact that the speed of polar wander decreases as a function of time as the shape relaxation proceeds at a rate determined by mantle viscosity.

The question of the accuracy of the direction of the secular drift of the pole that is derived on the basis of the ILS data may be at least as important as the speed. The reason for this has to do with the use of the rotational anomalies to constrain the rate of melting of polar ice that may be occurring at present due to the action of greenhouse gas-induced global warming. Depending upon the polar wander prediction due to the continuing action of the GIA effect, there will exist a residual between this prediction and the modern observations that may be employed to constrain the rate and geographical locations of modern sources of land ice melting (Greenland, Antarctica, small ice sheets and glaciers) as previously discussed in Peltier (e.g., 1998, see figure 46). Further comment on this issue follows in the next section, in which the theory reviewed in Section 9.10.3 will be applied to understanding the observational constraints upon polar wander described in this section.

9.10.5 Earth's Rotational Response to the Cyclic Reglaciation Cycle of Late Pleistocene Time: Data-Model Intercomparisons

Based upon the discussion in Section 9.10.3, it will be clear that accurate predictions of RSL history are a required preliminary to accurate predictions of the rotational response to the GIA process and thus to the understanding of Earth rotation history on millennial timescales. Since the best test of the accuracy of RSL history predictions based upon solution of the SLE is provided by radiocarbon-dated RSL curves from coastal locations, it will be clear that the confrontation of theory with observational 'truth' requires a voluminous compilation of such records, individual examples of which have been produced by innumerable scientists working in the area of Pleistocene geomorphology over the past half century. That a global database of such records is expected to record a wide range of signatures of the GIA process will be clear on the basis of **Figure 14**, from Peltier (2004), which shows predictions of the present-day rate of RSL rise for the ICE-4G (VM2) model both (a) including and (b) excluding the influence of rotational feedback. The difference between these predictions (a−b) is shown in **Figure 14**(**c**), which establishes the dominant role that the polar wander component of the rotational response to the GIA effect plays in contributing to sea-level history. The 'signature' of this feedback is the existence of the strong degree 2 and order 1 spherical harmonic component, a quadrapolar distribution that is the expected form of this feedback based upon eqns [13] in Section 9.10.3. **Figure 14**(**d**) shows the sum of the signal shown in **Figure 14**(**a**) for the present-day rate of RSL rise and the prediction for the same model of the present-day rate of radial displacement of the crust. As first discussed in Peltier (1999), this sum represents the time rate of change of geoid height due to the GIA process, a field that is measured by the Gravity Recovery and Climate Experiment (GRACE) dual-satellite system (see

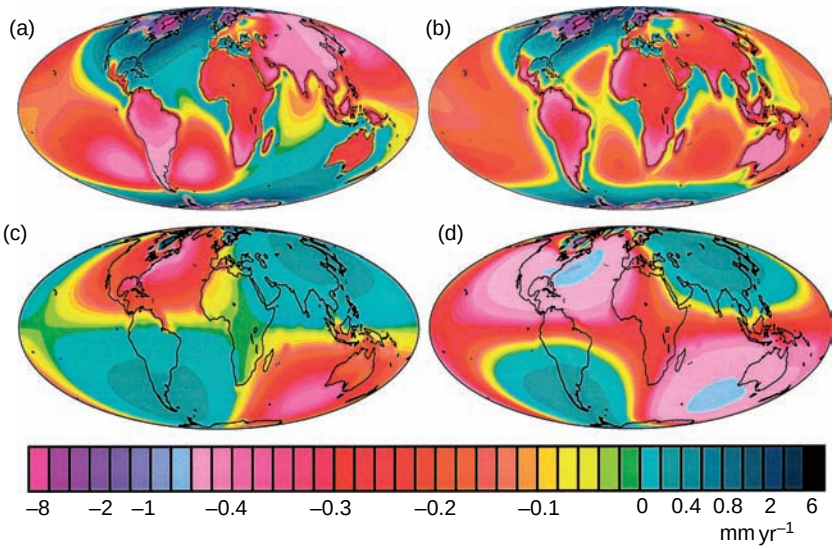

Figure 14 The ICE-4G (VM2) model prediction of (a) the present-day rate of sea-level rise relative to the deforming surface of the solid Earth, including the influence of rotational feedback; (b) same as (a) but excluding the influence of rotational feedback; (c) the difference between (a) and (b) illustrating the spherical harmonic degree 2 and order 1 pattern that dominates the influence due to rotational feedback on account of the control exerted by the polar wander effect; (d) the present-day geoid height time dependence predicted by the ICE-4G (VM2) model, obtained by adding to the field in (a) the prediction of the time rate of change of radial displacement of the surface of the solid Earth with respect to the center of mass of the planet.

Figure 15) that is now in space. In order to test the accuracy of predictions of the Earth's rotational response to the GIA process produced by the theory discussed in Section 9.10.4, an appropriate strategy is therefore to focus upon the observational constraints provided by geological recordings of postglacial RSL change through the Holocene interval of time in those regions in which the impact of rotational feedback is expected to be most intense.

9.10.5.1 A Database of Holocene RSL Histories

A location map of the positions on Earth's surface from which ^{14}C-dated RSL histories are available in the University of Toronto database is shown in **Figure 16** (from Peltier, 1998). Comparing the coverage provided by these many hundreds of individual RSL curves with the geographically intricate pattern evident in **Figure 14**, it will be clear that there exists, not surprisingly, much better coverage of this signature of the GIA process in the Northern Hemisphere than is available from the Southern Hemisphere. Yet, as will be made clear in what follows, the role of the available southern hemisphere data in confirming the important role that variations in Earth rotation play in forming the detailed signature of the GIA effect evident in Holocene RSL records is extremely important. **Figure 17**, from Peltier and Fairbanks (2006), intercompares a number of ^{14}C-dated RSL records from this database with the predictions of the ICE-5G (VM2) model that served as basis for the computation of the time series of the variations in the elements of the moment of inertia tensor that are required in the computation of the rotational response to the glaciation–deglaciation cycle. The locations of the individual sites are shown on the map of the prediction of the present-day rate of sea-level rise predicted by the ICE-5G (VM2) model of the GIA process.

9.10.5.2 The Influence of Rotational Feedback upon Postglacial RSL History and Its Impact upon Predictions of Earth Rotation Anomalies

Although the purpose of the present subsection is to explore the extent to which the most recent models of the GIA process may be employed to further reinforce the interpretation of the millenial timescale

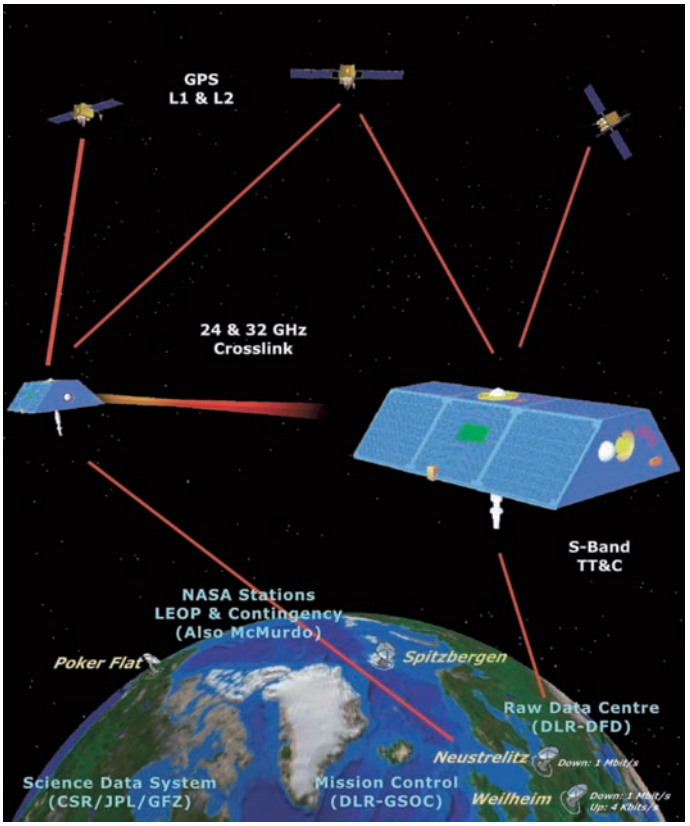

Figure 15 Schematic of the dual-satellite Gravity Recovery and Climate Experiment (GRACE) experiment designed to measure the time dependence of the gravitational field of the planet.

variations in Earth rotation anomalies in terms of the GIA process, it will be useful to begin by revisiting the results previously obtained by Peltier and Jiang (1996) who employed the ICE-4G deglaciation model of Peltier (1994, 1996) to investigate the extent to which both of the previously discussed anomalies were explicable in these terms. Their results are summarized in **Figure 18**, which shows the theoretical predictions of $\dot{\mathcal{J}}_2$ and polar wander speed as a function of the viscosity of the lower mantle of the Earth below a depth of 660 km, with the value of the viscosity of the upper mantle fixed to the nominally accurate value of 10^{21} Pa s, and the thickness of the surface lithosphere taken to be $L = 120$ km. Inspection of **Figure 18** demonstrates that both of the millennial timescale secular anomalies are fit by the same simple model of the radial variation of mantle viscosity. With the upper-mantle viscosity fixed to the above value, the lower-mantle viscosity required to fit the observations is approximately 2×10^{21} Pa s. It might be seen as unlikely, given that the two rotational anomalies depend upon entirely independent elements of the moment of inertia tensor, that this degree of agreement would exist if GIA were not the primary explanation for both observations.

Since publication of these results, further refinements of the required analyses have been performed. In particular, in Peltier (1996), the VM2 model of the radial viscosity structure was inferred on the basis of a full Bayesian inversion of the available data (see **Figure 19**). Equally important has been the considerable further refinement of the loading history that is represented by the ICE-5G model of Peltier (2004) and previously introduced in Section 9.10.3. **Table 1** lists the predictions of present-day polar wander speed and direction for the ICE-4G (VM2) and ICE-5G (VM2) models, assuming the validity of the VM2 model of the radial viscosity structure and a lithospheric thickness of $L = 90$ km, using versions of the theory that both include and exclude the influence of rotational feedback in the solution of the SLE that constitutes the first step in the analysis procedure. The most accurate predictions are of course those that

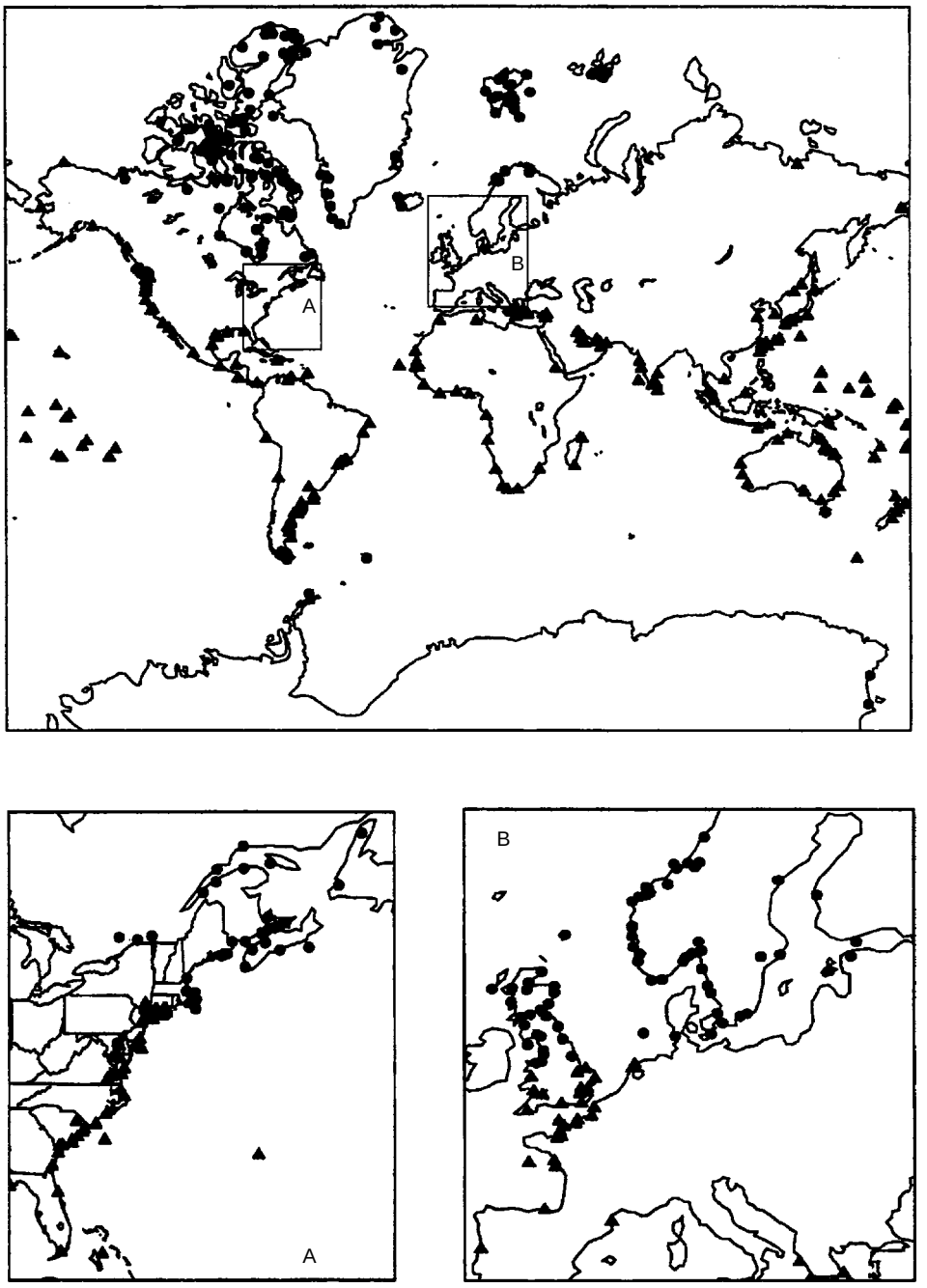

Figure 16 Global location map of the sites from which ^{14}C-dated time series of RSL history are available in the University of Toronto database.

include this critical feedback effect. Inspection of the results in **Table 1**, in which the observed values of the computed quantities are also listed according to the original analyses of the ILS data, will reveal a number of interesting properties of the TPW solutions (since the polar wander component of the rotational response is the most complicated to calculate, the initial focus here will be upon this element). First, concerning the predicted speeds of TPW, these results demonstrate that in the case of no rotational feedback the predictions of ICE-4G (VM2) and ICE-5G (VM2) are respectively on the lower and upper bounds of the observed speed of $\sim$0.8–1.1° My^{-1} according to the analysis of Dickman (1977). When the influence of rotational feedback is included, however, the prediction of the ICE-4G (VM2) model is

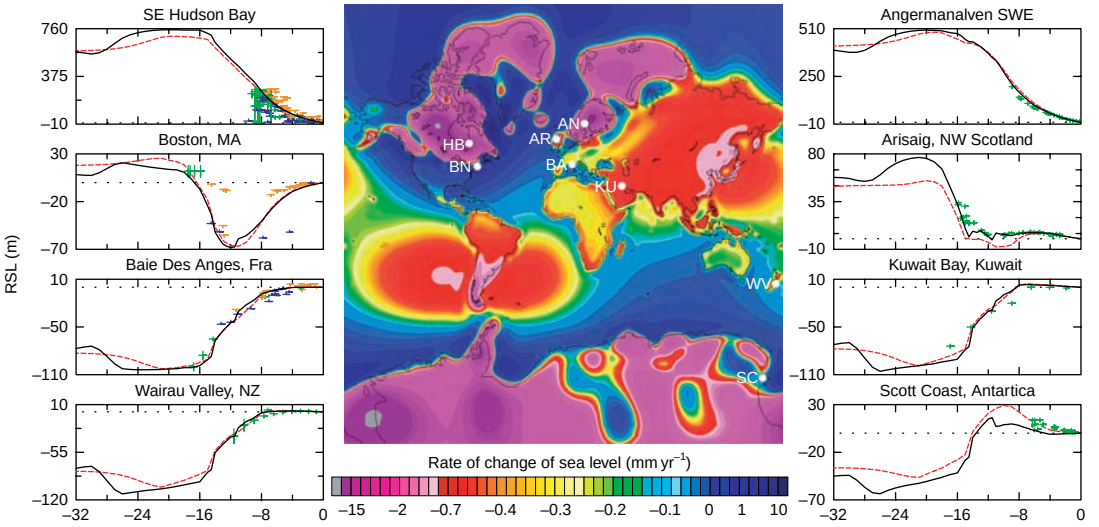

Figure 17 Illustrative suite of predictions of the history of RSL change at eight sample locations using the ICE-5G (VM2) model of the GIA process. The locations of the individual sites are superimposed upon a Mercator projection of the predicted present-day rate of RSL rise. Predictions are shown for two slightly different versions of the model that differ from one another only in terms of the assumption made concerning the timing of LGM. For one version of the model, LGM is assumed to have occurred at the conventional age of 21 ka; for the other, it is assumed, as illustrated in **Figure 7**, that LGM occurred considerably earlier at 26 ka.

reduced to 0.57° My^{-1}, too slow to fit the observed speed. The action of the same feedback also reduces the predicted speed for the ICE-5G (VM2) model to a value of 0.72° My^{-1} that is also slightly too slow to be acceptable.

Insofar as the predictions of polar wander direction are concerned, the predictions of the two models in the absence of rotational feedback are directed somewhat eastward of the observed direction of ~75.5° west longitude, at 69.9° west longitude, in the case of the ICE-4G (VM2) model, and somewhat westward of the observed direction, at 83.1° west longitude, in the case of the ICE-5G (VM2) model. When the influence of rotational feedback is included, the polar wander direction predicted by both models is shifted further westward. For ICE-4G (VM2) the shift is from 69.9° west longitude to 73.4° west longitude, whereas for ICE-5G (VM2) the shift is from 83.1° west longitude to 88.8° west longitude. That the predicted direction of present-day polar wander for the ICE-5G (VM2) model lies significantly to the west of the prediction for the ICE-4G (VM2) model is entirely expected on the basis of the fact previously mentioned and documented in Peltier (2004), that the primary difference between ICE-4G and ICE-5G is that the distribution of continental ice mass has been significantly shifted from the glaciated sites east of the North American continent to the North American continent itself.

In order to demonstrate the sensitivity of these predictions to certain special characteristics of the assumed loading history, results are shown in **Table 2** equivalent to those shown in **Table 1** for models designed to explore the sensitivity associated with two such characteristics. The first of these has to do with an assumption made in constructing the most widely distributed version 1.2 of the ICE-5G model, that the ice cover on Greenland continued to expand in the years following the mid-Holocene climate optimum. Although the initial Neoglacial expansion is required to understand the records of RSL history from southwest Greenland (see Tarasov and Peltier, 2002), version 1.2 of ICE-5G assumed that this Neoglacial expansion continued up to the present which is not required by the observations and is incompatible with modern measurements of the mass balance of this ice sheet (e.g., see Krabil *et al.* (2000)). If we remove the continuing addition of mass from this region that was assumed to be occurring from 2 ka onward, then the new results we obtain for polar wander speed and direction presented in **Table 2** are obtained. In the absence of rotational feedback, the speed now increases from 1.06° My^{-1} to 1.17° My^{-1}. With rotational feedback, the speed prediction changes from 0.72° My^{-1}, too slow to fit the observations, to 0.84° My^{-1}, which is now compatible with the observations. This demonstrates an extremely important characteristic of the planet's

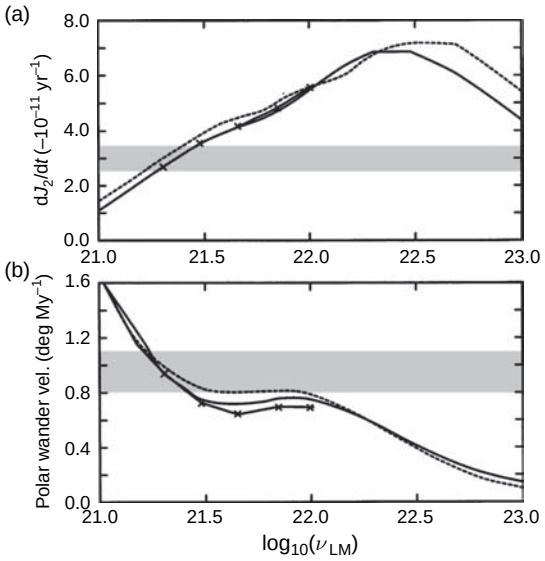

Figure 18 (a) $\dot{J}_2$ as a function of lower mantle viscosity with the upper-mantle viscosity held fixed to the value of 10^{21} Pa s. (b) Same as (a) but for polar wander speed. In each frame, the shaded region represents the observationally constrained range according to the analysis of Dickman (1977). Note that the millennium timescale secular anomalies in Earth rotation are 'explained' as a consequence of the GIA process by the same model of the radial variation of mantle viscosity. From Peltier WR and Jiang X (1996) Glacial isostatic adjustment and Earth rotation: Refined constraints on the viscosity of the deepest mantle. *Journal of Geophysical Research* 101: 3269–3290 (correction, *Journal of Geophysical Research* 102: 10101–10103, 1997).

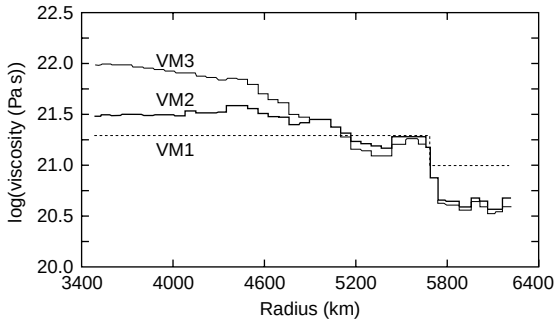

Figure 19 Viscosity models VM1, VM2, and VM3 originally inferred in Peltier (1994, 1996) on the basis of full Bayesian inversions of a subset of the observational constraints pertaining to the GIA process. Model VM1 was the starting model employed to initiate the Bayesian inversion that employed the methodology of Tarantola and Valette (1982a, 1982b). Control on the viscosity in the deepest mantle was provided solely by the rotational constraint provided by the observation of the parameter $\dot{J}_2$ as inferred by Cheng *et al.* (1989) in the analysis that delivered VM2 from the inversion. Model VM3 was obtained in an inversion that adjusted the observed value of $\dot{J}_2$ so as to allow for the influence of possible contamination due to the influence of modern climate change induced forcing due to melting from either the Greenland or Antarctic ice sheets. This inversion was based upon the assumption that one or the other of these was contributing to the current rate of global sea-level rise at the rate of 1–1.5 mm yr^{-1}.

response to surface loading and thus to the understanding of the history of the evolution of its rotational state, namely its extreme sensitivity. Insofar as the predicted polar wander direction is concerned, the pronounced westward shift of direction characteristic of ICE-5G v1.2 is now significantly subdued. In the no rotational feedback case, the direction shifts from 83.1° west longitude to 78.7° west longitude. With feedback, the shift is even more pronounced from 88.8° west longitude to 80.4° west longitude, results that are in much better accord with the observations, especially when the looser bounds allow by the analysis of Argus and Gross (2004) are taken into account.

The further results presented in **Table 2** explore the sensitivity to present-day melting of the Greenland ice sheet under the assumption that this system, after having ceased to expand by 2 ka, begins

Table 2 Predictions of the polar wander speed and direction for the ICE-5G models of the Late Pleistocene glacial cycle when the Neoglacial readvance of the Greenland Ice Sheet is assumed to cease at 2 ka and for a further variant in which, although the Neoglacial readvance ends at 2 ka, the ice sheet begins to lose mass at the rate of 0.1 mm yr^{-1} eustatic equivalent beginning 100 years before present

	Observation	ICE-5G (N) Neoglacial ends at 2 ka	ICE-5G (R) Neoglacial ends at 2 ka	ICE-5G (N) Modern mass loss at 0.1 mm year^{-1}	ICE-5G (R) Modern mass loss at 0.1 mm year^{-1}
Polar wander speed (deg My^{-1})	0.8–1.1	1.17	0.84	1.26	0.94
Polar wander direction (degrees west longitude)	75.5	78.7	80.4	75.1	74.2

to lose mass beginning 100 years ago at a rate equivalent to a rate of rise of ice equivalent eustatic sea level of 0.1 mm yr^{-1}. Since the modern rate of global warming-induced sea-level rise is now well understood on the basis of the analysis of tide gauge records covering the last 70 or so years of Earth history to be on the order of 1.85 mm yr^{-1} (e.g., see Peltier (2001)), the assumption of an 0.1 mm yr^{-1} equivalent rate of mass loss from Greenland must be considered modest. Inspection of the results listed in the last two columns of **Table 2** will show that the addition of this forcing to the system, in the case of no rotational feedback, further increases the predicted speed of TPW from 1.17° My^{-1} to 1.26° My^{-1}, both of which are too fast to fit the ILS observations. When rotational feedback is included, however, the speed once more increases, but now from 0.84° My^{-1} to 0.94° My^{-1}, both of which are fully compatible with the ILS-based observations. Insofar as the polar wander direction predictions are concerned, this swings from somewhat west of the observed direction (78.7° west longitude) to very close to the observed direction (75.1° west longitude). These results further reinforce the previous message concerning the extreme sensitivity of the rotational observables to surface mass loading and unloading associated with continental ice mass variations. Because of this sensitivity, these observables may provide an important means of inferring the locations and rates of present-day land ice melting, especially if one may assume that the influence of GIA due to the Late Pleistocene ice-age cycle may be modeled with sufficient accuracy.

Predictions of the nontidal acceleration of planetary rotation for the same sequence of models are listed in **Table 3**. The versions of the calculation for which results are listed are the same four versions as were employed to produce the list of results for polar wander in **Table 2**. In this case, however, two distinct methods were employed to calculate the results for $\dot{\mathcal{J}}_2$ listed in the table. The first of these methods is the same as that employed in Peltier and Jiang (1996; see their equation 37). An alternative method is that based upon exploitation of the connection between $\mathcal{J}_2$ and the planet's gravitational field. The GIA-induced time dependence of geoid height that is currently being measured by the GRACE satellite system may be computed based upon recognition of the fact (see Peltier, 1999) that this signal, denoted say by $\dot{G}(\theta, \lambda, t)$, is identically equal to the sum $\dot{R}(\theta, \lambda, t) + R\dot{S}L(\theta, \lambda, t)$ in which the first term is the time rate of change of the local radius of the solid Earth and the second term is the time rate of change of RSL. Since the instantaneous level of the sea is determined by the gravitational equipotential that is best fit to it and since the geoid is, by definition, this equipotential surface, the validity of this expression is clear. Now since the geoid height time dependence may also be expanded in spherical harmonics, it may be expressed as

$$\dot{G}(\theta, \lambda, t) = \sum_{l=0}^{\infty} \sum_{m=0}^{l} \dot{G}_{lm}(t)\, Y_{lm}(\theta, \lambda) \qquad [36]$$

Table 3 $\dot{J}_2$ (equivalent to the nontidal acceleration of rotation) predictions for the ICE-5G (VM2) model for which the Neoglacial readuance of Greenland ice is eliminated subsequent to 2 ka. Also shown are results for a version of the model that includes Greenland melting at a rate of 0.1 mm yr^{-1} beginning 100 years before present. Results are shown for two different methods of performing the calculation

	Observed	ICE-5G (N) Neoglacial readvance of Greenland ceases after 2 ka	ICE-5G (R) Neoglacial readvance of Greeland ceases after 2 ka	ICE-5G (N) Includes the influence of Greenland melting at the rate of 0.1 mm yr^{-1}	ICE-5G (R) Includes the influence of Greenland melting of the eustatic equivalent rate of 0.1 mm yr^{-1}
$\dot{J}_2 \times 10^{11}$, yr^{-1}, using the method of Peltier and Jiang (1996)	-2.7 ± 0.4	-3.22	-3.23	-2.83	-2.84
$\dot{J}_2 \times 10^{11}$, yr^{-1}, using the new method of Section 9.10.3.4	-2.7 ± 0.4	-4.05	-3.97	-3.71	-3.63

However, based upon the definition of the nondimensional quantities $\mathcal{J}_{lm}$, we may also write

$$\dot{G}(\theta, \lambda, t) = -a \sum_{l=2}^{\infty} \sum_{m=0}^{l} (\dot{\mathcal{J}}^1_{lm} \cos m\lambda + \dot{\mathcal{J}}^2_{lm} \sin m\lambda) P_l^m(\cos\theta) \quad [37]$$

Using the conventional normalization for the Legendre polynomials P_l^m, comparison of eqns [36] and [37] then requires the following result for $\dot{\mathcal{J}}_2$:

$$\dot{\mathcal{J}}_2 = \dot{\mathcal{J}}^1_{20} \quad [38]$$

In the second line of $\dot{\mathcal{J}}_2$ data in **Table 3**, the numbers listed are obtained using eqn [38]. In the first line they have been obtained using the Peltier and Jiang formulation. Inspection of the results in **Table 3** will show that the two methods have delivered somewhat different results, differences that are typically on the order of 20–25%, a difference that is similar in magnitude to the errors that have been ascribed to the measurement by the various authors that have performed the analysis. Although the observed estimates listed in **Table 3** are those of Cheng *et al.* (1989), those obtained by several other authors are somewhat higher as follows:

$$\dot{\mathcal{J}}_2 = (-3.5 \pm 0.3) \times 10^{-11}\,\mathrm{yr}^{-1}, \quad \text{Yoder } et\ al.\ (1983)$$

$$\dot{\mathcal{J}}_2 = (-3.5 \pm 0.8) \times 10^{-11}\mathrm{yr}^{-1}, \quad \text{Stephenson and Morrison (1995)}$$

Of the two methods employed to produce the $\dot{\mathcal{J}}_2$ estimates in **Table 3**, the most accurate should be that based upon the expansion of the gravitational field. Intercomparing the results in **Table 3**, one would therefore be led to conclude that the magnitude of the predictions for the ICE-5G (VM2) model, even in the best case in which the 0.1 mm yr^{-1} eustatic rise due to Greenland Ice Sheet melting is active, is too high if one accepts the estimate of Cheng *et al.* as the most accurate and even if one were to replace it by the number preferred in the more recent paper by Dickey *et al.* (2002). If one were to prefer the estimates of Yoder *et al.* or Stephenson and Morrison, however, the prediction for this model would be well within the observed bounds. Accepting the result of Cheng *et al.* as most accurate, the misfit may however be eliminated simply by slightly increasing the rate at which Greenland ice is assumed to be melting at present to, say, 0.3 mm yr^{-1}. By inspection of the results in **Table 2**, this would be expected to increase the rate of polar wander by an additional $\sim 0.2^\circ\,\mathrm{My}^{-1}$, leading to a polar wander prediction that remains within the error bounds on this observable.

It is important to understand, however, that Greenland is not the only contributor to the modern rate of rise of sea level that is associated with greenhouse gas-induced global warming. As documented most recently by Dyurgerov and Meier (2005), the small ice sheets and glaciers of the planet are also melting at rates such that they are collectively contributing to the ongoing rise of global sea level in the amount of approximately 0.5 mm yr^{-1}. In order to employ the rotational observables to accurately constrain the rate at which the great polar ice sheets are currently losing mass will require that this contribution be carefully taken into account using the methodology employed previously in Peltier (1998, see figure 46). The refined ICE-5G (VM2) model of the Late Pleistocene ice-age cycle will provide an important basis upon which a more accurate application of this methodology will be possible. Because the measurements of the rates of change of the rotational anomalies are essentially instantaneous on the millennial timescale characteristic of the GIA process, it is nevertheless important that the accuracy of our association of both anomalies with GIA be tested over a more extended range of time. As demonstrated in the following subsection, Holocene records of RSL history have enabled such a definitive test to be performed.

9.10.5.3 Measurements of the Strength of the Expected Quadrapolar 'Signature' of the Rotational Feedback Effect upon Postglacial Sea-Level Histories

In order to adequately test the veracity of the theory that has been developed to compute the Earth's rotational response to the glaciation–deglaciation cycle, and thereby to adequately test our understanding of the history of Earth rotation on millennial timescales, the use of the global patterns of postglacial RSL change predicted by the different versions of the calculation might be expected to be especially useful. As previously, these patterns are best illustrated by global predictions of the present-day rate of RSL rise that would be expected to be observed as a secular rate of change on a tide gauge installed in a coastal location if the only contribution to RSL history were the continuing impact of the GIA process. **Figure 20** shows Mollwiede projections of the global map of

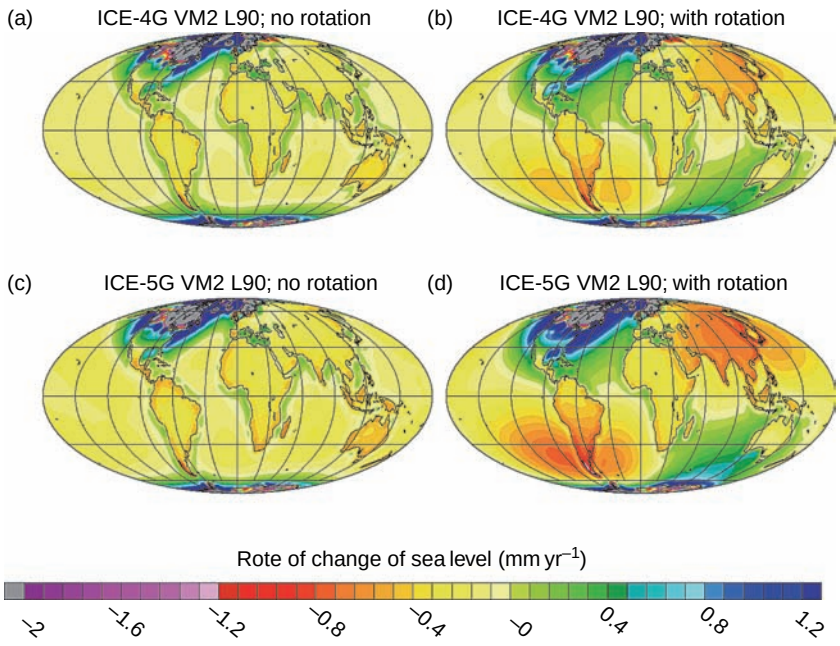

Figure 20 This compares the predictions of the ICE-4G (VM2) and ICE-5G (VM2) models of the present-day rate of RSL rise, both including and excluding the influence of rotational feedback as described by the second term in the integrand of the triple convolution integral in eqn [1]. Noticeable is the fact that the influence of rotational feedback has the form of a spherical harmonic of degree 2 and order 1 which exists as a consequence of the dominant role played in the feedback process by the polar wander component of the rotational response to the GIA process (see eqns [4c] and [4d]). Also evident is the fact that this feedback is stronger in model ICE-5G (VM2) than it is in ICE-4G (VM2).

this prediction for the ICE-4G and ICE-5G models, both including and excluding the impact of rotational feedback. These calculations have been made by solving the SLE using the 'full glacial cycle' methodology for incorporation of the influence of coastline migration discussed in Peltier (2005) and Peltier and Fairbanks (2006). Inspection of these figures further reinforces the fact that the impact of rotational feedback is such as to superimpose upon the pattern predicted by either model, a modification that has the form of a spherical harmonic of degree 2 and order 1, a pattern of 'quadrapolar' form. This characteristic of the RSL response to variations in Earth rotation was first demonstrated by Dahlen (1976) in the context of his analysis of the 'pole-tide' raised in the oceans by the Chandler wobble of the Earth. Initial attempts to incorporate the influence of rotational feedback upon the variations of sea level caused by the GIA process were described by Milne *et al.* (1996) and Peltier (1998), who employed the theory of Peltier (1982) and Wu and Peltier (1984) to estimate the magnitude of the effect, analyses that initially suggested it to be small enough to be neglected. The fact that the influence of rotational feedback has this quadrapolar structure is a consequence of the fact that the dominant impact of rotational feedback is due to the influence of TPW, as will be clear on the basis of inspection of eqns [13]. The ω_3 (nontidal acceleration of rotation related component) of the perturbation to the angular velocity of the planet controls the impact upon sea-level history of the GIA-induced change in the l.o.d. The ω_1 and ω_2 perturbations, on the other hand, control the polar wander contribution and it will be clear on the basis of eqns [13] that this will appear as a forcing of spherical harmonic degree 2 and order 1 form. Noticeable also on the basis of **Figure 20** is the fact that the magnitude of this impact is more intense in the ICE-5G (VM2) model than it is in the ICE-4G (VM2) model, a consequence of the fact, evident from **Table 1**, that the polar wander speed predicted for this model is higher than for ICE-4G (VM2), even though the two models have very similar LGM surface mass loads of glacial ice (although there is a 10% difference in LGM mass between the version of ICE-4G being employed here and ICE-5G, the difference in the polar wander speed predicted by the two models is 20%). This difference can be exploited to examine the extent to which the feedback effect is properly incorporated in the theory

based upon the 'equivalent Earth model' approach of Munk and MacDonald (1960). Since it is in the regions centered within the four 'bull's-eyes' of the spherical harmonic degree 2 and order 1 quadrapole pattern that the influence of rotational feedback will be most apparent, it is in these regions that we should expect to find its consequences most clearly revealed.

The most important region in which such intercomparison is possible concerns the extremum in rotational feedback that is located on the southern tip of the South American continent (see **Figure 14**). Although the west coast of this continent is strongly impacted by the deformation associated with the subduction of the Nazca plate, the east coastal margin is passive and therefore should provide an excellent region in which to attempt to measure, using postglacial histories of RSL change, the impact of rotational feedback. **Figure 21** shows a map of the South American continent, from Peltier (2005), on which, primarily along the east coast passive continental margin, are shown the locations at which, based upon the compilation of RSL histories in Rostami *et al.* (2000), radiocarbon-dated RSL history information is available. When such data are used to compare with the predictions of the theory previously described, they must of course be transformed onto the calendar-year timescale using the modern calibration procedure CALIB described by Stuiver and Reimer (e.g., 1993). The site numbers on the map of **Figure 21** correspond to the last two digits of the site numbers shown in **Figure 22** where the subset of locations for which model-data inter-comparisons are shown are named.

In Rostami *et al.* (2000), attention was drawn to the fact that there existed a systematic misfit of the theory for postglacial sea-level change based upon the ICE-4G (VM2) model without rotational feedback to the observed sea-level histories from this coastal region. The nature of this misfit, documented in figure 11 of Rostami *et al.* (2000), involved the variation with latitude of the so-called mid-Holocene 'highstand' of the sea. The prediction of the amplitude of this highstand using the ICE-4G (VM2) model without feedback was that this amplitude should decrease with increasing south latitude whereas the observation was that it actually increased very significantly, a qualitative difference easily resolved by the observational record. In Peltier (2002c), it was first demonstrated that the incorporation of rotational feedback into the theory would lead to the qualitative change in the nature of the prediction required to reconcile the observations. More

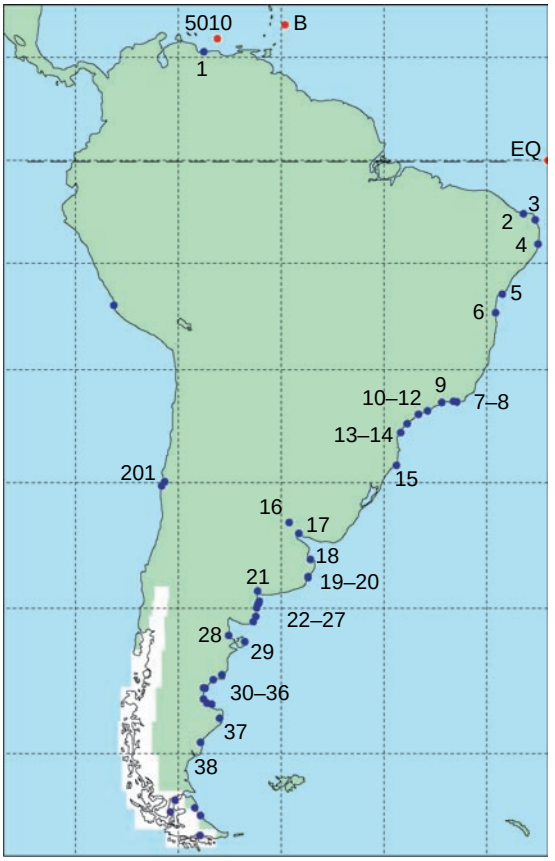

Figure 21 Location map for the South American sites from which radiocarbon-dated RSL histories are available. Also shown is the LGM location of the Patagonian ice-sheet complex.

recently, Peltier (2005) has more fully exploited these observations and the ICE-4G (VM2) model predictions to argue that this data set could be invoked to demonstrate that the impact of rotational feedback upon RSL history predicted by the ICE-4G (VM2) model was approximately correct. In fact, the data–model intercomparisons presented in both Peltier (2002c) and Peltier (2005) were incomplete, as several of the most anomalous of the observations were not discussed. As will be shown through intercomparisons between the predictions of the ICE-4G and ICE-5G models in what follows, these further analyses have sufficed to reconcile all of the remaining misfits to the data from this region.

The importance of including the ICE-4G calculations together with those for the ICE-5G model for present purposes is that the former model is characterized by a polar wander speed prediction that is slower than that predicted by the latter model by approximately 20%. This model may therefore be

seen as a surrogate for models that predict a polar wander speed that is unable to satisfy the observational constraints. Although it may be reasonable to argue that one could invoke some process other than GIA, say mantle convection, to explain some modest fraction of the present-day observed polar wander speed observation, it is extremely unlikely that a credible calculation of this effect could be performed that would deliver the correct time dependence of the speed and direction predictions that are required to understand the dominant contribution to this signal. Yet all of these aspects of the data are fully explicable as consequences of the GIA effect, with the computation modified perhaps to include the influence of a modest deviation from the 'equivalent Earth model' assumption of Munk and MacDonald (see Peltier (2007) for further discussion).

Figure 22 presents model–data intercomparisons for postglacial RSL history at 16 of the numbered sites from the east coast of South America, beginning at the northernmost site from coastal Venezuela and continuing southward through Brazil and Argentinian Pategonia toward Tierra del Fuego. For each site are shown the predictions for three different models from the set of four for which predictions of polar wander speed and direction are listed in **Table 1**.

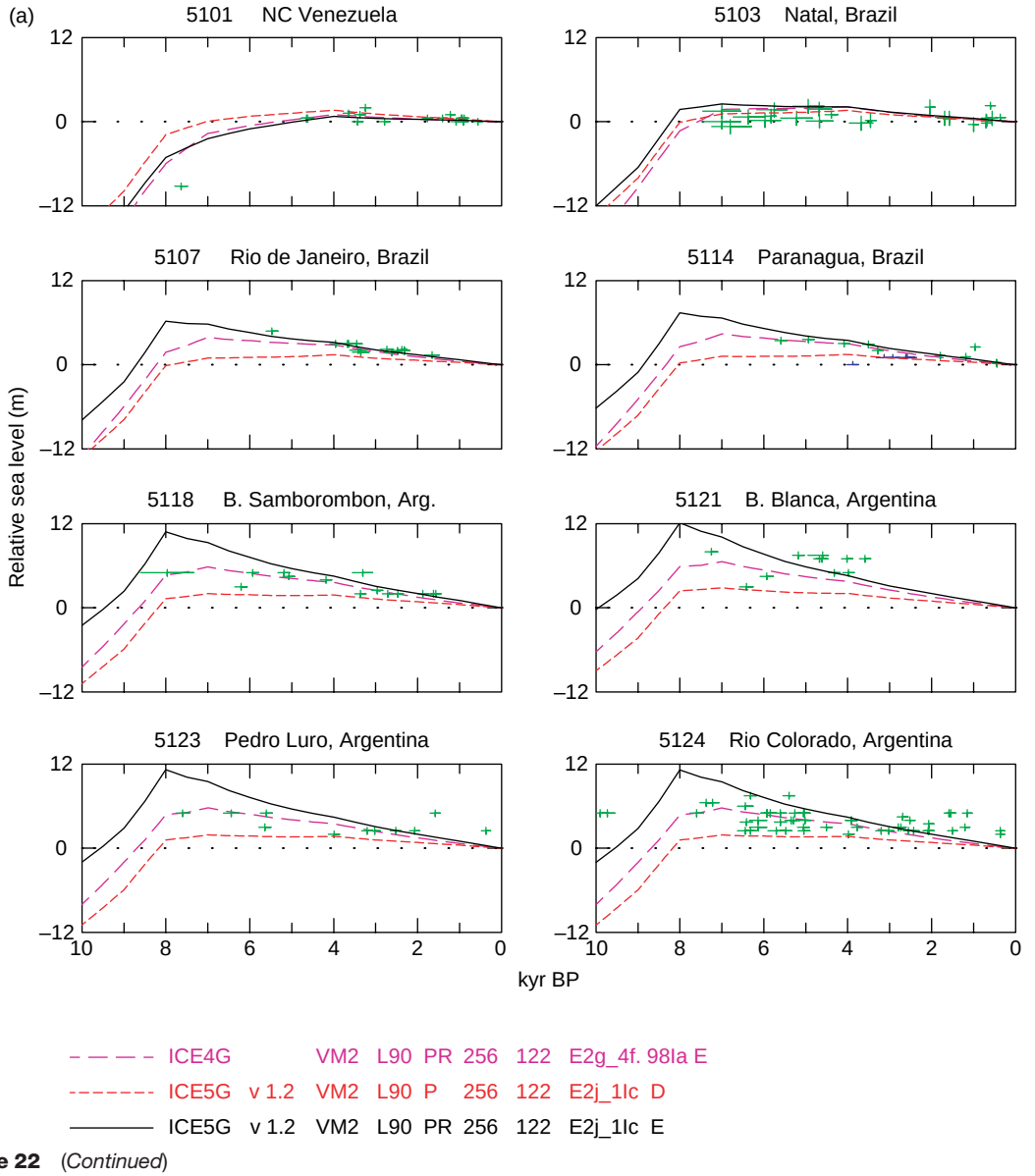

Figure 22 (*Continued*)

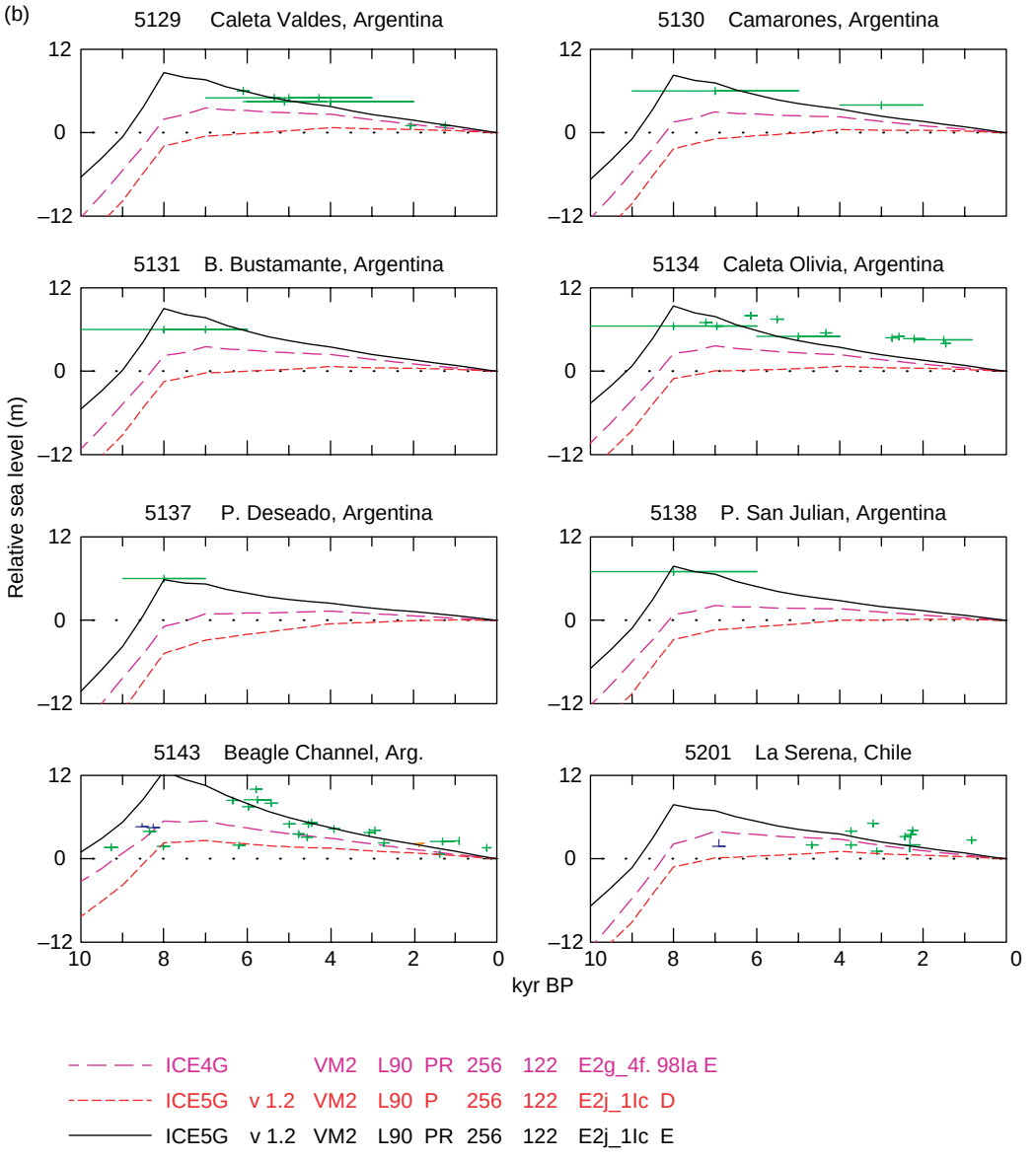

Figure 22 (a) Model–data intercomparisons for eight sites from the northern portion of the east coast of the South American continent. The last two digits of the site numbers correspond to the numbered locations on **Figure 21**. On each plate, the ^{14}C-dated sea-level index points are denoted by green crosses. RSL history predictions based upon eqn [1] are shown for three model variants, respectively: ICE-5G (VM2) with rotational feedback (black), ICE-5G (VM2) without rotational feedback (red), and ICE-4G (VM2) with rotational feedback (mauve). Notable is that based upon the comparisons at these north coastal sites the data are unable to unambiguously discriminate between the two models that include rotational feedback. However, the model that does not include rotational feedback is entirely rejected. (b). Same as (a) but for a set of eight sites from the southern (Patagonian) region of the east coast of the South American continent. At these locations, the results of the intercomparisons are now entirely unequivocal. Only the ICE-5G (VM2) model with rotational feedback satisfies the highstand observations.

These are for the ICE-4G (VM2) model that includes the influence of rotational feedback and for the ICE-5G (VM2) model both including and excluding this influence. It will be important to note that the first site in the list, denoted NC Venezuela (Valastro *et al.*, 1980), is the only site that is north of the equator (see **Figure 21**). This is important because the sign of the impact of rotational feedback changes across this line of 0° latitude, as expected based upon the spherical harmonic degree 2 and order 1 form of the

pattern of this influence. To the north of the equator, as will be clear by inspection of the intercomparisons at NC Venezuela, the impact of rotational feedback is to diminish the predicted elevation with respect to sea level throughout the Holocene interval from 10 ka onward. To the south of the equator, however, as the intercomparisons for the Natal, Brazil, site (Bezerra *et al.*, 2003) show, the opposite is the case, as at this site the impact of rotational feedback is such as to elevate the predicted sea levels for the Holocene epoch above that for which this influence is neglected entirely or for which the effect of rotational feedback is diminished as is the case for the ICE-4G prediction relative to that for the ICE-5G model. Based upon the results in **Table 1**, it will be clear that this influence is expected to be weaker in ICE-4G (VM2) than it is in ICE-5G (VM2) simply because the predicted polar wander speed for the former model is less than that for the latter model. As will be evident by inspection of the complete set of intercomparisons shown on **Figure 22**, this hierarchy is preserved at all locations. **Table 4** lists the references for the data from all of the sites for which data–model intercomparisons are shown in this section.

Very clearly evident also, based upon the results shown in **Figure 22**, is the fact that exceptionally high-'stands' of the sea above present sea level are predicted and observed to obtain at sites along this coast during mid-Holocene time between 6000 and 8000 years BP. Although there is considerable scatter in the data at the sites from NC Venezuela to Rio Colorado, Argentina, it is nevertheless clear that the influence of rotational feedback is required in order for the model to adequately reconcile the data. As discussed in detail in Rostami *et al.* (2000),

Table 4 References for the data from the sites for which data–model intercomparisons are provided in this chapter

Site number	Site name	References
5101	NC Venezuela	Valastro *et al.*, 1980
5103	Natal, Brazil	Bezerra *et al.*, 2003
5107	Rio de Janeiro, Brazil	Martin *et al.*, 1987; Fairbridge, 1976; Delibrias *et al.*, 1974; Angulo and Lessa, 1997
5114	Paranagua, Brazil	Angulo and Lessa, 1997
5118	B. Samborombon, Argentina	Codignotto *et al.*, 1992
5121	B. Blanca, Argentina	Codignotto *et al.*, 1992
5123	Pedro Luro, Argentina	Albero and Angiolini, 1983, 1985
5124	Rio Colorado, Argentina	Codignotto *et al.*, 1992
5129	Caleta Valdes, Argentina	Rostami *et al.*, 2000; Codignotto *et al.*, 1992; Albero and Angiolini, 1983
5130	Camarones, Argentina	Rostami *et al.*, 2000
5131	B. Bustamante, Argentina	Rostami *et al.*, 2000
5134	Caleta Olivia, Argentina	Rostami *et al.*, 2000
5137	P. Deseado, Argentina	Rostami *et al.*, 2000
5138	P. San Julian, Argentina	Rostami *et al.*, 2000
5143	Beagle Channel, Argentina	Porter *et al.*, 1984; Morner, 1991
11105	Pt. Adelaide/Gillman, Australia	Belperio *et al.*, 2002
11107	Pt. Wakefield, Australia	Belperio *et al*, 2002
11109	Pt. Pirie (Spencer Gulf), Australia	Belperio *et al.*, 2002
11110	Redcliffe, Australia	Belperio *et al.*, 2002
11111	Franklin HB, Australia	Belperio *et al.*, 2002
11113	Ceduna, Australia	Belperio *et al.*, 2002
11115	Weiti River, New Zealand	Gibb, 1986, Schofield, 1975
111123	Blue Skin Bay, New Zealand	Gibb, 1986
9003	Nouakchatt, Mauritania	Faure and Hebrard, 1977
9006	St. Louis, Senegal	Faure *et al.*, 1980
9022	Reunion	Camoin *et al.*, 1977, 2004
9023	Mauritius	Camoin *et al.*, 1997
11004	Shikoku Island, Japan	Pirazzoli, 1978
11006	Kikai-Jima Island, Japan	Pirazzoli, 1978; Sugihara *et al.* 2003
11008	S. Okinawa Island, Japan	Koba *et al.* 1982
11010	Uotsuri Island, Japan	Koba *et al.*, 1982

most of the data from this set of locations are from the older literature and therefore a legitimate question exists concerning its quality. However, this is not the case concerning the data from the set of locations between Caleta Valdes, Argentina, and P. San Julian, Argentina, all from Argentinian Patagonia, for which the data–model intercomparisons are shown in **Figure 22**. At these locations, the data have been carefully screened for quality (see discussion in Rostami *et al.* (2000)), and it is clear on the basis of them that only the ICE-5G (VM2) model is able to reconcile the 6–8 m mid-Holocene highstands of the sea that are observed to exist in the time window between 6000 and 8000 years BP. The ICE-5G (VM2) model, in the absence of rotational feedback, inevitably predicts that no such highstand should exist or that its amplitude should be very small. The ICE-4G (VM2) model predicts a highstand amplitude that is insufficient to explain the observations. These analyses very strongly reinforce the conclusion in Peltier (2002c, 2005) that this influence is a crucial determinant of the ability of the model to fit the observations. However, they also allow a considerably stronger conclusion to be reached. In particular, they force us to conclude that only if the time dependence of the predicted speed of TPW due to the influence of GIA is compatible with the presently observed speed and with the temporal evolution of the amplitude of the mid-Holocene highstand of the sea, is the record of postglacial RSL history understandable. Even a 20% reduction from the observed speed, as embodied in the version of the ICE-4G (VM2) model being employed here, leads to a significant misfit to the observations.

It is nevertheless the case that there is scatter in the data and one might reasonably hope that there might exist data from other locations where the influence of rotational feedback is also expected to be strong that might be invoked to confirm (or to deny) the robustness of this conclusion. To this end, **Figure 23** shows a location map for 16 additional sites from other regions, for some of which this influence is expected to be especially strong. Eight of these sites, for which intercomparisons are shown in **Figure 24**, are within the influence of the second Southern Hemisphere 'bull's-eye' of the spherical harmonic degree 2 and order 1 pattern that is produced by the influence of rotational feedback. The map in **Figure 23(c)** (in Mercator projection), on which these positions are located, is that of the difference between the present-day rate of sea-level rise

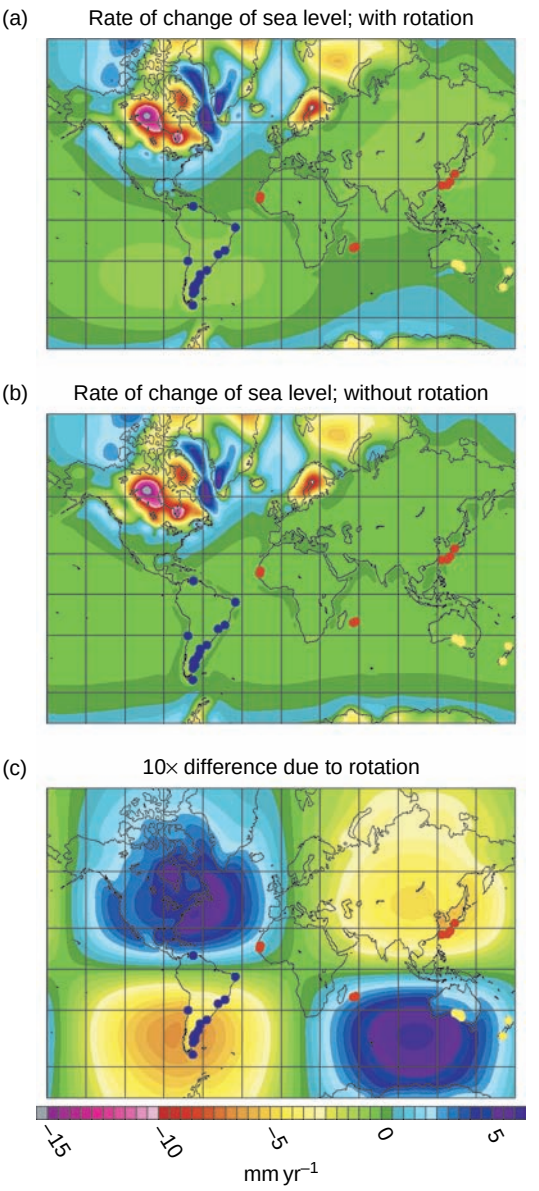

Figure 23 Mercator projections of the model predicted present-day rate of RSL rise for the ICE-5G (VM2) model both (a) including and (b) excluding the influence of rotational feedback. In (c), the difference between (a) and (b) is presented, demonstrating that the influence of the rotational feedback effect is dominantly of the form of a spherical harmonic of degree 2 and order 1. Superimposed upon each of the three plates of this figure are the locations of sites at which high-quality ^{14}C-dated RSL histories are available beyond those from the South American continent already discussed. The sites shown as yellow dots are located in a region (Australia–New Zealand) where the influence of rotational feedback is expected to have the opposite sign as the South American locations. At the sites shown as red dots the effect is either expected to the same as an Australia–New Zealand (in the Indian Ocean or West Africa) or the same as in South America (Japanese islands).

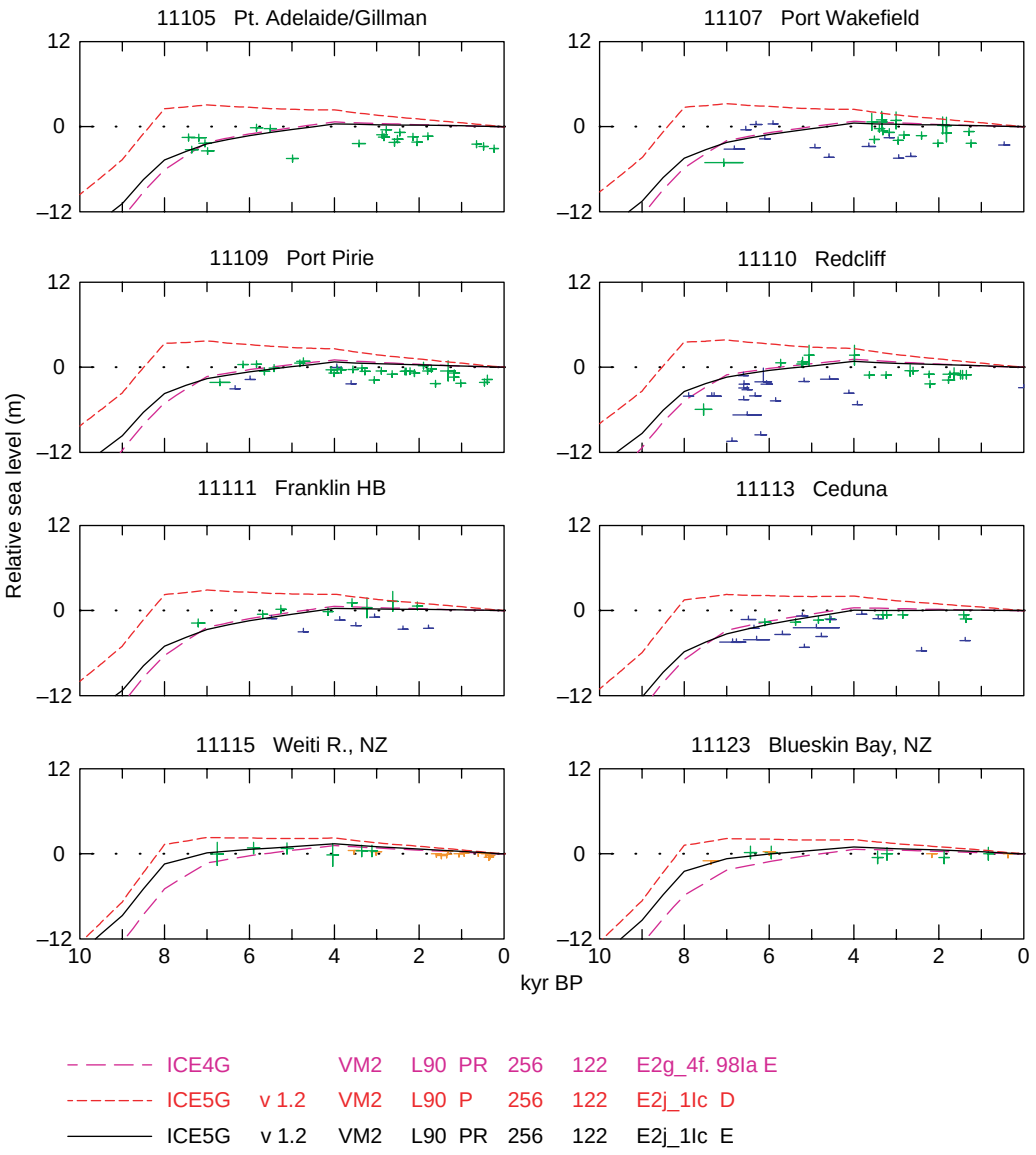

Figure 24 Same as **Figure 22**(**a**) but showing model–data intercomparisons for the Australia–New Zealand region. Inspection of these intercomparisons demonstrates that, as expected, the nature of the influence of rotational feedback is opposite to that observed at the South American locations. At these locations, the data are once more unable to discriminate between the two models that include the influence of rotational feedback, presumably because these sites are insufficiently close to the degree 2 and order 1 'bull's-eye', just as was the case for the sites along the northern part of the east coast of South America. Once more, however, the model without rotational feedback is totally rejected.

prediction for the ICE-5G (VM2) model with rotation (shown in **Figure 23**(**a**)) and that obtained when this influence is not included (shown in **Figure 23**(**b**)). Eight additional intercomparisons are shown in **Figure 25**, four of which are from locations in the Indian Ocean or the west coast of Africa, and four of which are from the third 'bull's-eye' located over the Japanese islands (see **Figure 23**(**c**)).

Inspecting first the intercomparisons shown in **Figure 24** for sites in the Australia–New Zealand region will show that at all of these sites there exists a striking anomaly between the prediction of the version of the ICE-5G (VM2) model without rotational feedback and the predictions for either of the models in which this influence is included. In the absence of rotational feedback, the theory predicts that a mid-Holocene highstand of the sea should exist

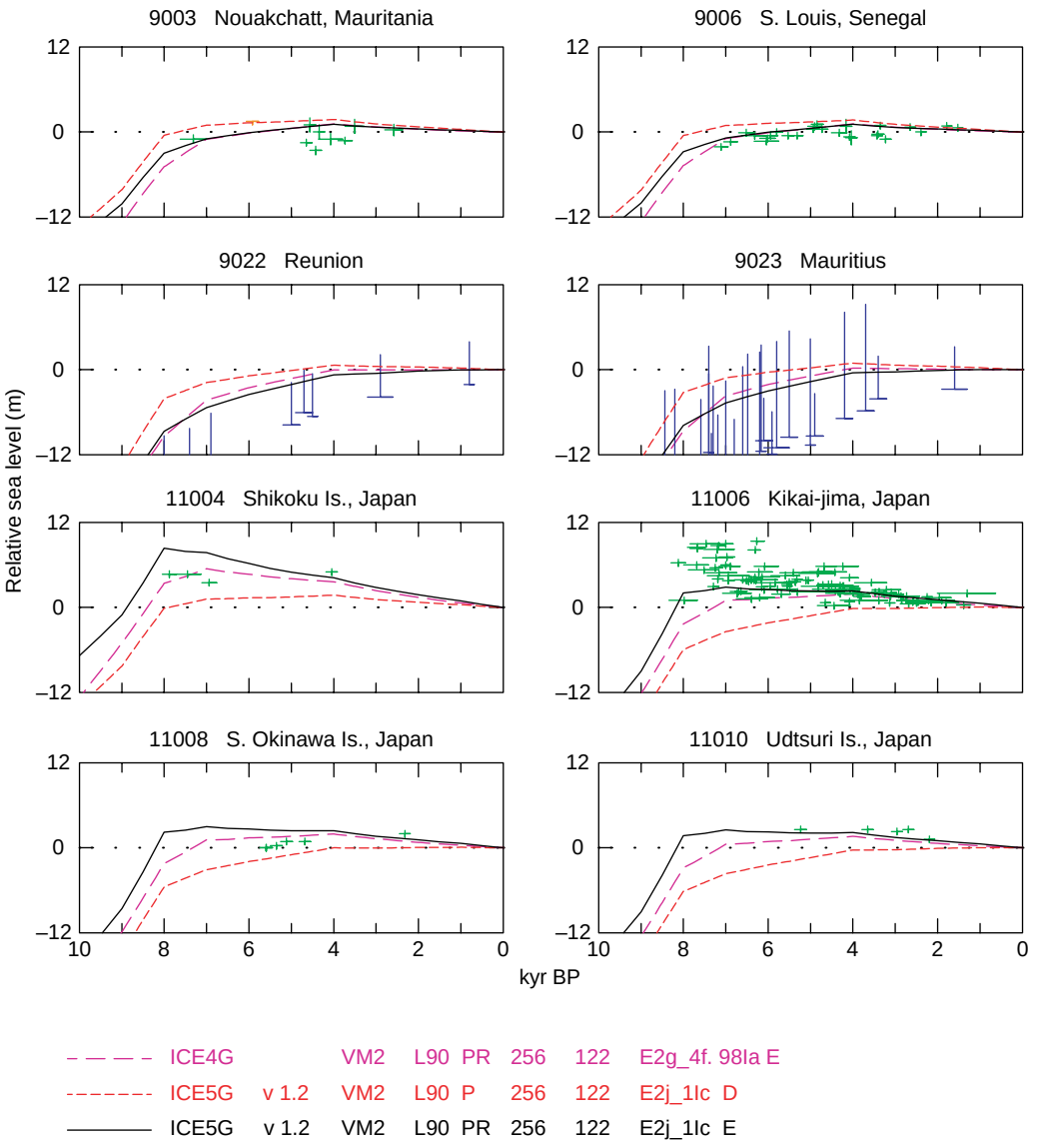

Figure 25 Same as for **Figure 22**(**a**) but showing model–data intercomparisons for both 'down sites' (Indian Ocean, West Africa) and 'up sites' (Japanese islands). For all sites, the sign of the rotational feedback effect is as expected, and all data reject the model from which the influence of rotational feedback has been eliminated.

with an approximately 3 m amplitude. However, the data at all eight locations show that no such feature is evident. At most of the locations for which results are shown in **Figure 24**, either of the two models with rotational feedback included suffice to fit the observed RSL record although at Blueskin Bay, NZ, the ICE-5G (VM2) model with feedback is again found to be superior to ICE-4G (VM2) with feedback. This set of intercomparisons is especially important because in this region the sign of the feedback effect is predicted to be opposite to that operating over the South American continent. Nevertheless, the necessity of the operation of a strong influence of rotational feedback in order to fit the observational constraints remains clear. It is perhaps especially interesting to note that the data from the coast of the Great Australian Bight of South Australia could be misconstrued to suggest that eustatic sea level must have continued to rise through Late Holocene time (e.g., see Lambeck, 2002), perhaps due to continuing melting of the Antarctica or Greenland ice sheets. The analysis presented here

demonstrates that such an interpretation would be incorrect. The absence of a mid-Holcene highstand of sea level in this region is due to the influence of rotational feedback onto postglacial sea-level history, not the continuing melting of land ice. In the ICE-4G and ICE-5G models, all melting of continental ice is assumed to have effectively ceased by 4000 years BP (e.g., see Peltier (2002), Peltier *et al.* (2002), and **Figure 7**).

The further model–data intercomparisons shown in **Figure 25** include information from sites in which the sign of the influence of rotational feedback is the same as that which operates in the Australia–New Zealand region, and sites in which the influence is qualitatively similar to that evident at locations along the southeast coast of the South American continent. Sites of the former type include those along the west coast of Africa (Nouakchatt, Mauritania, and St. Louis, Senegal) and the others from the Indian Ocean (Reunion, Mauritius). Sites of the latter type from the islands of Japan include Shikoku Island, Kikai-jima Island, S. Okimaura Island, and Uotsuri Island. At the former locations, theory once more predicts that in the absence of rotational feedback a mid-Holocene highstand of the sea should be observable. At these locations, however, no such highstand is evident. The addition of rotational feedback, either of the strength embodied in ICE-4G (VM2) or ICE-5G (VM2), allows the model to fully reconcile the data.

Turning next to the final set of four data–model intercomparisons shown in **Figure 25**, it will be clear that at each of the Japanese islands for which RSL intercomparisons are shown, the model without rotational feedback predicts that no mid-Holocene highstand of the sea should be evident at any of these locations. Yet the data in each case clearly reveal the presence of such a feature. As will be clear by inspection of this set of intercomparisons, the incorporation of the influence of rotational feedback suffices to reconcile the misfits of the theoretical predictions to the data that would otherwise exist. Once more, the data at these locations are only marginally able to distinguish between the strength of the feedback effect embodied in the ICE-4G (VM2) and ICE-5G (VM2) models. Only at Uotsuri Island and Kikai Island does there appear to exist a marginal preference for the latter model.

On the basis of the totality of these intercomparisons we may therefore conclude that there exists very strong evidence in the global variations of postglacial RSL history for the action of the influence of rotational feedback. Furthermore, the strength of this feedback appears to be quite accurately predicted by the theory of Peltier (1982) and Wu and Peltier (1984), a theory based upon the application of the 'equivalent Earth model' concept of Munk and McDonald (1960). On the timescale of thousands to hundreds of thousands of years in the most recent geological past, the history of Earth rotation has apparently been strongly dominated by the influence of the GIA process, as both the secular variation in the nontidal variation in the l.o.d and the TPW evident in the ILS path of the pole are accurately predictable by the same model of the GIA process that is employed to predict the histories of postglacial RSL change. In this same range of timescales, however, additional and even more subtle influences are active upon, rather than within, the Earth system that are connected to the history of the Earth's rotation as observed from space. These influences are discussed in the next section.

9.10.6 The Impact of Variations in the Geometry of Earth's Orbit around the Sun upon Earth System Evolution

In the previous sections of this chapter, the focus has been fixed upon the history of Earth rotation as observed in the body-fixed coordinate system, the terrestrial frame, in which the anomalies in the variations in the l.o.d. and polar motion are most usefully described. Equally important aspects of the evolution of Earth's rotation are, however, those that are most usefully described in the celestial frame provided by the field of stars of our own and more distant galaxies. In this celestial frame of reference, the orbit of the Earth in its rotation around the Sun is observed to be characterized by subtle time dependence in its geometry. These variations are due to the action of gravitational n-body effects in the solar system that cause the ellipticity of the otherwise Keplerian elliptical orbit to vary with time and similarly impose subtle time dependence upon orbital obliquity, that is to say upon the angle that the spin axis makes with the plane of the ecliptic (see **Figure 26**). As it happens, this aspect of the history of Earth rotation exerts a profound effect upon low-frequency climate variability and in particular is the ultimate cause of the Late Pleistocene ice-age cycle that was discussed in the last section of this chapter as the source of the excitation of millennial timescale variations in l.o.d. and polar

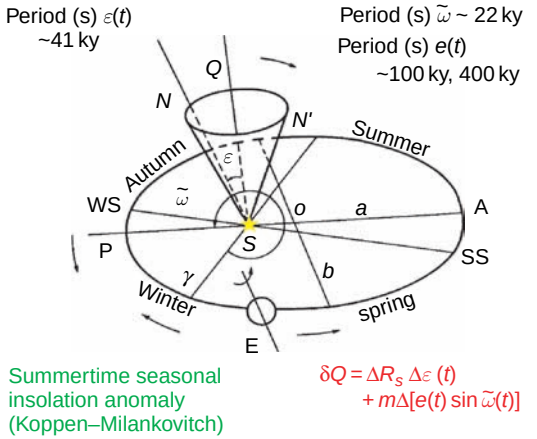

Figure 26 Geometry of Earth's orbit around the Sun depicting the present positions of the apogee and the perigee, as well as the summer and winter solstices and the spring and autumn equinoxes. The tilt of the spin axis with respect to the plane of the ecliptic is represented by the parameter ε, whereas the eccentricity of the orbit is represented by the parameter e. As a consequence of the influence of the precession of the spin axis in space, the position of the equinoxes and solstices rotates around the orbital ellipse with a period of approximately 22 000 years.

motion. This so-called astronomical theory of the ice ages, due originally to Milankovitch (e.g., 1940), was finally verified as essentially correct in the seminal paper by Hays *et al.* (1976) that was based upon the analysis of oxygen-isotopic data from deep-sea sedimentary cores such as the data set from ODP site 677 from the Panama Basin shown in **Figure 5** and which was analyzed in detail in Shackleton *et al.* (1990). The origins of the particular time series shown in this figure are in fact extremely important, both from the perspective of our understanding of the Late Pleistocene ice-age cycle and our appreciation of the crucial role that the history of Earth rotation has played in our understanding of the detailed characteristics of the process of plate tectonics itself.

Prior to the analysis presented in the Shackleton *et al.* paper, it had been widely believed, based upon potassium–argon dating of the age of the most recent Brunhes–Matuyama reversal of the polarity of Earth's magnetic field, that this event had occurred approximately 730 000 years BP. This assumed age was, until the appearance of this paper, universally employed in the construction of the chronology of all of the deep-sea sedimentary cores that were employed as constraints upon the understanding of climate system processes over the Pleistocene epoch. This date was also employed to constrain the speeds with which oceanic plates were assumed to 'spread' away from oceanic ridge crests in response to the underlying mantle convection process. The history of the process that led to our present understanding that the age of this critical control point for planetary chronology was 780 000 years rather than 730 000 years is important from the perspective of our appreciation of the role that Earth rotation history plays in our understanding of the system and so is worth reviewing in some detail.

9.10.6.1 The Astronomical Imprint on Oxygen-Isotopic Records from Deep-Sea Sedimentary Cores

Basic to this understanding is an appreciation of the extent to which modern astrophysical theory has been successful in the reconstruction of the evolving geometry of Earth's orbit around the Sun over the past several million years of Earth history. Early work on this problem was reviewed and significantly extended by Laskar (1988), who employed a mixture of analytical and numerical techniques to demonstrate that it was possible to perform stable integrations of the geometry of the orbit that extended in excess of several million years into the past. These reconstructions were tested by performing brute force initial value integrations, starting from a modern ephemeris, of the system of gravitational n-body equations governing the evolution of the entire solar system, a system of equations that included an accounting for tidal interactions among the planets and their satellites as well as for relativistic effects. The results of such brute force integrations were first described in an important paper by Quinn *et al.* (1991). These analyses demonstrated that the solution of Laskar (1988) was highly accurate and could therefore be employed with confidence to accurately predict the variation of the strength of the solar insolation received by the Earth in the course of its orbit around the Sun as a function of time and as a function of latitude. Earlier predictions of these variations produced by Berger (e.g., 1978) were thereby shown to become inaccurate prior to approximately 1 My BP. The numerical reconstructions of the evolving geometry of Earth's orbit consist of predicted time series for the evolution of orbital ellipticity and orbital obliquity. From these quantities, one may compute the latitude-dependent summertime seasonal anomaly in solar insolation

received at the top of the atmosphere that is presumed to drive the glaciation–deglaciation process according to the Koppen–Milankovitch hypothesis on the basis of the expression,

$$\delta Q\,(\theta,\ t) = \Delta R_s(\theta)\Delta\varepsilon(t) + m(\theta)\Delta[e(t)\sin(\tilde{\omega}t)] \quad [39]$$

in which $\delta Q\,(t)$ is the deviation, in W m^{-2}, of the insolation received at the surface of the Earth during the summer season relative to the average of summer insolation over, say, the timescale of the entire 900 000 year period during which the 100 000 year ice-age cycle has been an active element of climate system evolution. The latitude dependence of the summertime seasonal insolation anomaly is introduced through the quantities $\Delta R_s(\theta)$ and $m(\theta)$, whereas the time dependence is governed by the variation in orbital obliquity $\Delta\varepsilon(t)$ and time-dependent eccentricity of the orbit $e(t)$ which enters the expression for the insolation anomaly only through a modulation of the influence of orbital precession which occurs at an angular frequency $\tilde{\omega}$ due to the same oblateness of the figure of the Earth that is modulated so effectively by the ice-age cycle. This phenomenon of orbital precession is caused by the action of the gravitational field of the Sun upon the oblate form of the planet whose spin axis is tilted with respect to the ecliptic plane. **Figure 27** illustrates the time dependence of each of the quantities that appears in the expression for the orbital insolation anomaly in eqn [39]. **Figure 28** shows the actual distribution of the received insolation over the surface of the Earth as a function of latitude and time of year, both for the present day and for the deviations from this distribution at several fiducial times over the most recent 100 000 year cycle of Late Pleistocene glaciation. Inspection of the distribution of the anomaly for 116 000 years BP at the onset of the most recent of these cycles of continental ice-sheet expansion demonstrates that this event was in fact apparently triggered by a high-latitude summertime seasonal insolation anomaly of magnitude in excess of 60 W m^{-2}, in accord with expectations based upon the Milankovitch hypothesis. At LGM itself, the deviation of the insolation regime from that

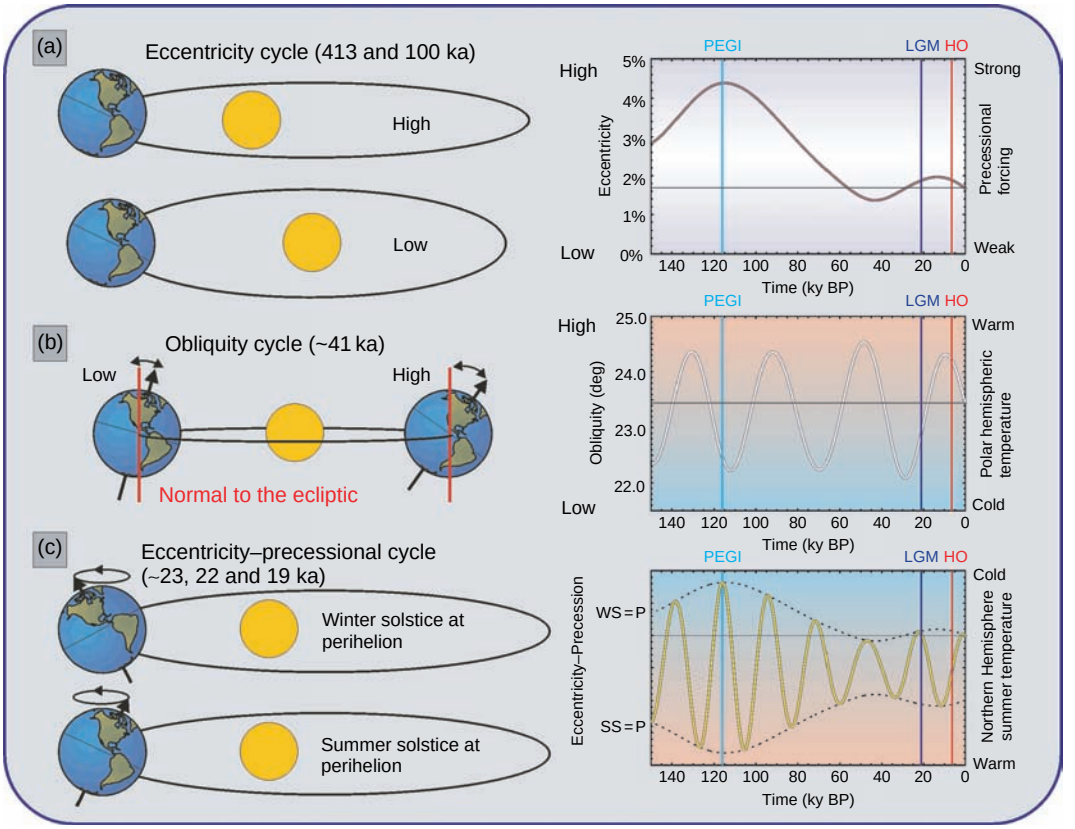

Figure 27 Evolution with time, over the most recent 100 000 year cycle of Late Pleistocene climate variability, of the parameters that control the variation of the solar insolation received at the top of the atmosphere.

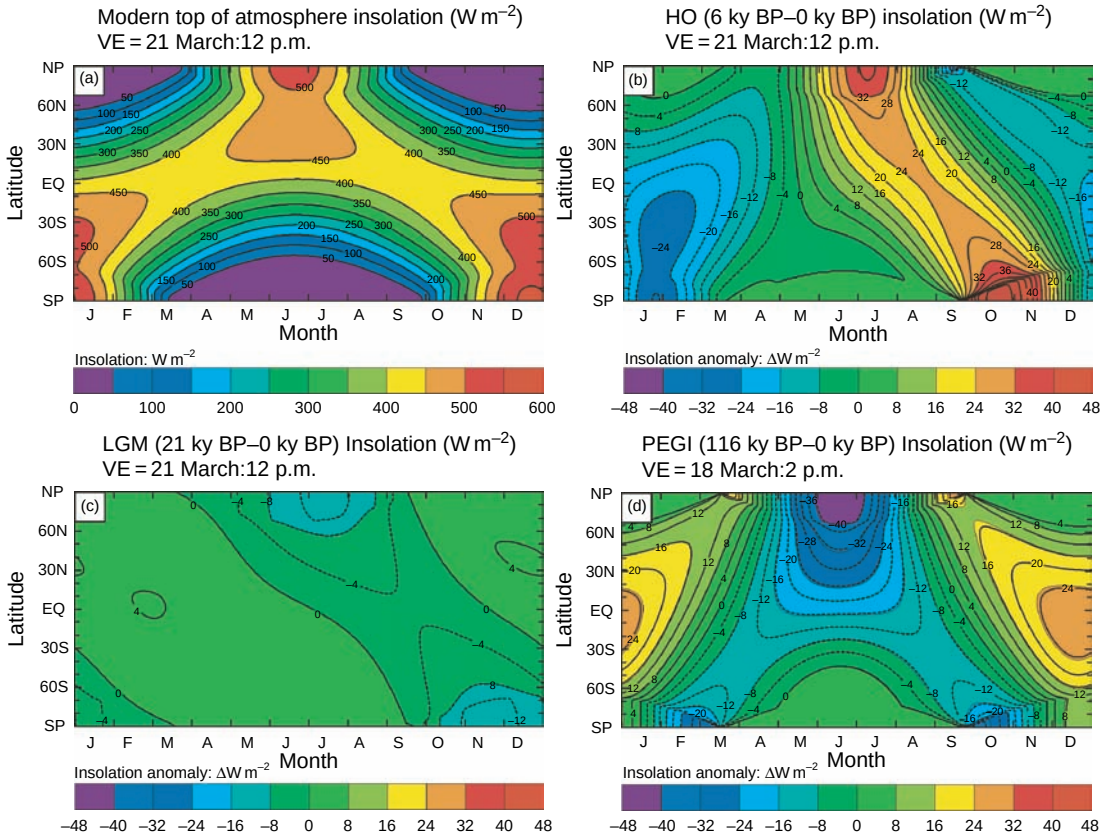

Figure 28 Distribution of solar insolation received at the top of the atmosphere as a function of time of year and latitude for three different epochs. (a) The present-day distribution; (b) and (c) the deviation from the modern distribution for the mid-Holocene warm period at 6000 years BP, for LGM at *c*. 21 000 years BP, and for the end of the Eemian interglacial at 116 000 years BP, the time during which the extremely strong negative summertime seasonal insolation anomaly existed that was responsible for the onset of the most recent 100 000 year glacial cycle.

characteristic of present climate was actually rather small. During the mid-Holocene interval centered upon 6 ka, the nature of the insolation forcing was such that the Northern Hemisphere continents would have been anomalously warm during the summer season, thus explaining the increased intensity of the summer monsoon circulations that were characteristic of the atmospheric general circulation at that time. **Figure 29** compares the power spectrum of the oxygen-isotope anomaly from deep-sea core OPD 677 to the power spectrum of the summertime seasonal insolation anomaly at 60° north latitude for both the first and last million years of the Pleistocene epoch. Inspection of this intercomparison shows that the power in the insolation forcing at the 100 000 year period on which the continental ice sheets expand and contract is miniscule. The implications of this intercomparison are profound as it provides a direct demonstration of the intensity of the nonlinearity of the climate system that is involved in converting the incoming insolation signature into the climate response. It is only through the action of such nonlinearity that the system may feel the effect of the 100 000 year modulation of the influence upon received insolation due to the effect of orbital precession that arises from the variation of orbital eccentricity. Precisely what the origin is of this nonlinearity remains a subject of intense debate but is presumably connected to the cause of the covariation of atmospheric carbon dioxide with continental ice volume that is so clearly revealed in the Vostock ice core from the continent of Antarctica (e.g., see Overpeck *et al.* (2007) for detailed discussion of the ice-core records and Shackleton (2000) for a discussion of the phase relationships between the atmospheric carbon dioxide record and the ice-volume record; Peltier (1998) has reviewed the current state of theoretical understanding).

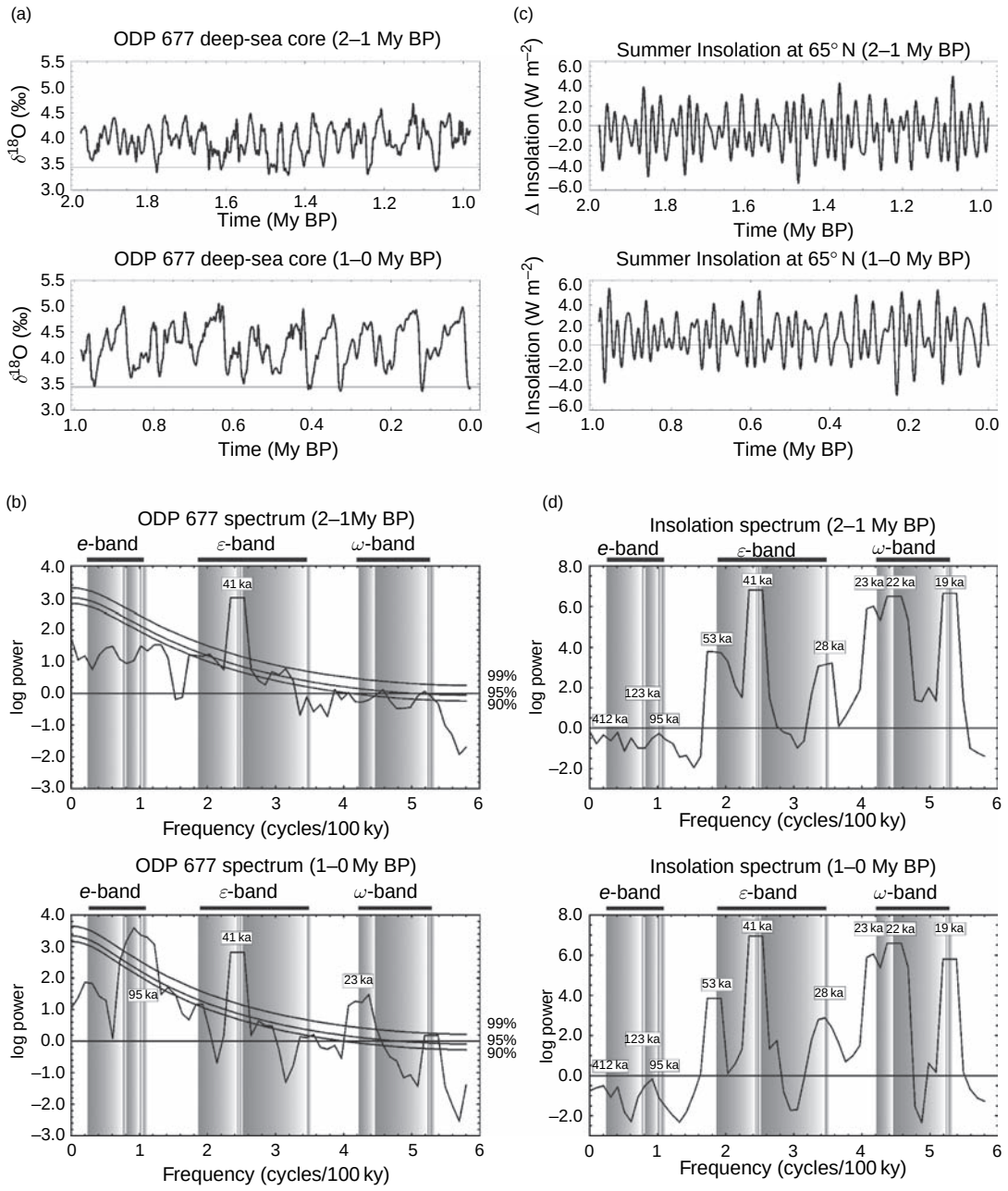

Figure 29 Intercomparison of the oxygen-isotopic time series from ODP core 677 and its power spectrum to the time series and power spectrum of the solar insolation forcing for both the first and last million years of these records. Notable is the extremely weak insolation forcing at the period of 100 000 years, which is the period at which the climate system response is strongest.

9.10.6.2 'Orbital Tuning' and the Age of the Brunhes–Matuyama Geomagnetic Polarity Transition

Given this background we may proceed to consider the analyses that led to the redating of the oxygen-isotopic record from ODP core 677 that has played such an important role in revising our understanding of the Pleistocene timescale. **Figure 31** shows the original depth versus time scale that was originally ascribed to this core by Shackleton (personal communication in 1988 when the data were passed to the present author for analysis). Notable is the 'dogleg' in this relationship that is apparent near the then-assumed age of 730 000 years of the

Brunhes–Matuyama transition that was widely accepted as correct at that time. Based upon the assumption of the validity of the Milankovitch hypothesis, the depth–age relationship for this core was refined in Toronto by applying the following strategy. First the relationship between depth in the core and calendar year age was refined by applying a band-pass filter to the isotopic time series with a central frequency equal to that of the obliquity timescale of 41 000 year and the depth–time relationship was adjusted iteratively so as to maximize the coherence between the astronomical forcing at this period and the ice-volume response. Next the same process was applied to the variability in the eccentricity–precession band, in which the modulation of the precession effect due to the eccentricity variation occurs. Once more, the age–depth relationship was adjusted in order to optimize the coherence between astronomical signal and ice-volume response. The frequency domain form of the band-pass filters employed in this analysis together with the power spectrum of the oxygen-isotope time series is shown in **Figure 30**. The process of refinement of the age–depth relationship was continued by returning to the obliquity band and then returning to the eccentricity–precession band, etc., until an entirely stable result was obtained. The new age–depth relationship for the 677 core is also shown in **Figure 31** as the dashed line labeled Model II, where it is observed to correspond to a very nearly linear relationship between depth and age, suggesting that in fact the sedimentation rate at this site had been very nearly constant throughout the entire Pleistocene interval. The initial depth–age model provided to the author by N. J. Shackleton is shown as model IV. The models denoted I and III in the figure are intermediate results obtained in the iterative sequence of steps in the 'orbital tuning' process. The quality of the fits between the astronomical forcing and ice-volume response records in the two pass bands employed in the application of this methodology are shown in **Figures 32**(**a**) and **32**(**b**), where a very nearly precise agreement was obtained (see Peltier (1994) in which the original results that led to the paper by Shackleton *et al.* (1990) were eventually published).

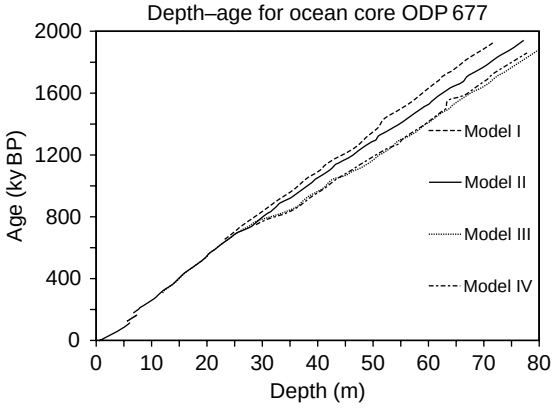

Figure 30 Oxygen-isotopic record from ODP core 677 as originally provided by N. J. Shackleton to the author in 1988 on the depth vs time scale constrained to fit the assumed age of 730 000 years of the Brunhes–Matuyama geomagnetic reversal. Notable in the original record is the 'dogleg' that was forced to occur in the depth–time relationship by virtue of this assumption. Also shown are the revised depth–time relationships deduced by 'orbital tuning' of this record that was accomplished at the University of Toronto and which led to the prediction of the necessity of revising the age of this geomagnetic reversal.

This analysis suggested that there must have been an error in the previously accepted age of the Brunhes–Matuyama transition in the polarity of Earth's magnetic field, with the actual age of the transition being very close to 780 000 years rather than to the originally assumed age of 730 000 years, a difference of approximately 7% or 50 000 years. In the paper by Shackleton *et al.* (1990), the initial Toronto result was checked against a large number of other oxygen-isotopic records from deep-sea cores and found to be reproducible in every instance. Very soon after appearance of the Shackleton *et al.* publication, and in response to it, the age of the Brunhes–Matuyama transition was redated using the argon 39–argon 40 method by Baksi (1992), whose analysis immediately confirmed the validity of the new age for this most recent polarity transition in the Earth's magnetic field, an age that had been determined by application of the 'orbital tuning' methodology. It should be clear that this combination of results has served to fully verify the validity of our present understanding of the Late Pleistocene ice-age cycle as being caused by the history of the variations in the geometry of Earth's rotation around the Sun.

9.10.7 Earth Rotation Variations and Mantle Convective Mixing

On the longest timescales of hundreds of millions of years on which the thermal evolution and internal structure of the Earth are governed by the mantle

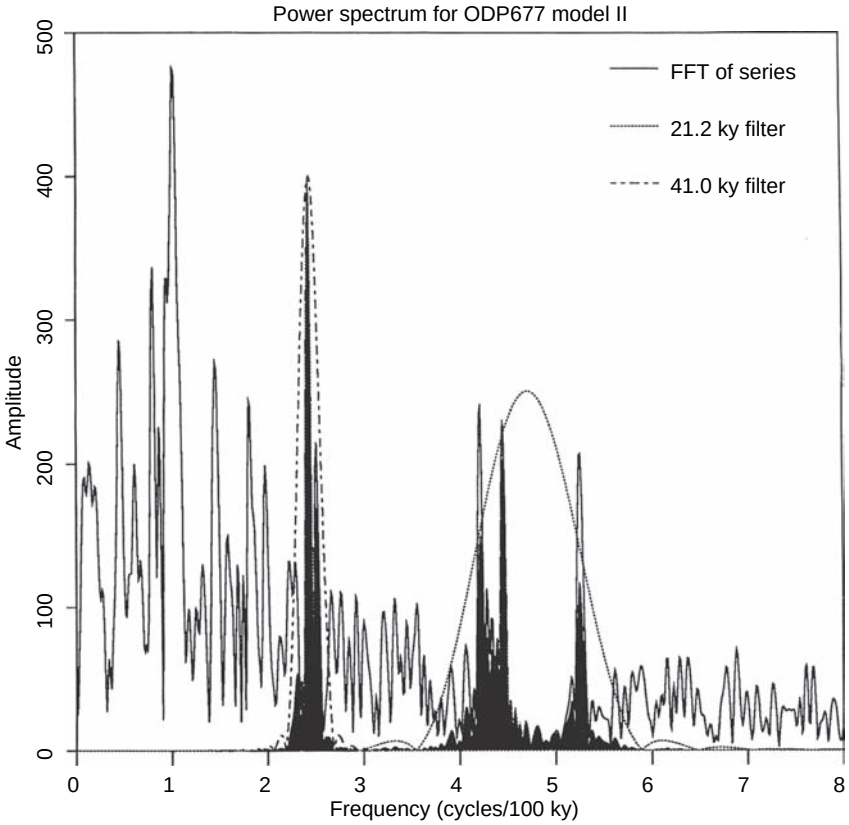

Figure 31 Frequency domain forms of the band-pass filters employed in the Toronto application of the orbital tuning methodology to the $\delta^{18}O$ record from ODP core 677.

convection process, debate continues concerning the issue as to whether the relative latitudinal positions of the continents and the variations of their positions through time are to be ascribed solely to the action of the mantle convection-driven process of continental drift. If it were possible for the relative positions of the continents with respect to the axis about which the planet rotates to be spontaneously modified by a TPW event that resulted in a reorientation of geography with respect to the rotation pole, then it would be possible to misinterpret paleomagnetic inferences of paleolatitude as arising due to the action of the convection process when in fact these were due to the influence of TPW. Recent interest in the possible importance of this process has come to be focused upon the possibility of occurrence of a so-called 'inertial interchange' instability (e.g., Goldreich and Toomre, 1969; Fisher, 1974, Kirschvink *et al.*, 1997) during which, as a consequence of the axis of greatest moment of inertia being 'suddenly' (on geological timescales) changed, the geographical positions of the continents with respect to the rotation pole would be subject to a secular shift. This would clearly require that the modification, whether by reorganization of the convective flow or some other process, be strong enough to overcome the stabilizing influence of the equatorial bulge due the basic rotation, as previously discussed in Section 9.10.4. It remains an issue as to whether the process of convective overturning is capable of effecting such a profound influence upon the rotational state of the planet. After all, the magnitude of the density variations associated with the convection process are hardly more than a few percentage, and these variations are not obviously organized in a sufficiently coherent pattern as to be effective in exerting direct control upon the rotational state of the object.

There does exist, however, one potential phenomenon that has been suggested to be a characteristic of the mantle convection process that could, at least in principle, exert 'coherent control' upon Earth

rotation. This is the so-called 'avalanche effect' discussed at length by Peltier and Solheim (1992) and Solheim and Peltier (1994a, 1994b), an effect upon the temporal variability of the convection process that is controlled by the action of the phase transition from spinel to a mixture of perovskite and magnesiowustite that exists at 660 km depth and which separates the so-called transition zone of the mantle above this level from the lower mantle beneath. The avalanche effect is found to be strong in models of the mantle convection process in which the effective viscosity of the planetary mantle is sufficiently low, as it is in the VM2 model that has been developed on the basis of fits to observations of the GIA process discussed in the previous sections of this chapter (see **Figure 19**). Peltier (1998) has argued that this model, or a close relative derived on the basis of analyses of the GIA process, may be equally applicable on the much longer timescale characteristic of convection in Earth's mantle, although this issue remains a subject of active debate.

Insofar as effort is concerned to confirm the possibility that IITPW may have occurred in the past, a primary era of Earth history that has been suggested as a candidate has been the Early Cambrian period (Kirschvink *et al.*, 1997). Of course, this is an extraordinarily important period of time from the perspective of Earth evolution in general and biological evolution in particular as well as from the perspective of tectonophysics. From the perspective of biological evolution, it was the time of especially rapid biological diversification that occurred during

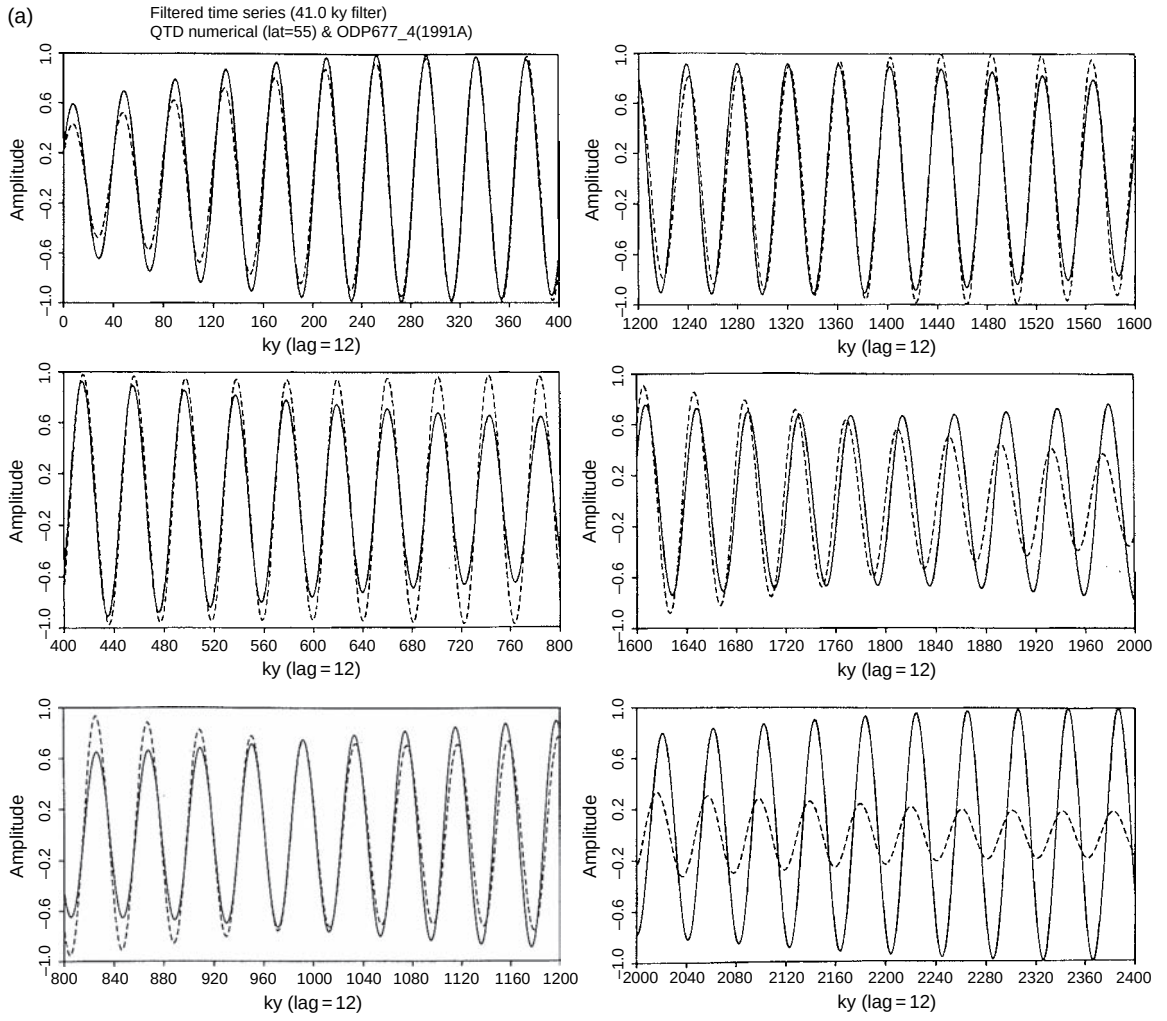

Figure 32 (*Continued*)

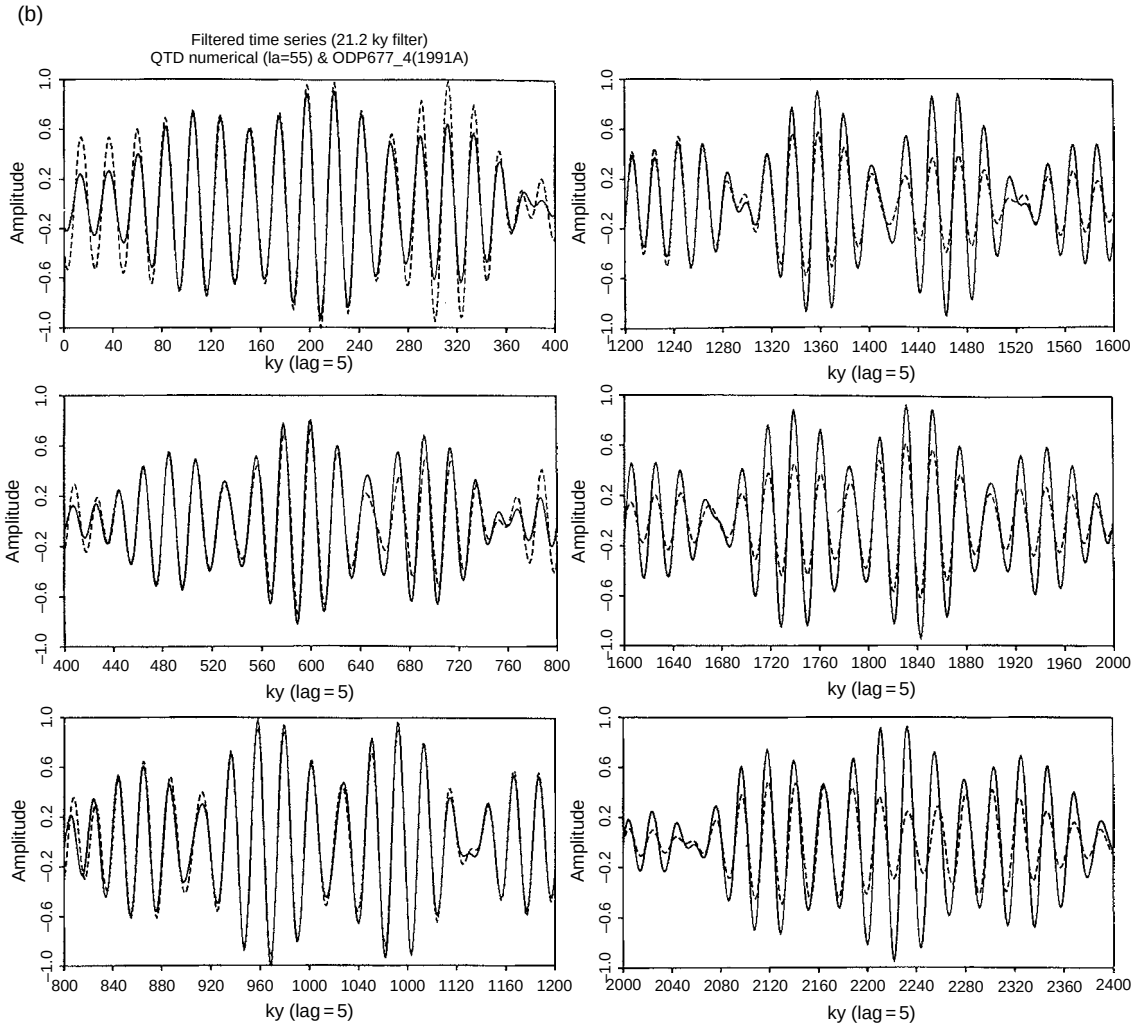

Figure 32 (a) Coherence between the astronomical forcing at the period of 41,000 years and the oxygen isotopic variability at the same period after orbital tuning at the University of Toronto. (b) Same as Figure 31a but showing the coherence in the eccentricity-precession band between astronomical forcing and oxygen-isotopic (climate) response. This is the original work that led to the results reported in Shackleton et al. (1990).

the so-called 'Cambrian explosion of life'. From the perspective of tectonophysics, it was a time immediately following the final phase of the Neoproterozoic breakup of the supercontinent of Rodinia during which a series of especially severe episodes of global glaciation are believed to have occurred (e.g., Kirschvink, 1991; Hoffman and Schrag, 2000, 2002). These hypothesized glaciation events have been termed 'snowball glaciations', during which it is imagined that the surface of the Earth may have become entirely ice covered, the oceans by a thick veneer of sea ice and the continents by thick continental ice sheets such as those that were confined primarily to the north polar regions during times of ice-age maxima within the Pleistocene era. Although the plausibility of occurrence of the 'hard snowball' state envisioned by these authors has been questioned (e.g., Hyde *et al*, 2000; Peltier *et al*., 2004), there is no doubt that the period of transition between the Neoproterozic and the Cambrian eras, a transition that occurred at approximately 541 Ma, was a time in Earth history during which plausibly large variations in the elements of the moment of inertia tensor of the planet could have occurred. Not only was the process of mantle convection highly disturbed during the process of the rifting and dispersal of Rodinia but

there were also highly significant exchanges of mass occurring between the oceans and the highly glaciated continents at the end of the final Neoproterozoic snowball event. Li *et al.* (2004) have in fact proposed that the inferred equatorial location of this supercontinent during the earliest (Sturtian) episode of intense Neoproterozoic glaciation could have arisen as a consequence of a complete 90° inertial interchange instability event during which the supercontnent was shifted from the pole to the equator. It may therefore be the case that the Sturtian ice mass was not emplaced on the supercontinent while it was at the equator but rather when it was in the initial polar location. This is an idea that is suggested as a possibility by the Li *et al.* analysis of the paleomagnetic data but which was not explicitly envisioned by them.

Figure 33 illustrates the temporal interrelationships that existed in the Earth system during this critical period in Earth history between the tectonophysical events associated with the mantle convection process and the events that were simultaneously occurring in surface climate variability. The climate-related signal shown on this time series is for the carbon-isotopic anomaly denoted $\delta^{13}C$ which is measured in carbonate rocks on land such as those from Namibia which constitute the type section for much of the work that has been accomplished in support of the snowball Earth hypothesis (Hoffman and Schrag, 2000). The importance of this isotopic measurement derives from the fact that it is strongly influenced by photosynthetic activity as an isotopic fractionation occurs such that the organic matter produced in photosynthesis is enriched in ^{12}C

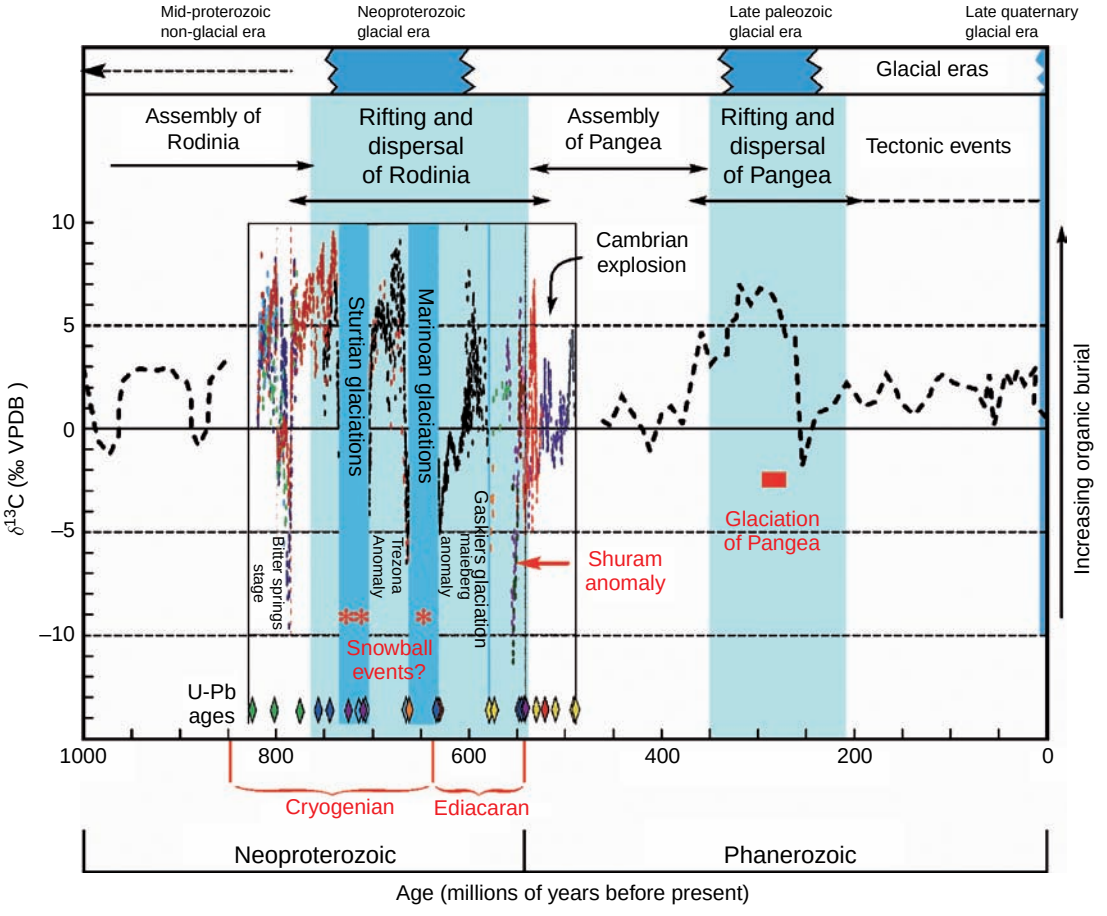

Figure 33 The variation of carbon isotopes, denoted $\delta^{13}C$, over the last 1.6 Gy of Earth history shown together with the times of occurrence of periods of significant continental glaciation and the times of creation and destruction of supercontinents that accompany the so-called 'Wilson cycle'. The $\delta^{13}C$ time series is from Kauffman (1997) and Hoffman and Schrag (1999), whereas the insert for the Neoproterozoic era is based upon the composite data set from Halverson *et al.* (2005).

relative to the heavier isotope ^{13}C. A time when the $\delta^{13}C$ that is measured in carbonate rocks that were precipitated from the ocean is high therefore corresponds to a time of high photosynthetic biological productivity. This is because such episodes correspond to times, as indicated in **Figure 33**, when the rate of burial of the organic matter produced in photosynthesis is significantly elevated, leaving behind an ocean that is enriched in ^{13}C. The sharp minima that are observed to characterize the time series shown on **Figure 32** have therefore been taken to correspond to times in Earth history of intense 'snowball' glaciation during which photosynthetic activity was either sharply diminished or eliminated altogether, as would have been the case during a 'hard snowball' event. Also indicated in **Figure 33** is the timing of the episodes of intense tectonic activity that would have been associated with the breakup of the supercontinents of Rodinia and, much later during the Carboniferous period, Pangea. The period of transition between the Neoproterozoic and the Cambrian that Kirschvink has suggested as a possible time of occurrence of an inertial interchange instability event was therefor a time of profound change in Earth history, perhaps the most important such period since the birth of the planet from the primitive solar nebula.

In an attempt to establish the Early Cambrian IITPW hypothesis of Kirschvink (1997) as viable, Mound *et al.* (1999) performed a calculation of the expected impact of such an event upon RSL history. Their idea was to see whether observations of RSL history over timescales of millions of years might be employed as a means of determining whether an IITPW event had occurred and the analyses presented were interpreted to imply that the hypothesis was not only viable but was supported by their initial analysis of the observational constraints they described. An important issue concerning the validity of these analyses concerns the strong dependence of the results obtained upon the thickness of the lithosphere assumed to be characteristic of the Maxwell viscoelastic model employed for the purpose of analyzing the sea-level response to the rotational excitation. Their assumption in this analysis was that the lithosphere could be treated as a complete 'unbroken-by-plate-tectonics' elastic shell over the tens of millions of years during which the IITPW event was imagined to occur. Their results, however, suggested a very strong dependence upon the thickness assumed such that the response rapidly diminished as the assumed thickness of the lithosphere was reduced. In Sections 9.10.3 and 9.10.5, the question as to how the thickness of the lithosphere was to be treated, insofar as the computation of the rotational response to surface glaciation and deglaciation is concerned, was discussed. The issue of the role of lithospheric thickness in global geodynamics in general, including its action in determining the manner in which Earth's rotation state responds to time variability in the mantle convection circulation, remains outstanding. It may in fact be possible during a period of rapid reorganization of the convection process, when the strong correlation that exists under modern plate-tectonic conditions between plate boundaries and deep mantle upwellings and downwellings may no longer obtain. In such conditions, an influence of finite lithospheric thickness may therefore have existed in which case the Mound *et al.* results could be fully applicable.

In searching for a sufficiently intense process of reorganization of the convective circulation that might be responsible for an IITPW event, such as that suggested by Kirschvink to have occurred in the Early Cambrian or Li *et al.* in the Neoproterozoic, the author is inclined to focus upon the times of occurrence of events related to the supercontinent cycle such as the rifting process during which an initially compact supercontinent is fragmented following the occurrence of 'avalanche' events during which the convective circulation may have made a rather sudden transition from a state of whole mantle flow to a state of layered convection (e.g., see Peltier (1996) for a review). Peltier *et al.* (1997) has in fact suggested a close linkage between the so-called 'Wilson cycle' of supercontinent creation and destruction and the continuously recurrent 'avalanche effect' that some detailed fluid mechanical models of the convection process have predicted (e.g., Peltier and Solheim, 1994a, 1994b). Such models do apparently predict the inferred timescale of several hundred million years that appears to separate the times in Earth history during which supercontinents existed. That timescale is most visibly evident in histograms of the sample density of continental rocks of a given age as a function of their age. Such suggestions of the mechanism that could underlie these most dramatic events of all that may have occurred in the history of Earth rotation must however remain a subject of speculation in search of firm quantitative justification.

References

Albero MC and Angiolini FE (1983) INGEIS Radiocarbon Laboratory dates I. *Radiocarbon* 25: 831–842.

Albero MC and Angiolini FE (1985) INGEIS Radiocarbon Laboratory dates II. *Radiocarbon* 27: 315–337.

Angulo RJ and Lessa GC (1997) The Brazilian sea level curves: A critical review with emphasis on the curves from Paranagua and Cananeia regions. *Geology* 140: 141–166.

Argus DF and Gross RS (2004) An estimate of motion between the spin axis and the hotspots over the past century. *Geophysical Research Letters* 31: L06614 (doi:10.1029/2004GL019657).

Baksi AK (1992) $^{40}Ar/^{39}Ar$ dating of the Brunhes–Matuyama geomagnetic field reversal. *Science* 256: 356–359.

Belperio AP, Harvey N, and Bousman RP (2002) Spatial and temporal variability in the Holocene sea-level record of the South Australian coastline. *Sedimentary Geology* 150: 153–169.

Berger A (1978) Long-term variations of daily insolation and Quaternary climatic changes. *Journal of the Atmospheric Sciences* 35: 2362–2367.

Bezerra F, Barreto A, and Sugio K (2003) Holocene sea-level history on the Rio Grande do Norte State coast, Brazil. *Marine Geology* 196: 73–89.

Broecker WS and Van Donk J (1970) Insolation changes, ice volumes, and the $\delta^{18}0$ record in deep sea cores. *Geophysics and Space Physics* 8: 169–198.

Calaya MA, Wahr JM, and Bryan FO (1999) Climate-driven polar motion. *Journal of Geophysical Research* 104: 12813–12829.

Camoin GF, Colonna M, Montaggioni LF, Casanova J, Faure G, and Thomassin BA (1997) Holocene sea level changes and reef development in the southwestern Indian Ocean. *Coral Reefs* 16: 247–259.

Carter WE, Robertson DS, Pyle TE, and Diamante J (1986) The application of geodetic radio interferometric surveying to the monitoring of sea level. *Geophysical Journal of the Royal Astronomical Society* 87: 3–13.

Camoin GF, Montaggioni LF, and Braithwaite CJR (2004) Late glacial to to post glacial sea levels in the western Indian Ocean. *Marine Geology* 206: 119–146.

Codignotto JD, Kokott RR, and Marcomini SC (1992) Neotectonism and sea-level changes in the coastal zone of Argentina. *Journal of Coastal Research* 8: 125–133.

Chandler SC (1891) On the variation of latitude, I. *Astronomical Journal* 11: 59–61.

Chao BF, O'Conner WP, Chang ATC, Hal DK, and Foster JL (1987) Snow load effect on the Earth's rotation and gravitational field, 1979-1985. *Journal of Geophysical Research* 92: 9415–9422.

Cheng MK, Eanes RJ, Shum CK, Schutz BE, and Tapley BD (1989) Temporal variations in low degree zonal harmonics from Starlette orbit analysis. *Geophysical Research Letters* 16: 393–396.

Clark JA, Farrell WE, and Peltier WR (1978) Global changes in postglacial sea levels: A numerical calculation. *Quaternary Research* 9: 265–287.

Clark PU, Mitrovica JX, Milne GA, and Tamasea ME (2002) Sea level finger printing as a direct test of the source of meltwater pulse 1a. *Science* 295: 2438–2441.

Cox CM and Chao BF (2002) Detection of a large-scale mass redistribution in the terrestrial system since 1998. *Science* 297: 831–833.

Dahlen FA (1976) The passive influence of the oceans upon the rotation of the Earth. *Geophysical Journal of the Royal Astronomical Society* 46: 363–406.

Dalmau W (1997) Critical remarks on the use of medieval eclipse records for the determination of long-term changes in the Earth's rotation. *Surveys in Geophysics* 18: 213–223.

Daly L and Le Goff M (1996) An updated and homogeneous world secular variation database. Part 1. Smoothing of the archeomagnetic results. *Physics of the Earth and Planetary Interiors* 93: 159–190.

Dahlen FA and Smith ML (1975) The influence of rotation on the free oscillations of the Earth. *Philosophical Transactions of the Royal Society* 279: 583–629.

Deblonde G and Peltier WR (1991) A one dimensional model of continental ice-volume fluctuations through the Pleistocene: Implications for the origin of the mid-Pleistocene climate transition. *Journal of Climate* 4: 18–34.

Deblonde G and Peltier WR (1993) Late Pleistocene ice-age scenarios based upon observational evidence. *Journal of Climate* 6: 709–727.

Delibrias G and Laborel J (1971) Recent variations of the sea level along the Brazilian coast. *Quaternia* 14: 45–49.

Dickey JO, Marcus SL, de Viron O, and Fukumori I (2002) Recent Earth oblateness variations: Unravelling climate and postglacial rebound effects. *Science* 298: 1975–1977.

Dickman SR (1977) Secular trend of the Earth's rotation pole: Consideration of motion of the latitude observatories. *Geophysical Journal of the Royal Astronomical Society* 57: 41–50.

Domack E, Duran D, Leventer A, *et al.* (2005) Stability of the Larsen B ice shelf on the Antarctic Peninsula during the Holocene epoch. *Nature* 436: 681–685.

Dyurgerov MB and Meier MF (2005) *Glaciers and the changing Earth system: A 2004 snapshot. Occassional Paper No. 58*. Boulder, Colorado: Institute of Arctic and Alpine Research, University of Colorado.

Dunberry M and Bloxham J (2006) Azimuthal flows in the Earth's core and changes in length of day at millennial timescales. *Geophysical Journal International* 165: 32–46.

Dziewonski AM and Anderson DL (1981) Preliminary reference Earth model. *Physics of the Earth and Planetary Interiors* 25: 297–356.

Fairbridge RG (1976) Shellfish-eating preceramic indians in coastal Brazil. *Science* 191: 353–359.

Faure H and Hebrard L (1977) Variations des lignes de ravages au Senegalet au Mauritania au cours de l'Holocene. *Studia Geologica Polonica* 52: 143–157.

Faure H, Fontes JC, Hebrasd L, Monteillet J, and Pirazolli PA (1980) Geoidal changes and shore-level tilt along Holocene estuaries: Senegal River area, west Africa. *Science* 210: 421–423.

Farrell WE (1972) Deformation of the Earth by surface loads. *Reviews of Geophysics* 10: 761–797.

Farrell WE and Clark JA (1976) On postglacial sea level. *Geophysical Journal of the Royal Astronomical Society* 46: 647–667.

Fisher D (1974) Some more remarks on polar wandering. *Journal of Geophysical Research* 79: 4041–4045.

Gegout P and Cazenave A (1991) geodynamic parameters derived from 7 years of laser data on LAGEOS. *Geophysical Research Letters* 18: 1739–1742.

Gibb JG (1986) A New Zealand regional Holocene eustatic sea-level curve and its application to determination of vertical tectonic movements. *Royal Society New Zealand Bulletin* 24: 377–395.

Gold T (1955) Instability of the Earth's axis of rotation. *Nature* 175: 526–529.

Goldreich P and Toomre A (1969) Some remarks on polar wandering. *Journal of Geophysical Research* 74: 2555–2567.

Gross RS (1986) The influence of earthquakes on the Chandler wobble during 1977–1983. *Geophysical Journal of the Royal Astronomical Society* 85: 161–177.

Gross RS (2000) The excitation of the Chandler wobble. *Geophysical Research Letters* 27: 2329–2342.
Halverson Galen P, Hoffman PF, *et al.* (2005) Toward a Neoproterozoic composite carbon-isotopic record. *GSA Bulletin* 117: 1181–1207.
Hays JD, Imbrie J, and Shackleton NJ (1976) Variations in the Earth's orbit: Pacemaker of the ice-ages. *Science* 194: 1121–1132.
Hide R, Birch NT, Morrison LV, Shea DJ, and White AA (1980) Atmospheric angular momentum fluctuations an changes in the length of the day. *Nature* 286: 114–117.
Hoffman PF and Schrag DF (2000) Snowball Earth. *Scientific American* 282: 68–75.
Hoffman PF and Schrag DA (2002) The snowball Earth hypothesis: Testing the limits of global change. *Terra Nova* 14: 129–155.
Hongre L, Hulot G, and Khoklov A (1998) An analysis of the geomagnetic field over the past 2000 years. *Physics of the Earth and Planetary Interiors* 106: 311–335.
Hyde WT, Crowley TJ, Baum SK, and Peltier WR (2000) Neoprpterozoic 'snowball Earth' simulations with a coupled climate/ice sheet model. *Nature* 405: 425–430.
Imbrie J, Hays JD, Martinsen DG, *et al.* (1984) The orbit theory of Pleistocene climate: Support from a revised chronology of the marine $\delta^{18}0$ record. In: Berger A, Imbrie J, Hays J, Kukla G, and Saltzman B (eds.) *Milankovitch and Climate*, pp. 269–306. Norwell, Mass: D. Reidel.
Jault D and Le Mouel J-L (1993) Circulation in the liquid core and coupling with the mantle. In: Singh RP, Feissel M, Tapley BD, and Shum CK (eds.) *Advances in Space Research: Observations of Earth from Space*, vol: 13, pp. (11)221–(11)233. Oxford: Pergamon.
Kirschvink JL (1991) Late Proterozoic low-latitude global glaciation: The snowball Earth. In: Schopf JW and Klein C (eds.) *The Proterozoic Biosphere, A Multi-discipliary Study*, pp. 51–52. New York: Cambridge University Press.
Kirschvink JL, Ripperdan RL, and Evans DA (1997) Evidence for a large-scale reorganization of Early continental masses by inertial interchange true polar wander. *Science* 277: 541–545.
Koba M, Nakata T, and Takahashi T (1982) Late Holocene eustatic changes deduced from geomorphological features and their C-14 dates in the Ryuku Islands, Japan. *Palaeogeography Palaeoclimatology Palaeoecology* 39: 231–260.
Korte M and Constable C (2003) Continuous global geomagnetic field models for the past 3000 years. *Physics of the Earth and Planetary Interiors* 140: 73–89.
Krabil W, Abdalati W, Frederick E, *et al.* (2000) Greenland Ice Sheet: high elevation balance and peripheral thinning. *Science* 289: 428–430.
Kuehne J and Wilson CR (1991) Terrestrial water storage and polar motion. *Journal of Geophysical Research* 96: 4337–4345.
Lambeck K (1980a) Changes in length-of-day and atmospheric circulation. *Nature* 286: 104–105.
Lambeck K (1980b) *The Earth's variable Rotation: Geophysical Causes and Consequences*, 449 pp. New York: Cambridge University Press.
Lambeck K (2002) Sea level change from mid-Holocene to recent time: An Australian example with global implications. In: Mitrovica JX and Vermeersen LA (eds.) *AGU Monographs, Vol.* 29: *Ice Sheets, Sea Level and the Dynamics of the Earth*, pp. 33–50. Washington, DC: AGU.
Lambeck K and Chappell J (2001) Sea level change through the last glacial cycle. *Science* 292(5517): 679–686.
Laskar J (1988) Secular evolution of the solar system over 10 million years. *Astronomy and Astrophysics* 198: 341–362.
Li ZX, Evans DAD, and Zhang S (2004) A 90 degree spin on Rodinia: possible causal links between the Neoproterozoic supercontinent, superplume, true polar wander and low latitude glaciation. *Earth and Planetary Science Letters* 220: 409–421.
Markowitz W (1960) Latitude and longitude and the secular motion of the pole. *Methods and Techniques in Geophysics* 1: 325–361.
Martin L, Sugio K, Flexor JM, Dominguez JML, and Bittencourt ACSP (1987) Quaternary evolution of the central part of the Brazilian coast, the role of relative sea-level variation and of shoreline drift. *Quaternary Coastal Geology of West Africa and South America. UNESCO Reports in Marine Science* 43: 97–145.
Mikhailov AA (1971) On the motion of the Earth's poles. *Astronomichrskij Zhurnal* 48: 1301–1304.
Milne GA and Mitrovica JX (1996) Post-glacial sea level change on a rotating Earth: first results from a gravitationally sel-consistent sea-level equation. *Geophysical Journal International* 126: F13–F20.
Mitrovica JX, Wahr J, Matsuyama I, and Paulson A (2005) The rotational stability of an ice-age Earth. *Geophysical Journal International* 161: 491–506.
Morner NA (1991) Holocene sea level changes in the Tierra del Fuego region. *Bol. IG-USP Publ. Esp* 8: 133–151.
Morrison LV (1973) Rotation of the Earth and the constancy of G. *Nature* 241: 519–520.
Morrison LV and Stephenson FR (2001) Historical eclipses and the variability of the Earth's rotation. *Journal of Geodynamics* 32: 247–265.
Mound JE, Mitrovica JX, Evans DAD, and Kirschvink JL (1999) A sea-level test for inertial interchange true polar wander events. *Geophysical Journal International* 136: F5–F10.
Muller RA and Stephenson FR (1975) The acceleration of the Earth and Moon from early observations. In: Rosenburg GD and Runcorn SK (eds.) *Growth Rhythms and History of the Earth's Rotation*, pp. 459–534. New York: John Wiley.
Munk WH and MacDonald (1960) *The Rotation of the Earth*. New York: Cambridge University Press.
Nakiboglu SM (1982) Hydrostatic theory of the Earth and its mechanical implications. *Physics of the Earth and Planetary Interiors* 28: 302–311.
Nakiboglu SM and Lambeck K (1980) Deglaciation effects on the rotation of the Earth. *Geophysical Journal of the Royal Astronomical Society* 62: 49–58.
Nakiboglu SM and Lambeck K (1981) Deglaciation related features of the Earth's gravity field. *Tectonophysics* 72: 289–303.
Newton RR (1972) *Medieval Chronicals and the Rotation of the Earth*. Baltimore, MD: Johns Hopkins University Press.
Overpeck J and Jansen E *et al.* (2007) Paleoclimatology. In: Soloman S (ed.) *Climate Change 2007: The Scientific Basis, Working Group 1 Report of the Intergovernmental Panel on Climate Change*. ch. 6, Cambridge, UK: Cambridge University.
Peltier WR (1974) The impulse response of a Maxwell Earth. *Reviews of Geophysics and Space Physics* 12: 649–669.
Peltier WR (1976) Glacial isostatic adjustment. Part II: The inverse problem. *Geophysical Journal of the Royal Astronomical Society* 46: 669–706.
Peltier WR (1982) Dynamics of the ice-age Earth. *Advances in Geophysics* 24: 1–146.
Peltier WR (1983) Constraint on deep mantle viscosity from LAGEOS acceleration data. *Nature* 304: 434–436.
Peltier WR (1985) The LAGEOS constraint on deep mantle viscosity: Results from a new normal mode method for the inversion of visco-elastic relaxation spectra. *Journal of Geophysical Research* 90: 9411–9421.

Peltier WR (1994) Ice-age paleotopography. *Science* 265: 195–201.

Peltier WR (1996a) Physics of the ice-age cycle. In: Duplessy J-C (ed.) *Long Term Climate Variations*, pp. 453–481. New York: Springer-Verlag Inc.

Peltier WR (1996b) Mantle viscosity and ice-age ice-sheet topography. *Science* 273: 1359–1364.

Peltier WR (1996c) Phase transition modulated mixing in the mantle of the Earth. *Philosophical Tansactions of the Royal Society (London) Series A* 354: 1425–1447.

Peltier WR (1998) Postglacial variations in the level of the sea: implications for climate dynamics and solid-Earth geophysics. *Reviews of Geophysics* 36: 603–689.

Peltier WR (1999) Global sea level rise and glacial isostatic adjustment. *Global and planetary change* 20: 93–123.

Peltier WR (2002a) Comments on the paper of Yokoyama *et al*. (2000) entitled 'Timing of the last glacial maximum from observed sea level minima. *Quaternary Science Reviews* 21: 409–414.

Peltier WR (2002b) One eustatic sea level history, Last Glacial Maximum to Holocene. *Quarternary Science Reviews* 21: 377–396.

Peltier WR (2002c) Global glacial isostatic adjustment: Paleo-geodetic and space-geodetic tests of the ICE-4G (VM2) model. *Journal of Quarternery Sciences* 17: 491–510.

Peltier WR (2004) Global glacial isostasy and the surface of the ice-age Earth: the ICE-5G(VM2) model and GRACE. *Annual Review of Earth and Planetary Sciences* 32: 111–149.

Peltier WR (2005) On the hemispheric origins of meltwater pulse 1a. *Quaternary Science Reviews* 24: 1655–1671.

Peltier WR and Fairbanks RG (2006) Global glacial ice-volume and Last Glacial Maximum duration from an extended Barbados Sea Level record. *Quarternary Science Reviews* 25: 3322–3337.

Peltier WR, Farrell WE, and Clark JA (1978) Glacial isostatsy and relative sea-level: A global finite element model. *Tectonophysics* 50: 81–110.

Peltier WR and Solheim LP (1992) Mantle phase transitions and layered chaotic convection. *Geophysical Research Letters* 19: 321–324.

Peltier WR and Jiang X (1996) Glacial isostatic adjustment and Earth rotation: Refined constraints on the viscosity of the deepest mantle. *Journal of Geophysical Research* 101: 3269–3290 (correction *Journal of Geophysical Research* 102: 10101–10103, 1997).

Peltier WR, Shennan I, Drummond R, and Horton B (2002) On the postglacial isostatic adjustment of the British Isles and the shallow visco-elastic structure of the Earth. *Geophysical Journal International* 148: 443–475.

Peltier WR and Solheim LP (2004) The climate of the Earth at Last Glacial Maximum: statistical equilibrium state and a mode of internal variability. *Quarternary Science Reviews* 23: 335–357.

Peltier WR, Tarasov L, Vettoretti G, and Solheim LP (2004) Climate dynamics in deep time: modeling the 'snowball bifurcation' and assessing the plausibility of its occurrence. In: Jenkins G, McMennamin MAS, McKay CP, and Sohl L (eds.) *AGU Monograph* 146: *The Extreme Proterozoic: Geology, Geochemistry, and Climate*, pp. 107–124. Washington, DC: AGU Press.

Pirazzoli P (1978) High stands of Holocene sea levels in the NW Pacific. *Quaternary Research* 10: 1–29.

Platzman GW (1971) Ocean tides and related w.aves. In: William HR (ed.) *Mathematical Problems in the Geophysical Sciences, Vol 2: Inverse Problems, Dynamo Theory and Tides*, pp. 239–291. Providence Rhode Island: American Mathematical Society.

Ponte RM, Stammer D, and Marshall J (1998) Oceanic signals in observed motions of the Earth's pole of rotation. *Nature* 391: 476–479.

Porter SC, Stuiver M, and Heusser CJ (1984) Holocene sea level changes along the straits of Megellan and Beagle Channel, Southernmost South America. *Quaternary Research* 22: 59–67.

Proverbio E and Quesada V (1974) Secular variation in latitudes and longitudes and continental drift. *Journal of Geophysical Research* 79: 4941–4943.

Quinn TR, Tremaine S, and Duncan M (1991) A three million year integration of the Earth's orbit. *Astronomical Journal* 101: 2287–2305.

Rochester MG and Smiley DE (1965) Geomagnetic core–mantle coupling and the Chandler wobble. *Geophysical Journal of the Royal Astronomical Society* 10: 289–315.

Rostami K, Peltier WR, and Mangini A (2000) Quarternary marine terraces, sea level changes and uplift history of Patagonia, Argentina: Comparisons with predictions of the ICE-4G (VM2) model of the global process of glacial isostatic adjustment. *Quaternary Science Reviews* 19: 1495–1525.

Rubincam DR (1984) Postglacial rebound observed by LAGEOS and the effective viscosity of the lower mantle. *Journal of Geophysical Research* 89: 1077–1087.

Sabadini R and Peltier WR (1981) Pleistocene deglaciation and the Earth's rotation: implications for mantle viscosity. *Geophysical Journal of the Royal Astronomical Society* 66: 553–578.

Sauriau A and Cazanave A (1985) Re-evaluation of the seismic excitation of the Chandler wobble from recent data. *Earth and Planetary Science Letters* 75: 410–416.

Shackleton NJ (1967) Oxygen isotope analysis and Pleistocene temperatures re-addressed. *Nature* 215: 15–17.

Shackleton NJ (2000) The 100,000 year ice-age cycle identified and found to lag temperature, carbon dioxide, and orbital eccentricity. *Science* 289: 1897–1902.

Shackleton NJ and Opdyke ND (1973) Oxygen isotope and paleomagnetic stratigraphy of equatorial Pacific core V28-238: Oxygen isotope temperatures and ice volumes on a 10^5-year time scale. *Quaternary Research* 3: 39–55.

Shackleton NJ, Berger A, and Peltier WR (1990) An alternative astronomical calibration of the lower Pleistocene timescale based upon ODP 677. *Transactions of the Royal Society of Edinburgh: Earth Sciences* 81: 251–261.

Schofield JC (1975) Sea-level fluctuations cause periodic post-glacial progradation, South Kaipara Barrier, North Island, New Zealand. *New Zealand Journal of Geology and Geophysics* 18: 295–316.

Solheim LP and Peltier WR (1994a) Avalanche effects in phase transition modulated thermal convection: A model of Earth's mantle. *Journal of Geophysical Research* 99: 6997–7018.

Solheim LP and Peltier WR (1994b) 660 km phase boundary deflections and episodically layered isochemical convection. *Journal of Geophysical Research* 99: 15861–15875.

Stephenson ER and Morrison LV (1995) Long term fluctuations in the earth's rotation: 700 B.C. to A.D. 1990. *Philosophical Transactions of the Royal Society (London) Series A* 351: 165–202.

Stuiver M and Reimer PJ (1993) Extended ^{14}C data base and revised calib. 3.0 ^{14}C age calibration program. *Radiocarbon* 35: 215–230.

Sugihara K, Nakamori T, Iryu Y, Sasakai K, and Blanchon P (2003) Holocene sea-level change and tectonic uplift deduced from raised reef terraces, Kikai-jima, Ryuku Islands, Japan. *Sedimentary Geology* 159: 5–25.

Tarantola A and Valette B (1982a) Inverse problems=quest for information. *Journal of Geophysics* 50: 159–170.

Tarantola A and Valette B (1982b) Generalized nonlinear inverse problems solved using the least squares criterion. *Reviews of Geophysics* 20: 219–232.

Tarasov L and Peltier WR (2002) Greenland glacial history and local geodynamic consequences. *Geophysical Journal International* 150: 198–229.

Tarasov L and Peltier WR (2005) Arctic freshwater forcing of the Younger-Dryas cold reversal. *Nature* 435: 662–665.

Tarasov L and Peltier WR (2006) A calibrated deglacial chronology for the North American continent: Evidence of an Arctic trigger for the Younger-Dryas event. *Quarternary Science Reviews* 25: 659–688.

Valastro S, Jr., Davis EM, Vallrela AG, and Ekland-Olson C (1980) University of Texas at Austin radiocarbon dates XIV. *Radiocarbon* 22: 1090–1115.

Vincente RO and Yumi S (1969) Co-ordinates of the pole (1899-1968) returned to the conventional international origin. *Publication of the International Latitude Observatory of Mizusawa* 7: 41–50.

Vincente RO and Yumi S (1970) Revised values (1941-1961) of the co-ordinates of the pole referred to the CIO. *Publications of the International Latitude Observatory of Mizusawa* 7: 109–112.

Vondrak J (1984) Long period behaviour of polar motion between 1900.0 and 1984. *Annals of Geophysics* 21: 351–356.

Waelbroeck C, Labyrie L, Michel E, *et al.* (2002) Sea-level and deep water temperature changes derived from benthic foraminifera isotopic records. *Quaternary Science Reviews* 21(1–3): 295–305.

Wahr JM (1982) The effects of the atmosphere and oceans on the Earth's wobble-I. Theory. *Geophysical Journal of the Royal Astronomical Society* 70: 349–372.

Wahr JM (1983) The effects of the atmosphere and oceans on the Earth's wobble and on the seasonal variations in the length of day-II. Results. *Geophysical Journal of the Royal Astronomical Society* 74: 451–487.

Widder DV (1946) *The Laplace Transform, ch. V*. Princeton, NJ: Princeton University Press.

Williams GE (2000) Geological constraints on the Precambrian history of Earth's rotation and the Moon's orbit. *Reviews of Geophysics* 38: 37–59.

Wilson CR and Haubrich RA (1976) Meteorological excitation of the Earth's wobble. *Geophysical Journal of the Royal Astronomical Society* 46: 707–743.

Wilson CR and Vincente RO (1990) Maximum likelihood estiumates of polar motion parameters. In: McCarthy DD and Carter WE (eds.) *American Geophysical Union Monograph Series: Variations in Earth Rotation*, pp. 151–155. Washington DC: AGU.

Wu P and Peltier WR (1984) Pleistocene deglaciation and the Earth's rotation: A new analysis. *Geophysical Journal of the Royal Astronomical Society* 76: 202–242.

Yoder CF, Williams JG, Dickey JO, Schutz BE, Eanes RJ, and Tapley BD (1983) Secular variation of the Earth's gravitational harmonic J_2 coefficient from LAGEOS and non-tidal acceleration of Earth rotation. *Nature* 303: 757–762.

Yoder CF (1995) Astrometric and geodetic properties of Earth and the solar systems. http://www.agu.org/reference/gephys/4_oder.pdf.

Yokoyama Y, Lambeck K, DeDekkar P, Johnston P, and Fifield LK (2000) Timing of the Last Glacial Maximum from observed sea level minima. *Nature* 406: 713–716 (correction 2001, *Nature* 412: 99).